

**ALMA MATER STUDIORUM  
UNIVERSITA' DI BOLOGNA**

**SCUOLA DI INGEGNERIA E ARCHITETTURA**  
Sede di Forlì

**Corso di Laurea Magistrale in  
INGEGNERIA AEROSPAZIALE**  
Classe 8197

**TESI DI LAUREA**

**In**

**DINAMICA E CONTROLLO ORBITALE LM**

**Magnetic Actuators for Nanosatellite Attitude Control**

**CANDIDATO**

**Niccolò Bellini**

**RELATORE**

**Prof. Paolo Tortora**

**CORRELATORE**

**Prof. Jordi Puig-Suari**

**Anno Accademico 2013/2014**  
**Sessione II**



## Abstract

La ricerca e le attività presentate nella seguente relazione di tesi sono state condotte presso il California Polytechnic State University (USA) sotto la supervisione del Prof. Jordi Puig Suari.

L'obiettivo della ricerca ha riguardato lo studio di attuatori magnetici, comunemente chiamati magnetorquer, per il controllo di assetto di nanosatelliti. Tali attuatori si dividono generalmente in tre diverse tipologie: avvolgimenti air-core, avvolgimenti integrati e torquerod. Si tratta di dispositivi che, alimentati con modeste quantità di corrente, permettono di generare un campo magnetico il quale, interagendo col campo magnetico terrestre, può essere controllato per imprimere determinate rotazioni al satellite effettuando così manovre di puntamento.

In una prima fase dell'attività, ogni tecnologia è stata analizzata, definendo vantaggi e svantaggi, studiando le procedure di fabbricazione, ricavando equazioni per il dimensionamento basate su modelli matematici del comportamento fisico. Questi ultimi sono stati implementate in software numerici per creare uno strumento che permettesse di determinare la configurazione ottimale in base a determinati vincoli e specifiche di input.

In una seconda fase delle attività i modelli creati sono stati validati sfruttando prototipi già esistenti e realizzandone di nuovi. Sono dunque state effettuate misure delle grandezze caratteristiche di tali attuatori che permettessero un confronto tra il comportamento reale e quello teorico. Gli strumenti e il materiale sfruttati per esperimenti e prototipi sono stati forniti dai laboratori PolySat e CubeSat.

I risultati ottenuti hanno portato alla creazione di routines di dimensionamento complete per la progettazione di tali dispositivi e alla definizione di una procedura di design basata sulla completa libertà di scelta di tutti i parametri. Oltre a ciò è stata fatta anche un'analisi approfondita dei costi per ogni tipo di soluzione.

I modelli e gli strumenti sono stati mantenuti completamente parametrici per offrire la possibilità di riscalarli tali tipi di attuatori per satelliti di classe e dimensione diversa.



## Abstract

The research and the activities presented in the following thesis report have been led at the California Polytechnic State University (US) under the supervision of Prof. Jordi Puig Suari.

The objective of the research has been the study of magnetic actuators for nanosatellite attitude control, called magnetorquer. These actuators are generally divided in three different kinds: air core torquer, embedded coil and torquerod.

In a first phase of the activity, each technology has been analyzed, defining advantages and disadvantages, determining manufacturing procedures and creating mathematical model and designing equation. Dimensioning tools have been then implemented in numerical software to create an instrument that permits to determine the optimal configuration for defined requirements and constraints.

In a second phase of the activities the models created have been validated exploiting prototypes and proper instruments for measurements. The instruments and the material exploited for experiments and prototyping have been provided by the PolySat and CubeSat laboratories.

The results obtained led to the definition of a complete designing tool and procedure for nanosatellite magnetic actuators, introducing a cost analysis for each kind of solution.

The models and the tools have been maintained fully parametric in order to offer a universal re-scalable instrument for satellite of different dimension class.



# Index

1.Nanosatellite Attitude Control System .....	10
1.1 Magnetorquer .....	11
1.2 Magnetorquer design parameter .....	14
1.2.1 Generated Dipole.....	14
1.2.2 Mass.....	14
1.2.3 Power Consumption .....	15
1.3 Magnetorquer Designing procedure .....	16
2. Fundamentals of Magnetism .....	18
2.1 Magnetic field strength and magnetic flux density.....	18
2.2 Magnetization .....	19
2.3 The demagnetizing factor .....	22
2.4 Diamagnetic Materials.....	23
2.5 Paramagnetic Materials .....	24
2.6 Ferromagnetic Materials.....	25
2.6.1 Hysteresis Cycle .....	25
2.6.2 Magnetic anisotropy .....	27
2.6.3 Soft and hard ferromagnetism .....	28
2.6.4 Temperature influence .....	30
2.6.5 Eddy Current .....	30
3. Embedded coil.....	32
3.1 Description and manufacturing .....	32
3.2 Model.....	33
3.2.1 Magnetic dipole.....	33
3.2.2 Balanced spiral in multilayer magnetorquer.....	39
3.2.3 Magnetic field strength.....	40
3.3 Designing issues .....	44
3.4 Experimental measures on embedded coil .....	48
3.4.1 No Solar cell mounted panel .....	53
3.4.2 Solar cell mounted panel .....	55
3.4.3 Comparison between the two case.....	59
3.4.7 Corrective parameters.....	61
4. Air Core Magnetorquer .....	67

4.1 Description and Manufacturing .....	67
4.2 Model.....	68
4.2 Designing issues .....	68
4.7 Experimental measures on air core magnetorquer.....	76
4.7.1 No Solar Cell mounted Panel .....	78
4.7.2 Solar Cell Mounted Panel.....	80
4.7.3 Comparison between the two case.....	81
4.7.4 Corrective parameters.....	84
5. Torquerod magnetorquer .....	88
5.1 Description and Manufacturing .....	88
5.2 Torquerod Designing issues .....	89
5.2.1 Demagnetization Issues .....	90
5.2.2 Mass.....	93
5.2.3 Control mode .....	94
5.2.4 Choice of the core material.....	95
5.3 Dimensioning equation for torquerod.....	99
5.4 Experimental measures on torquerod prototype .....	116
6. Design of a 3axis torquerod for CubeSat.....	127
7. Magnetorquer preliminary design .....	135
8. Cost Analysis.....	146
9. Conclusion .....	148
Bibliography .....	150



## Table of Figures

Fig. 1 Magnetorquer basic principle of operation [4] .....	12
Fig. 2 Principle of operation of a solenoid without core [6] .....	18
Fig. 3 Magnetization tends to align the magnetic dipole depending to the external applied field [6] .....	21
Fig. 4 Paramagnetic and diamagnetic materials behavior [6] .....	24
Fig. 5 Domains orientation in a ferromagnetic sample [6] .....	26
Fig. 6 Typical hysteresis cycle of ferromagnets [6] .....	27
Fig. 7 Iron and Nickel crystal hysteresis cycle [6] .....	28
Fig. 8 Example of easy and hard magnetizations according to crystallographic orientation [6] .....	28
Fig. 9 Hard and soft ferromagnetic hysteresis cycle [6] .....	29
Fig. 10 Example of commercial embedded coil for CubeSat application [8] .....	32
Fig. 11 Schematic example of square spiral embedded coil surrounded by magnetic field .....	33
Fig. 12 The torque (in yellow) tends to align the normal direction with the magnetic field .....	35
Fig. 13 Schematization of square spiral for embedded coil analysis .....	37
Fig. 14 Comparison between the simplified model and the spiral model .....	38
Fig. 15 Possible scheme of balanced multilayer embedded coil .....	39
Fig. 16 Square spiral scheme for H field analysis .....	40
Fig. 17 Square spiral scheme for H field analysis. Same colored segments give equal contribute .....	42
Fig. 18 Comparison between simplified model and spiral model for the H field estimation .....	44
Fig. 19 Magnetic dipole reduction due to increase of spiral concentration .....	46
Fig. 20 Power consumption for a multilayer embedded coil .....	47
Fig. 21 Estimated mass increase for multilayer embedded coil .....	48
Fig. 22 Helmholtz cage exploited for embedded coil experimental measurements .....	51
Fig. 23 Embedded coil experimental layout .....	51
Fig. 24 Current Profile 1 .....	52
Fig. 25 Current Profile 2 .....	52
Fig. 26 No-solar cells mounted panel layout (photo 1) .....	53
Fig. 27 N-solar cells mounted panel layout (photo 2) .....	53
Fig. 28 Magnetic Flux in z direction for no-solar cells mounted panel .....	54
Fig. 29 Comparison between positive and negative magnetic flux profile .....	55
Fig. 30 Solar cells mounted panel experiment layout .....	56
Fig. 31 No-solar cells mounted panel cage calibration result .....	56
Fig. 32 Solar cells mounted panels cage calibration result .....	57
Fig. 33 Magnetic flux in z direction for solar cells mounted panel .....	58
Fig. 34 Comparison between positive and negative magnetic flux profile for solar cells mounted panel .....	58
Fig. 35 Comparison between magnetic flux for solar cells and No-solar cells mounted panel (Profile 1) .....	59
Fig. 36 Magnetic flux difference between the solar cell case and no solar cells case(Profile 1) .....	60
Fig. 37 Comparison between magnetic flux for solar cells and No-solar cells mounted panel (Profile 2) .....	60
Fig. 38 Magnetic flux difference between the solar cell case and no solar cells case(Profile 2) .....	61
Fig. 39 Evaluated artificial permeability from experimental results .....	62
Fig. 40 Ratio between the artificial permeability in the two case (Solar cells / No-solar cells) .....	63
Fig. 41 Evaluated artificial permeability of the entire panel .....	64

Fig. 42 Expected dipole and adverse dipole evaluation .....	65
Fig. 43 Example of air core magnetorquer [11].....	67
Fig. 44 Magnetic dipole variation depending on wire's diameter.....	70
Fig. 45 Power consumption model.....	71
Fig. 46 Mass model.....	71
Fig. 47 Magnetorquer 1 expected performances.....	72
Fig. 48 Magnetorquer 2 expected performances.....	73
Fig. 49 Magnetorquer 3 expected performances.....	73
Fig. 50 Effective dipole corrective factor.....	75
Fig. 51 Air core magnetorquer prototype exploited for measurements.....	76
Fig. 52 Air core magnetorquer mounted on the panel .....	76
Fig. 53 Air core experimental setup .....	76
Fig. 54 Air core magnetorquer prototype expected performances .....	77
Fig. 55 Current profile 1 (Air Core experiment).....	78
Fig. 56 Current profile 2 (Air Core experiment).....	78
Fig. 57 Magnetic Flux in z direction for profile 1with no solar cells mounted .....	79
Fig. 58 Magnetic flux in z direction for profile 2 with no solar cells mounted.....	80
Fig. 59 Magnetic flux in z direction for profile 1 with solar cells mounted .....	80
Fig. 60 Magnetic flux in z direction for profile 2 with solar cells mounted.. .....	81
Fig. 61 Comparison between solar cell and no solar cells mounted (Profile 1) .....	82
Fig. 62 Magnetic flux difference between the two case (Profile 1) .....	82
Fig. 63 Comparison between solar cell and no solar cells mounted (Profile 2). .....	83
Fig. 64 Magnetic flux difference between the two case (Profile 2) .....	83
Fig. 65 Evaluated permeability for air core experiment (Profile 1) .....	84
Fig. 66 Evaluated permeability for air core experiment (Profile 2) .....	85
Fig. 67 Ratio between the artificial permeability in the two case (Solar cells / No-solar cells) - profile 2.....	86
Fig. 68 Ratio between the artificial permeability in the two case (Solar cells / No-solar cells) - profile 1.....	86
Fig. 69 Example of minor hysteresis cycles [12] .....	91
Fig. 70 Demagnetizing slope [12] .....	92
Fig. 71 Example of apparent demagnetization exploiting minor hysteresis cycle [12].....	93
Fig. 72 Resume table for main ferromagnetic materials [13] .....	96
Fig. 73 Magnifer 7904 characteristic slope [16] .....	98
Fig. 74 Magnifer 7904 permeability variation with respect to frequency [16] .....	98
Fig. 75 Demagnetizing factor dependence on L/r ratio.....	101
Fig. 76 Geometric parameter for different volumes of the core .....	103
Fig. 77 Alloy 79 first magnetization curve [16].....	104
Fig. 78 Magnetic dipole dependence for different core's shape .....	105
Fig. 79 Power consumption dependence for different core's shape .....	106
Fig. 80 Magnetic dipole and power consumption magnitude for different core's shape.....	107
Fig. 81 Mass relation depending on core's shape .....	108
Fig. 82 Example of magnetic flux density for a defined core (10x80mm).....	110
Fig. 83 Example of magnetic flux density for a defined core (7x80mm).....	111
Fig. 84 Minimum wire's diameter to reach saturation for a defined core ( $3.07 \cdot 10^{-6} \text{ mm}^3$ ) .....	112

Fig. 85 Power consumption relation for different wire's diameter (10x80mm) .....	113
Fig. 86 Magnetic dipole relation (10x80mm) .....	113
Fig. 87 Relation between magnetic flux and intrinsic magnetization [12] .....	114
Fig. 88 Ferrite core hysteresis loop reconstruction at 100 KHz.....	118
Fig. 89 Torquerod prototype design (1).....	118
Fig. 90 Torquerod prototype design (2) .....	118
Fig. 91 Realized prototype (1).....	119
Fig. 92 Realized prototype (2).....	119
Fig. 93 Experiment layout scheme .....	121
Fig. 94 Experiment layout.....	122
Fig. 95 Current profile for torquerod experiment.....	122
Fig. 96 Magnetic flux density in x direction; experimental results and mathematical model .....	123
Fig. 97 Evaluated operative region during experiment.....	124
Fig. 98 Remanence of the core (measured in experiment configuration) .....	125
Fig. 99 Evaluated remanence inside the core .....	126
Fig. 100 Air core magnetorquer integration.....	127
Fig. 101 Embedded magnetorquer integration [8] .....	127
Fig. 102 Air core and embedded magnetorquer average encumbrance .....	128
Fig. 103 Designed torquerod integrated in CubeSat structure (1) .....	130
Fig. 104 Designed torquerod integrated in CubeSat structure (2) .....	130
Fig. 105 Optimal wire's diameter evaluation .....	131
Fig. 106 Performances for 0.3 mm wire's diameter .....	132
Fig. 107 Different possible performances for different wire's diameter @3.3V.....	133
Fig. 108 Different possible performances for different wire's diameter @5V.....	133
Fig. 109 Operative range for different designs (850 turns and variable wire's diameter) .....	134
Fig. 110 Magnetorquer optimal design procedure .....	137
Fig. 111 Design 1 AirCore.....	139
Fig. 112 Design 2 AirCore.....	139
Fig. 113 Design 3 AirCore.....	140
Fig. 114 Design 4 AirCore.....	140
Fig. 115 Design 5 AirCore.....	140
Fig. 116 Design 1 EmbeddedCoil .....	142
Fig. 117 Design 2 EmbeddedCoil .....	142
Fig. 118 Design 3 EmbeddedCoil .....	142
Fig. 119 Design 4 EmbeddedCoil .....	143
Fig. 120 Design 5 EmbeddedCoil .....	143

## 1. Nanosatellite Attitude Control System

Satellites for space application are divided in different category according to their mass. It's considered a nanosatellite a satellite whose mass is below 10 Kg, while a microsatellite a satellite has mass which doesn't exceed 50 Kg.

Among the first, one of the most famous is the CubeSat [1]: this kind of nanosatellite has been standardized in 2003 by prof. Jordi Puig Suari with the intent to offer the access to space to University and research institute exploiting a low cost platform. A CubeSat has in fact standard dimensions and size (100x100x100 – 1KG) and the cost for the launch results drastically reduced. Due to its versatility and simplicity, the CubeSat became the most launched satellite during the last years becoming one of the main commercial platforms for space application. Generally, due to its reduced dimensions and mass, CubeSat subsystems are often critical aspects and performances optimization is crucial: the few available power and volume pose many limitations to the use of certain technologies for subsystems.

Among these, most of nano and micro satellites need an appropriate attitude control system (ACS) that permits to the satellite to perform maneuver, fundamental for mission operations in orbit [2] [3].

For example, every satellite with a directional instrument, such as antenna or camera, need to be accurately oriented on target. Although, many satellite need to compensate torque disturbances to perform their task

Therefore, it is clear that ACS is an essential subsystem that must be carefully chosen and evaluated in the design phase of the mission. Furthermore, when the constraints are very stringent it is necessary that such a system is designed in an optimal way in order to avoid waste in terms of mass, volume and power consumption. There are multiple possible choices to design the ACS subsystem, exploiting different technologies and consisting mostly in two different categories: active controls (momentum wheels, magnetic dipole, and propulsion) and passive controls (gravity gradient boom, aerodynamic devices).

Passive control permits to impose the attitude of the satellite without controlling it directly according to the need: they provide stabilization in a defined attitude that can't be changed during mission operation. The advantage of these devices consists in the fact that they do not require power to the satellite but do not offer

any flexibility. An example is a gravity gradient boom that forces the satellite to align with the radial direction of the earth, or permanent magnets that permits to align the satellite continuously in the direction of earth magnetic field.

On the contrary, active controls consist in real controls that permit to decide and change the attitude during on orbit operation according to the need. These kinds of devices request a power supply and control algorithm to work and for that reason their design represents one the most critical aspect of the whole satellite development. Reaction wheels consist of wheels that allow to transfer momentum to the satellite and to control its rotation: these are devices with masses and volumes that are not negligible and therefore very sensitive from a design point of view. Propulsion systems exploit a pressurized propellant that through appropriate nozzles allows even in this case to induce rotations and angular velocities with respect to the center of gravity of the satellite itself. Even in this case, the presence of tanks and pressurized substances poses great limits above all in nanosatellite application.

The last kind of active control is the so called magnetorquer. These kinds of control that will be deeply analyzed in this project are the more compact solution for nano and microsatellites, presenting both advantages and disadvantages with respect to the other devices presented.

## 1.1 Magnetorquer

A magnetorquer or magnetic torquer is a system for attitude control, detumbling and stabilization, based on the interaction between a generated magnetic dipole and earth magnetic field [2]. Through this interaction is generated a torque that is used to control the rotation of the satellite around its gravity center.

A magnetorquer is built using electromagnetic coils. When the coil is subject to a current generates the magnetic dipole control. This is a vector whose intensity is strictly connected to the geometry and the current provided. In the easiest case of a simple wounded coil this is expressed by the following formula:

$$m = nIS$$

Where  $m$  is the magnetic dipole intensity (measured in  $\text{Am}^2$ ),  $S$  is the area of the coil and  $n$  is the number of turns for a simply wounded coil. The direction of the

magnetic dipole is aligned with the axes of the coil and depending to the verse of the current.

The dipole tends to align with the external magnetic field environment or in our case the Earth's magnetic field. Since the dipole is rigidly bounded with the satellite, this is oriented accordingly.

The two parameters that determine the control are the direction of the torque vector and its intensity.

The torque vector is expressed by the formula:

$$\vec{T} = \vec{m} \times \vec{B}$$

Where T is the torque, m is the magnetic dipole, and B is the external magnetic field.

The vector of the torque generated lies always in the plane of the coil and is perpendicular to the vector of the external magnetic field (Fig. 1). Therefore, in order to fully control the orientation and generate a torque vector with arbitrary direction, it is required to exploit 3 magnetorquer placed perpendicular. Nevertheless, in some circumstances could be required to control only one or two degree of freedom, reducing the number of needed magnetorquer and the complexity of the control law.

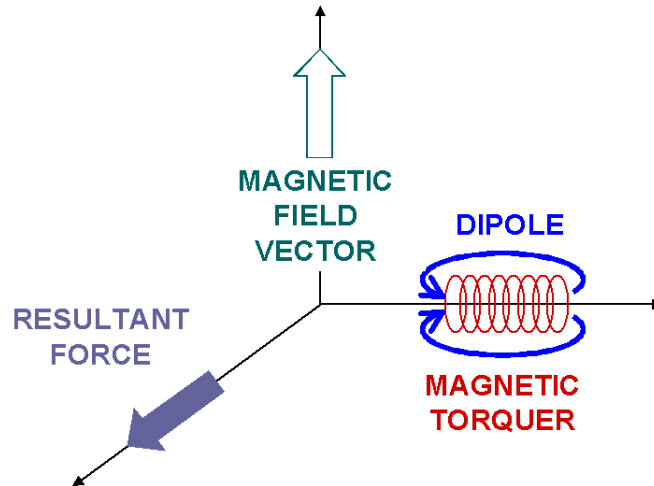


*Fig. 1 Magnetorquer basic principle of operation [4]*

The intensity of the controlling torque depends on the intensity of the dipole, the intensity of the magnetic field and their respective orientation, thus being maximum when the dipole generated and the external magnetic field are perpendicular, then vanish once aligned.

The advantage of this kind of technology is linked to easy construction, high reliability, small mass and small power consumption, making it suitable for nanosatellite application. Considering that for the functionality isn't needed any kind of propellant, they are a resource always potentially usable as long as solar panels can provide a current.

Among disadvantages it appears clear that the functionality of the system strictly depends both on the efficiency of the magnetorquer its self, both on the external magnetic field that, for the earth magnetic field case, decreases moving to higher orbits: it means that in order to have appreciable torque at high altitude it would be required to have really high dipole intensity that means really high current with consequent high power consumption.

Generally the torques provided are very small and not sufficient in case of really accurate and fast orientation, differently than momentum wheels and propulsion.

There are substantially three kind of magnetorquer:

- **Embedded magnetorquer:** This magnetorquer is obtained directly on the PCB design and the wire is substitute by the copper trace of the board. The shape of the coil is a square spiral on a plane.
- **Air Core Magnetorquer:** this magnetorquer consists in a certain number of turns of wire wrapped in wide circles. They are called "air core" because there is no material placed in the interior. Are usually installed in the side panels of the satellites.
- **Torquerod Magnetorquer:** although the principle is the same of the air core magnetorquer, in this case, the winding is made in the form of a solenoid and in the volume contained by the coils is introduced a certain material with magnetic properties which amplifies the effectiveness of the device.

## 1.2 Magnetorquer design parameter

There are several aspects that are to be considered designing a magnetorquer. These issues have to respect the constraints and the requirements of the mission:

- Generated dipole
- Mass
- Power Consumption
- Occupied volume and interference

### 1.2.1 Generated Dipole

This is of course one of the most important features of the magnetorquer because it determines the efficiency of the control torque. The generated dipole cannot be determined arbitrarily, but must be determined in the design phase taking into account the key performance of the mission. Oversize the dipole has a significant impact on the budgets of mass and power available for attitude control subsystem of a satellite. These can be seen in the formula:

$$m = nIS$$

This general formula is exacted for air core magnetorquer, an approximation for embedded coil, and not applicable for torqueroed. A higher requested momentum consists in higher current (consumption increase) or bigger area and turns (increase mass). It's important to evaluate the needed momentum to satisfy mission requirements in order to find the correct compromise.

### 1.2.2 Mass

As already said, both the number of turns and the area of the coil affect the total mass of the magnetorquer.

It can be possible to evaluate the mass of the wounded wire knowing the length and the size of the wire:

$$M = \rho_w L a_w$$



Where  $\rho_w$  is the density of wire's material,  $a_w$  is the area of the cross section  $L$  is the total length.

Increasing the area of the coil would cost in terms of total length and so in terms of total mass.

In general:

$$L = nC$$

Where  $C$  is the length of a single coil and  $n$  the number of turns [5].

$C$  is directly connected to shape of the coil. For a fixed mass and size it would be useful to increase the number of turns reducing wire diameter. On one side this could help to increase the generated dipole, but it would costs in term of power consumption.

Besides that each magnetorquer needs proper support structure: for embedded coil this consists in the PCB substrate while for air core and torquerod there are proper structure with different mass and dimensions.

For torquerod the total mass is affected also by the presence of the metal core that represent the bigger percentage.

### 1.2.3 Power Consumption

The power consumption of the coil is connected to the total resistance of the wire. This is due to two main factors: the resistivity of the wire's material, the cross section of the wire and its total length.

$$R = \sigma_w \frac{L}{a_w}$$

Where  $\sigma_w$  is the resistivity of wire's material and  $R$  the total resistance.

The power consumption can be expressed as

$$P = RI^2$$

Where  $R$  is the resistance,  $I$  is the current across the wire and  $P$  is the power absorbed.

The resistance is function of the temperature of the conductor and tend to decrease with the increase of the temperature. That means that, if the magnetorquer is driven with a constant voltage it's important to perform a thermal analysis expecting some fluctuation on the current across it and in that way the magnetic dipole. In following analysis this aspect won't be taken into account because strictly depend to the operative regime of the device and external condition.

As already said, increasing the current would increase significantly the power consumption, and the same increasing the resistance. Expressing the dependence of the power from the wire dimension it's possibly to put on evidence that the choice of wire diameter directly affects the performance of the device.

$$P = \sigma_w \frac{nC}{a_w} I^2$$

### 1.3 Magnetorquer Designing procedure

As presented, a magnetorquer is characterized by the power consumption, its mass, its dimension and of course the generated dipole. These aspects are strictly connected and it's always necessary to find the best compromise between the minimum performance required and the maximum power and dimensional budget. It's really important to define the main constraints for the system in order to have a starting input for the system optimization. It's not possible to define a universal strategy to obtain the best compromise because each mission or each scenario can be driven by different constraints that could lead to completely different choice.

Generally, for a nanosatellite mission, especially for a CubeSat, one of the starting points is the needed torque: this come from evaluation concerning the requested pointing or despinning time and desaturation efficiency of the system. Through the definition of these specifics it's possible to define the requested magnetic dipole as a key performance parameter.

Concerning the constraints of the system, one of the most important can be the available power dedicated to the system: generally in fact, power budget is one of the most delicate aspects of each nanosatellite mission considering also that batteries are limited in Ampere per hour availability.

To define a designing strategy it's necessary to fix some inputs that permit to generate different solution depending to the variability of the other parameter. The

methodology that will be presented for all kind of magnetorquer will exploit as initial input the dimensions of the system and the nominal voltage supply. This choice seems quite logical since the area of the magnetorquer defined by its dimensions is the parameter that, in proportion, affects less the others maximizing the magnetic dipole that is the reason for which the system is designed. Especially considering the small size of a CubeSat it is not uncommon to be in a situation of forced dimensions for a subsystem, and exploiting the **maximum available dimension is the most obvious solution to achieve the best performances**. The **voltage supply instead is a parameter that is almost standard depending to the class of the satellite (3.3 or 5 V for CubeSat)**, being the most of subsystem designed for standard voltage input and output.

The procedure will be fully parametric in every single variable: this allows to rescale the design for every satellite classes, from 1 to 50 Kg, simply changing the parameters.

To define properly the methodology and make it applicable to every kind of magnetorquer it's necessary to obtain a **mathematical model (equations) for the design for each technology**. To do that, a study of the magnetic properties involved is necessary, especially for the torquerod system. Where possible, the model obtained needs to be compared with real data from experimental results to validate it and to understand eventual unexpected issues.

## 2. Fundamentals of Magnetism

### 2.1 Magnetic field strength and magnetic flux density

As well known, every conductive wire crossed by a current induces in the nearest space a magnetic field. This, depending on the medium in this space determines a magnetic flux density. The magnitude and the direction of the magnetic field, variable in space, depend to the geometry of the structure that carry the current and the current intensity.

Taking in consideration a solenoid as example (Fig. 2), the magnetic field is constant in the inner volume and the strength is expressed by the formula [6]:

$$H = \frac{NI}{l}$$

Where N is the number of turns, I the intensity of the current, and l the length of the solenoid. The unit of the magnetic field H is Ampere per meter (A/m).

The magnetic induction, or magnetic flux density, denoted by B and measured in Tesla, represents the magnitude of the internal field strength within a substance that is subjected to an H field. Both B and H are field vectors, being characterized not only by magnitude, but also by direction in space.

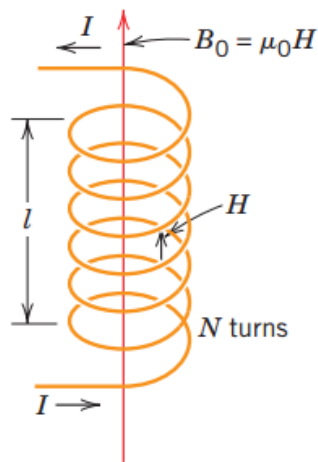


*Fig. 2 Principle of operation of a solenoid without core [6]*

B and H are related according to the law

$$B = \mu H$$

$\mu$  represents the permeability of the medium and it's a property of the specific material through which H passes. Permeability is measured in H/m.

For a solenoid without metal core (assumed in vacuum)

$$B_0 = \mu_0 H$$

Where  $\mu_0$  is a universal constant equal to  $1.257^{10^{-6}}$  H/m.

When we introduce a core bar in the solenoid we substantially change the permeability of the medium.

The resulting Magnetic Flux density change and become

$$B = \mu_0 H + \mu_0 M$$

Where M is called magnetization. The presence of the core subjected to a magnetic field H reinforce the magnetic flux density B. The term  $\mu_0 M$  is a measure of the contribution of the core.

## 2.2 Magnetization

Magnetization can be seen as the **vector field that expresses the density of magnetic dipole moments in a material.**

Magnetic dipole moments at atomic level are due to two different contributes: the first is the orbit of the electron around the nucleus that, being a moving charge, behave like a small current loop. The second contribution is due to electron spin along his axes. This spin magnetic moment can be in "up" direction or "down" direction [6].

In a single atom, the different magnetic moment due to orbital loop and spin may cancel each other's. We call net magnetic moment the sum of all the magnetic moment contribution, spin and orbital, taking into account the eventual moment cancellation.

The net magnetic moment is strictly connected to the filling of atom's shells: for an atom having completely filled electron shells or subshells, when all electrons are considered, there is total cancellation of both

orbital and spin moments.

That's why these kinds of materials composed by these kinds of atoms can't be permanently magnetized.

We can then define different types of magnetism: diamagnetism, paramagnetism, and ferromagnetism:

Diamagnetic materials show a weak magnetization with verse opposite to the external magnetic fields. For that reason these materials are not suitable at all to increase the magnetic dipole thus they weakly reduce it.

Paramagnetism on the contrary is the property of certain material to be weakly magnetized in presence of an external magnetic field in the same direction of it: this kind of magnetization doesn't persist without the external field and completely disappear when the exciting field is removed.

Ferromagnetism is the property of certain material to be strongly magnetized in presence of an external magnetic field and maintain the magnetization even when the external field is removed. They generally follow a hysteresis cycle, and for that reason it's not possible to find a linear and constant law to determine the intensity of the phenomena.

For the application studied it appears obvious that diamagnetism isn't the right solution, while paramagnetic and ferromagnetic materials are the possible solution that could be used to improve the efficiency of a magnetorquer, both with advantages and disadvantages.

As already said, magnetization is the vector that represents the density of magnetic dipoles moment in a material, both permanent and induced (Fig. 3).

An easy definition of magnetization is expressed by the formula

$$M = \frac{N}{V}m$$

Where M represents magnetization, m is the vector that defines the magnetic moment, V represents volume and N is the number of magnetic moments in the sample. The quantity N/V is usually written as n, the number density of magnetic moments. The M-field is measured in amperes per meter (A/m) in SI units.

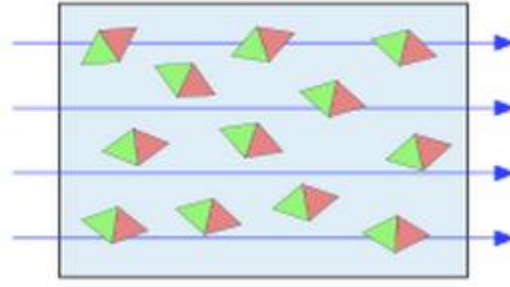


*Fig. 3 Magnetization tends to align the magnetic dipole depending to the external applied field [6]*

Another interesting expression for  $M$  is given by the following formula

$$M = \frac{\Delta m}{\Delta \tau}$$

$\Delta m$  over  $\Delta \tau$  represents the variation of momentum over volume. In this expression  $M$  represent the density of dipole in a certain volume  $\tau$ .

When  $M$  is constant in the medium we call it uniform magnetization.

We can understand the formula thinking about a cylinder shared in many slice, each with height  $dz$ . Each slice is shared in equal portion with area  $da$ . Then each prism with volume  $\Delta \tau$  has a dipole oriented according to  $M$  that is the total magnetization. So we can consider:

$$\Delta m = M \Delta \tau$$

Integrating over all the volume we can obtain the total dipole of the medium. In fact,  $M$  is measured in  $A/m$  that multiplied for a volume gives  $Am^2$  that is a magnetic dipole.

This relation is important because, once defined a magnetization  $M$  (depending on the material properties and external field) it's possible to determine the induced dipole of the medium.

A useful relation between  $M$  and  $H$  exists:

$$M = \chi_m H$$

Where  $\chi_m$  is the volume magnetic subscptibility, a dimensionless quantity.

Taking in consideration the formula:

$$B = \mu_0 H + \mu_0 M$$

We can rewrite

$$B = \mu_0 (1 + \chi_m) H$$

Where

$$\mu_0 (1 + \chi_m) = \mu$$

$$(1 + \chi_m) = \mu_r = \frac{\mu}{\mu_0}$$

$\mu_r$  is called relative permeability of the material;  $\mu$  is called magnetic permeability of the material.

The relation is correct for diamagnetic and paramagnetic materials, while for ferromagnetism it's not possible to find a linear relation because of the magnetic hysteresis phenomena.

## 2.3 The demagnetizing factor

The magnetic behavior of samples does not only depend on its intrinsic properties but also on its shape and dimensions. The surface of a magnetic sample and the volume magnetic pole density generate an  $H_d$  field that tends to reduce the magnetization. The  $H_d$  field is called stray field [7].

When an external magnetic field is applied, the total magnetic field in a certain point is equal to

$$H = H_a + H_d$$

Where  $H_a$  is the magnetic field applied and  $H_d$  is the stray field.



The H field is reduced due to the presence of the core of a quantity that is related to the magnetization.

The demagnetizing factor is the parameter that relates the stray field to the shape and the dimension of the ferromagnetic core.

The average volume magnetization of a sample is related to the demagnetizing field  $H_d$

$$H_d = -N_d M_{vol}$$

Where  $N_d$  is the demagnetizing tensor. For some samples in which the  $H_a$  field is applied according to the principal direction of the samples the two fields can be assumed parallel and the tensor is reduced to a scalar factor called in fact demagnetizing factor [7].

The effect could be understood in a simplified way taking in consideration the magnetic flux density B of the core:

$$B = \mu H_a$$

Rewriting B

$$\mu H_a = \mu_0 H + \mu_0 M$$

Where H is the H field induced with the presence of the core

$$\mu_0 H = \mu H_a - \mu_0 M$$

The core reduces in a certain way the magnetic field intensity depending on the core magnetization and the demagnetizing factor that becomes really important to relate the H field to the dimension and the shape of the core.

## 2.4 Diamagnetic Materials

Diamagnetism is a weak form of magnetism nonpermanent that persists only while an external field is being applied. The external magnetic field induces a magnetic moment that is really small, and in a direction opposite to that of the exciting field

(Fig. 4). The relative permeability is less than unity, and the magnetic susceptibility is of course negative (the magnetization reduces the magnetic flux density with respect to the vacuum). The volume susceptibility for diamagnetic solid materials is in the order of  $10^{-5}$ .

## 2.5 Paramagnetic Materials

Paramagnetic materials are those materials that present a really weak magnetization that increase the magnetic flux density (Fig. 4). These are generally characterized by a low susceptibility value with respect to ferromagnetic materials and the magnetic behavior disappears when the external  $H$  field is removed.

The  $B$  versus  $H$  slope of paramagnetic material is a line whose angular coefficient is related to the relative permeability.

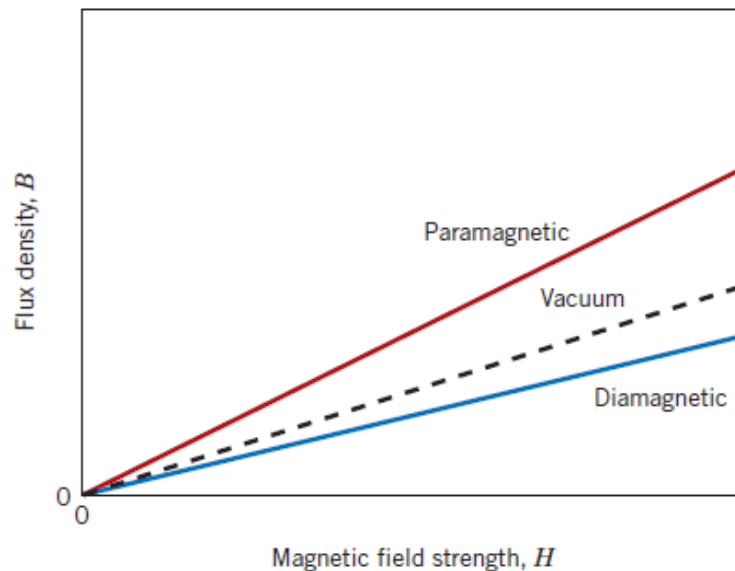


*Fig. 4 Paramagnetic and diamagnetic materials behavior [6]*

Typical values of some paramagnetic materials are presented below in Tab. 1. As it's possible to see the general value of susceptibility are really low.

	Susceptibility $\chi_m$	Density [ $\text{kg/m}^3$ ]
Aluminum	$2.07 \times 10^{-5}$	2700
Chromium	$3.13 \times 10^{-4}$	7140
Chromium Chloride	$1.51 \times 10^{-3}$	2870
Manganese Sulfate	$3.70 \times 10^{-3}$	3250

Molybdenum	$1.19 \times 10^{-4}$	10280
Sodium	$8.48 \times 10^{-6}$	968
Titanium	$1.81 \times 10^{-4}$	4507
Zirconium	$1.09 \times 10^{-4}$	6511

*Tab. 1 Typical paramagnetic materials properties [6]*

## 2.6 Ferromagnetic Materials

Ferromagnetic materials generally present stronger magnetization with respect to paramagnetic materials, and this persists even when the external field is removed. Their magnetic susceptibility could reach values around  $10^6$ .

The permanent magnetic moment derives from the atomic magnetic moments due to the structure of the atom that lead to uncanceled electron spins. Moreover interactions cause net spin magnetic moments of adjacent atoms to align with one another, even in the absence of an external field. When all the magnetic dipole are mutually aligned with the magnetic field there is no more margin for the alignment possible and then the saturation magnetization is reached. It exists therefore a saturation flux density  $B_s$ .

The saturation magnetization is equal to the product of the net magnetic moment for each atom and the number of atoms present [6].

$$M_s = n_b N \mu_b$$

Where  $\mu_b$  is the magnitude of Bohr magnetons,  $N$  is the number of atoms per cubic meter and  $n_b$  is the number of bohr magnetons per atom.

### 2.6.1 Hysteresis Cycle

A ferromagnetic material is composed by many small region characterized by the mutual alignment of all the magnetic dipole contained. These regions are called domains.

Each sample is composed of many adjacent domains, each one with its own direction of magnetization, and separated by domain boundaries or walls. Here the direction of magnetization gradually changes to the direction of the adjacent domains (Fig. 5).

The total magnetization of a solid is the sum of all the magnetization of its domain with each contribution that depends to the volume fraction of the domain. In general, for an unmagnetized sample, the direction of the magnetization of the domains is random thus the sum lead to a total magnetization equal to zero.

A ferromagnetic material starts to be magnetized when an H field is applied; Increasing the H field it's increased also the magnetic flux density in the material, starting slowly for low level of H and then growing faster. At a certain level of the applied external field, the magnetic flux gets independent of H because the saturation magnetization occurs and therefore the saturation of the magnetic flux density. The phenomena inside the material consist in a change of the domains size and structure due to the alignment of the dipole and the movement of domain boundary. The typical relation between H and B is presented below.

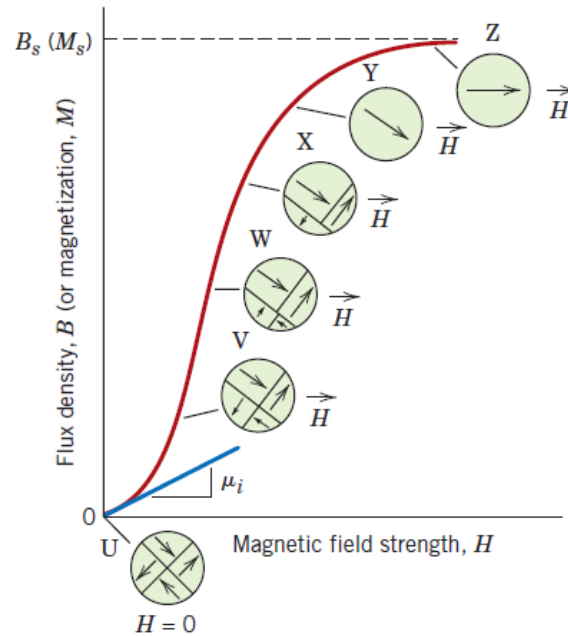


*Fig. 5 Domains orientation in a ferromagnetic sample [6]*

The variation of the B field with respect to the variation of the H field doesn't follow a linear law, that's why it's not possible to define a coefficient to express the relation between H and B as for  $\mu$  in paramagnetic materials. Normally is defined the initial permeability  $\mu_i$  for  $H=0$ .

When the saturation occurs we can assume the specimen as a single domain oriented according to the H field. Once the H field start to decrease the B field

doesn't follow the same slope of its growth but it starts a hysteresis cycle (Fig. 6). When  $H$  returns to zero the specimen presents a residual magnetic flux that is called remanence. This is the residual magnetization of ferromagnetic materials. To reduce the  $B$  field to zero it's necessary to apply a reverse  $H$  field whose intensity  $H_c$  is called coercivity. At  $H = -H_c$ ,  $B$  is equal to 0. Increasing the reversal  $H$  field it's possible to reach saturation in the opposite direction obtaining in that way the same hysteresis cycle for negative value of  $B$ , reaching so a negative residual magnetization  $-B_r$  and a positive coercivity  $H_c$ .

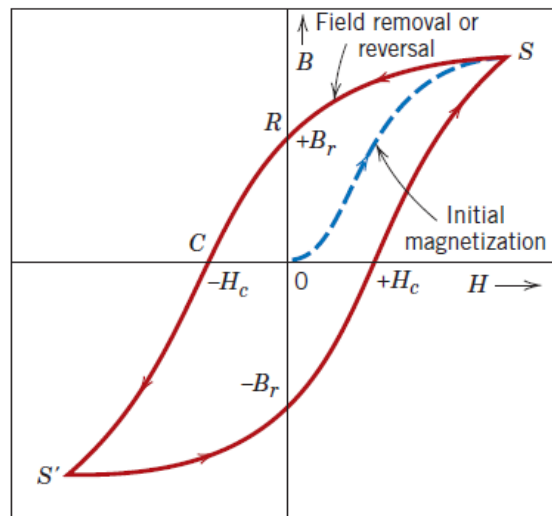


*Fig. 6 Typical hysteresis cycle of ferromagnets [6]*

One of the possibilities to demagnetize a sample consists in applying different cycle of  $H$  field alternating the direction and reducing its amplitude. In that way it's possible to create minor hysteresis cycles that collapse to the condition of  $B=H=0$  (or closer).

The cycle changes also with the frequency of the exciting  $H$  field: the effect is a reduction of the slope and increase of the hysteresis area.

In general the permeability of a ferromagnetic material decreases with the increase of the frequency depending of the kind of ferromagnets.

## 2.6.2 Magnetic anisotropy

The hysteresis cycle can vary depending on the chemical composition of the material and the crystal composition and orientation in its structure.

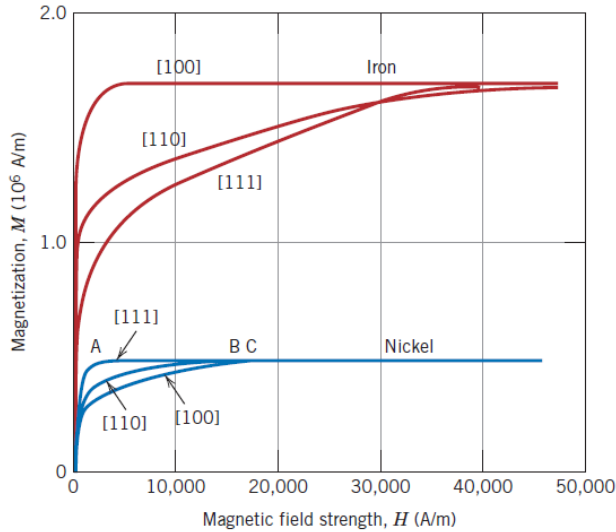


Fig. 7 Iron and Nickel crystal hysteresis cycle [6]

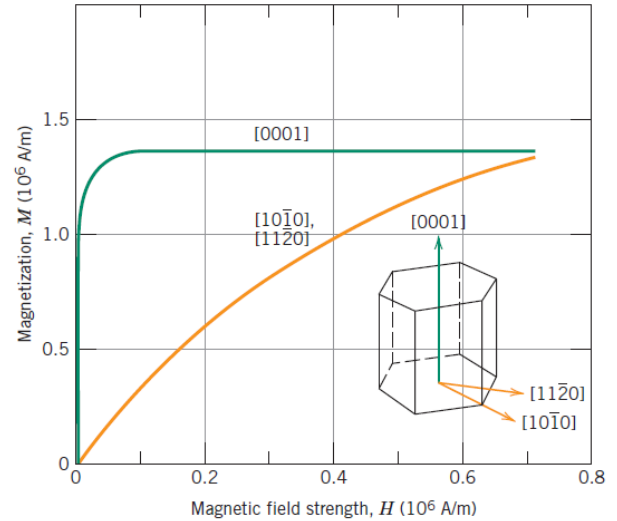


Fig. 8 Example of easy and hard magnetizations according to crystallographic orientation [6]

In the image above is presented the different hysteresis cycle for a single crystal of iron (red) and nickel (blue) (Fig. 7). The slope presents different shape depending to the different crystallographic orientation of the external magnetic field. Each direction is represented by the sequence of number [111], [110], [100].

The behavior is an example of magnetic anisotropy: the slope changes according to the crystal structure of the sample, determining directions of magnetization more or less favorable (Fig. 8).

Observing the magnetization envelope for a crystal cobalt as example is possible to define two kind of behavior according with the direction of the magnetization: the green slope represents the direction of "easy magnetization" where it's possible to obtain the saturation with lower value of H field applied, while the yellow slope represents the "hard direction" of magnetization where the saturation is harder to achieve and higher intensity of the H field is required.

### 2.6.3 Soft and hard ferromagnetism

Depending on the material composition it's possible to observe different shapes for the B-versus-H hysteresis cycle. In general ferromagnetic materials are divided in "soft ferromagnetic" and "hard ferromagnetic". The difference is represented by the typical area of the hysteresis cycle that can be narrow and thin (soft ferromagnetic)

or larger and wide (hard ferromagnetic) as possible to observe in Fig. 9. The area has a practical importance because it represents a magnetic energy loss per unit volume of material per magnetization–demagnetization cycle [6].

The difference in the hysteresis cycle can be seen in the graph below:

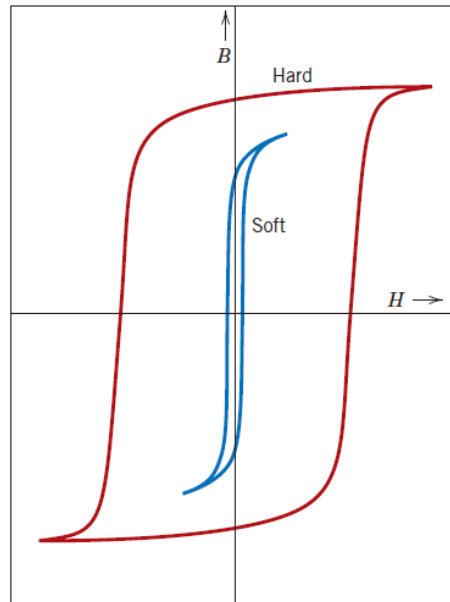


*Fig. 9 Hard and soft ferromagnetic hysteresis cycle [6]*

The soft ferromagnetic material area characterized by a hysteresis cycle thin that consists in low energy loss. The initial permeability of these materials is generally high and the saturation occurs for low values of the applied field. The important features of these kind of material is also the low value of coercivity  $H_c$  that permit to bring the B field to zero with a low reverse magnetic field. The shape of the hysteresis cycle makes this material suitable for application in which it's necessary to achieve easy magnetization-demagnetization exploiting a low applied field that in the case of torquerod consists in low power consumption.

The saturation field is function only of the composition of the material while the susceptibility and coercivity is linked also to the structure of the crystals. To obtain low values of coercivity it's necessary to achieve the easy movement of domains boundaries: this can be obtained minimizing the presence of imperfection or voids in material's structure.

Commercially magnetically soft materials are made using alloys of nickel and iron with different composition. These products called Permalloy, Hymu and Mumetal.

They typically have coercivity values in the order of less than 10 to 40 Am<sup>-1</sup> and typical value of saturation flux density in the order of 1 T. The main parameter, often used as a figure of merit for soft magnetic materials, is the relative permeability, which is a measure of how readily the material responds to the applied magnetic field.

#### 2.6.4 Temperature influence

The temperature influences the behavior of a ferromagnetic material: increasing the temperature the vibration energy of the atoms increases and in that way the ordered and the alignment of the dipole can be disrupted.

Over a certain temperature called Curie Temperature a ferromagnetic material behaves as a paramagnetic following the curie law where the magnetization decreases with the increase of the temperature.

$$M = C \frac{B}{T}$$

Where T is the absolute temperature in Kelvin, C is the curie constant and B the magnetic flux density.

In general this problem doesn't occur for space application because the lowest curie temperature for a soft ferromagnetic material is in the order of 570 K (295°). Some special materials are designed to have a curie temperature close to ambient temperature for specific application.

On the contrary this temperature represents the correct way to demagnetize a ferromagnetic core but as obvious is not applicable for designed purpose.

#### 2.6.5 Eddy Current

Another important property to be considered for soft magnetic materials is electrical resistivity. In addition to the hysteresis energy losses, there could be further losses due to electrical currents induced in the sample by a time-varying magnetic field in magnitude and direction. These currents are called eddy currents. To reduce this effect it is important to increase the resistivity of the material that tends to reduce the formation of this current: in general iron-silicon and iron-



nickel alloys present good properties from this point of view. The ceramic ferrites are also used for applications in which low losses are requested being intrinsically electrical insulators.

This issue is strictly related to the operation of the core at high frequency depending to the variation in time of the magnetic field: for torquerod application in general the eventual time variation doesn't create substantial problems in these terms.

### 3. Embedded coil

#### 3.1 Description and manufacturing

Embedded coil consists in a magnetorquer where the coil winding is obtained with a copper trace in the design of the side PCB for solar panels (Fig. 10). Generally this kind of magnetorquer have the advantage of the low volume occupied being integrated in a thick board while there is a limit in the number of turns obtainable. The low resistance of the copper trace causes high current for a defined applied voltage and obtained dipole, thus this kind of magnetorquer are characterized by high power consumption.

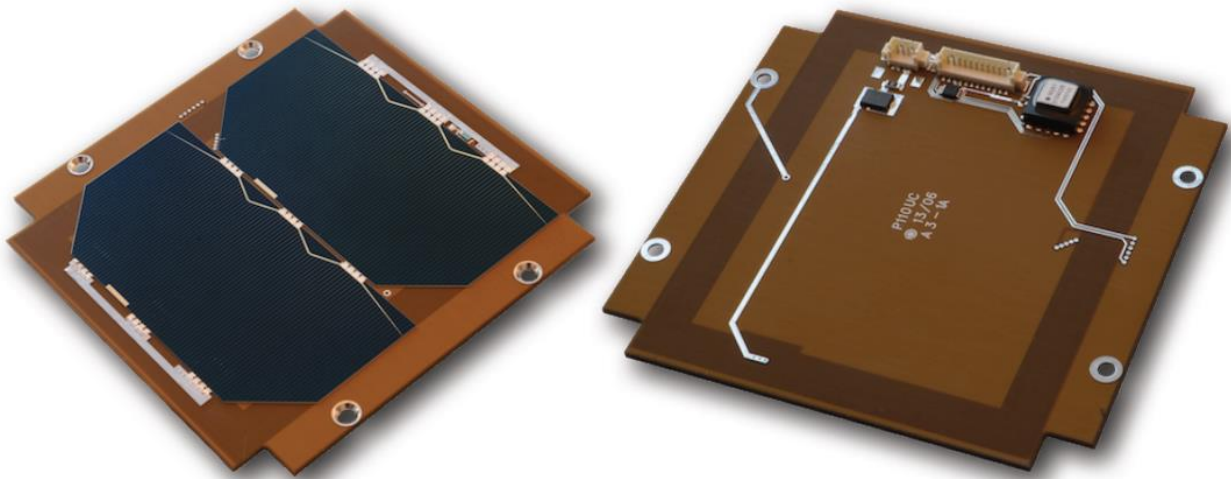


*Fig. 10 Example of commercial embedded coil for CubeSat application [8]*

Being part of a more complex electronic board it's always necessary to consider the presence of electronic components and traces that can't be interrupted by the coil: that's why normally, the inner region of the board needs a certain free area to setup the main electronic circuit causing limit to the coil design. Being embedded in an electronic board manufactured by a machine the precision of the winding is higher and more ordered then the one of an air core that in general can be made also manually. Another advantage is the possibility to exploit the technology of PCB and realize a multilayer magnetorquer in a really small volume: this possibility is fundamental because it will be shown that it's the only solution to reduce the power consumption of this device.

### 3.2 Model

In general, for a wounded coil the magnetic dipole is defined:

$$m = nIS$$

The expression of the magnetic dipole is exact in the case of a wounded wire where the average area of the winding it's really close to the nominal one and the number of turns are well defined. This is the case of an air core torquer in which the characteristic dimensions are order of magnitude bigger than the thickness.

On the contrary in a spiral plane wounded coil there is no specific distinction between every single turn because doesn't not exist a complete turn with closed area.

#### 3.2.1 Magnetic dipole

To study the magnetic dipole of a spiral coil it's easy to refer to a simple model considering spiral square coil in a magnetic field (Fig. 11). The problem is simplified assuming the B field and n normal to coil's surface on the same plane ( $B_n$ ) that is perpendicular to the coil plane.

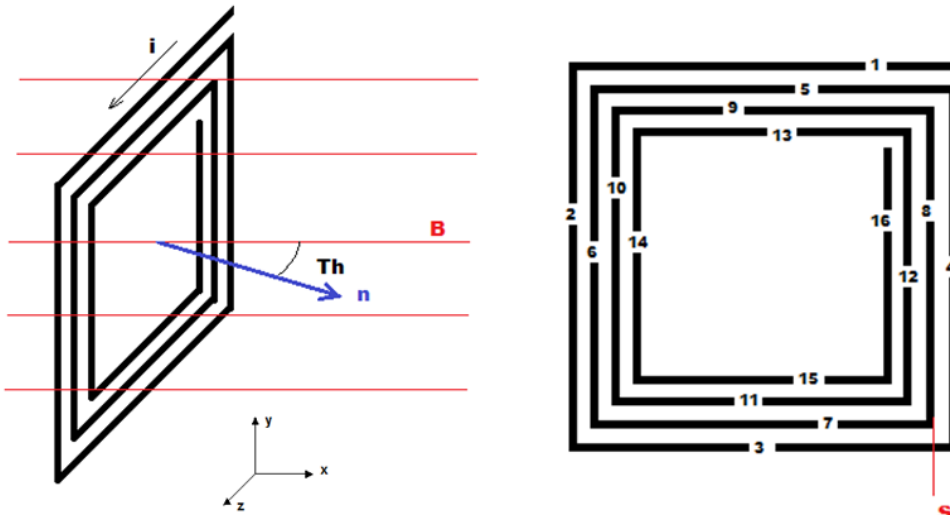


Fig. 11 Schematic example of square spiral embedded coil surrounded by magnetic field

The Lorentz force on a single segment of wire is equal to:

$$F = i\vec{dl} \times \vec{B}$$

The analysis can be separated in 2 different part, firsts the segment parallel to the plane XZ (1,3,5,7,9,11,13,15) in y direction and then the segments perpendicular to the plane XZ (2,4,6,8,10,12,14,16) in z direction (Fig. 11).

### **Z direction:**

The strength of each part of the coil parallel to the plane  $B_n$  gives a contribution that is alternately opposite in z direction. Part 1-5-9-13 would give a contribution that is in positive direction, while 3-7-11-15 will give a contribution in negative direction. Due to the fact that each piece is shorter than the previous one of a factor called s (wire diameter and space between two turns), the force at every turn will not be balanced by the following segment.

$$\begin{aligned} F_1 &= ilB\sin(90 + \theta) \\ F_3 &= -ilB\sin(90 + \theta) \\ F_5 &= i(l - s)B\sin(90 + \theta) \\ F_7 &= -i(l - 2s)B\sin(90 + \theta) \\ F_9 &= i(l - 3s)B\sin(90 + \theta) \\ F_{11} &= -i(l - 4s)B\sin(90 + \theta) \\ F_{13} &= i(l - 5s)B\sin(90 + \theta) \\ F_{15} &= -i(l - 6s)B\sin(90 + \theta) \end{aligned}$$

The sum of this contribution will provide a resultant force in positive direction of y equal to:

$$F_R = 3s iB\sin(90 + \theta)$$

### **Y direction:**

Repeating the same procedures for the vertical segment in z direction (2,4,6,8,10,12,14,16) it's possible to obtain the following forces in XZ plane:

$$\begin{aligned}
F_2 &= ilB \\
F_4 &= -i(l - s)B \\
F_6 &= i(l - 2s)B \\
F_8 &= -i(l - 3s)B \\
F_{10} &= i(l - 4s)B \\
F_{12} &= -i(l - 5s)B \\
F_{14} &= i(l - 6s)B \\
F_{16} &= -i(l - 7s)B
\end{aligned}$$

Where the direction is alternating every time as the previous case.

In this case each segment will provide a torque to the coil that tends to align the normal direction  $\mathbf{n}$  with the direction of the magnetic field  $\mathbf{B}$  (Fig. 12).

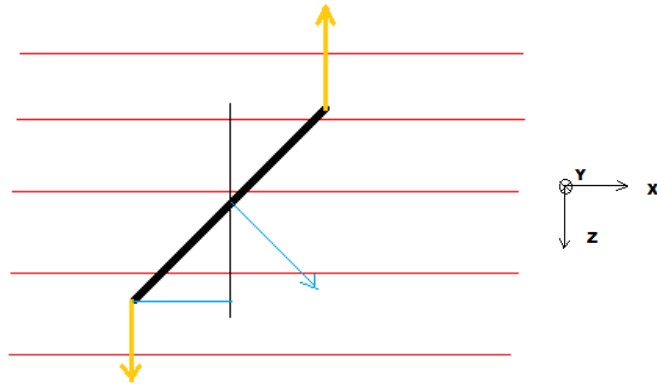


*Fig. 12 The torque (in yellow) tends to align the normal direction with the magnetic field*

The arm of each force can be evaluated considering each segment and then calculate the torque. All the torques agree with the same sign.

$$\begin{aligned}
T_2 &= F_2 \frac{l}{2} \sin(\theta) \\
T_4 &= F_4 \frac{l}{2} \sin(\theta) \\
T_6 &= F_6 \left( \frac{l}{2} - s \right) \sin(\theta) \\
T_8 &= F_8 \left( \frac{l}{2} - s \right) \sin(\theta)
\end{aligned}$$

$$T_{10} = F_{10} \left( \frac{l}{2} - 2s \right) \sin(\theta)$$

$$T_{12} = F_{12} \left( \frac{l}{2} - 2s \right) \sin(\theta)$$

$$T_{14} = F_{14} \left( \frac{l}{2} - 3s \right) \sin(\theta)$$

$$T_{16} = F_{16} \left( \frac{l}{2} - 3s \right) \sin(\theta)$$

Summing the torque with the same arm

$$T_{2,4} = \frac{l}{2} \sin(\theta) [(2il - is)B]$$

$$T_{6,8} = \left( \frac{l}{2} - s \right) \sin(\theta) [(2il - 5is)B]$$

$$T_{10,12} = \left( \frac{l}{2} - 2s \right) \sin(\theta) [(2il - 9is)B]$$

$$T_{14,18} = \left( \frac{l}{2} - 3s \right) \sin(\theta) [(2il - 13is)B]$$

The total torque can be written as series

$$T = \sum_{j=0}^3 [2il - (4j + 1) is] \left( \frac{l}{2} - js \right) B \sin(\theta)$$

Taking out the constant parameter from the series:

$$T = i B \sin(\theta) \sum_{j=0}^3 [2l - (4j + 1) s] \left( \frac{l}{2} - js \right)$$

Where it clearly appear the vector product:

$$T = \left[ i \sum_{j=0}^3 [2l - (4j + 1) s] \left( \frac{l}{2} - js \right) \right] \times \vec{B}$$

Remembering the expression of the torque as cross product between  $\vec{m}$  and  $\vec{B}$

$$\vec{T} = \vec{m} \times \vec{B}$$

In this expression the magnetic dipole is equal to

$$\vec{m} = i \sum_{j=0}^{n-1} [2l - (4j + 1)s] \left( \frac{l}{2} - js \right) \hat{n}$$

The series substitutes the term  $nA$  that is not evaluable for a spiral because the number of turns and the area of each loop is indefinable. A solution could be to use a simplified model in which it is assumed as Area the average area between the inner loop and the outer loop and as number of turns the number obtained counting the tracks from the first going to the inner (Fig. 13).

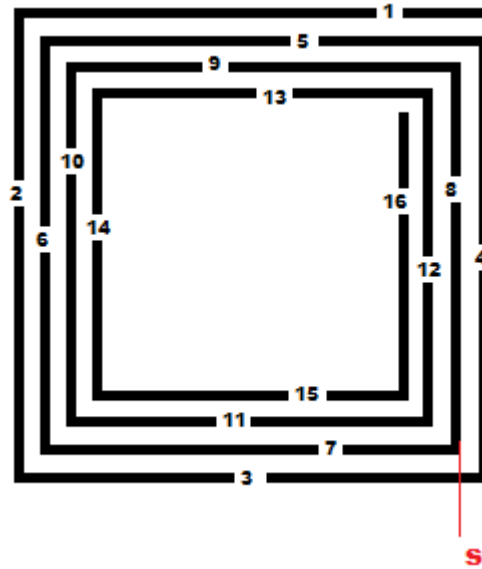


*Fig. 13 Schematization of square spiral for embedded coil analysis*

In the example the number of turns can be assumed equal to 4.

The difference in the results obtained with the two method gives the magnitude of the mistakes committed evaluating the magnetic dipole of the spiral coil with the simplified model (Fig. 14).

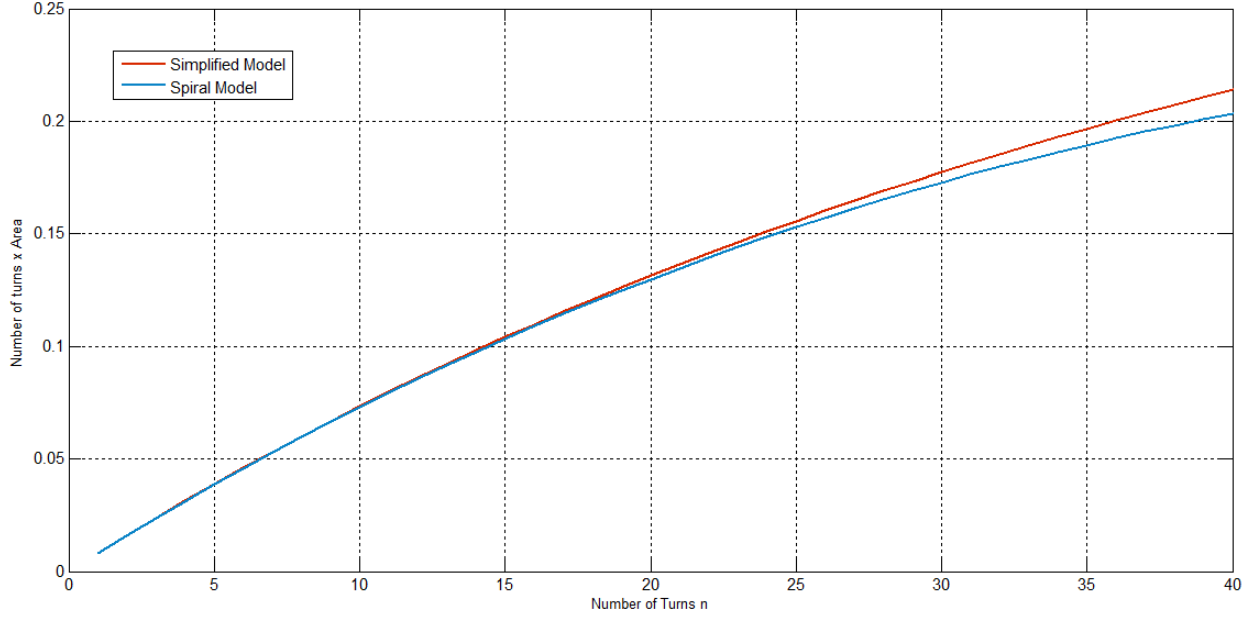


Fig. 14 Comparison between the simplified model and the spiral model

Assuming  $l=0.08$  m and  $s=0.0005$  the result show that for small number of turns the two model are pretty equivalent, while with the increase of the number of turns the overestimation made with the simplify model get more consistent. This is due to the fact that assuming a closed area for each loop it's an overestimation considering that no one loop is actually closed but is connected with the further. Increasing the number of turns increase also the error committed that could lead to a consecutive overestimation of the dipole moment.

The presence of a residual force parallel to the plane of the coil in up direction could consists in an attitude disturbance for the satellite

$$F_{R1} = 3s iB \sin(90 + \theta)$$

$$F_{R2} = nsiB$$



### 3.2.2 Balanced spiral in multilayer magnetorquer

Even if these residual forces are really low, these would tend to misalign the versor  $n$  with respect to the direction of  $B$ . But when this happens an arm for the torque would be created tending to realign  $n$  with  $B$ .

To compensate the residual force  $F_{R1}$  should be enough to reduce the starting segment of quantity equal to  $3s$  that represent the total amount not balanced (Fig. 11).

Would be therefore not possible to compensate at the same time also  $F_{R2}$ . The solution to completely balance the magnetorquer could anyway to rotate the spiral in a multilayer embedded coil. Exploiting an even number of layer and alternating the position is possible to compensate the residual forces in pairs of two (Fig. 15).

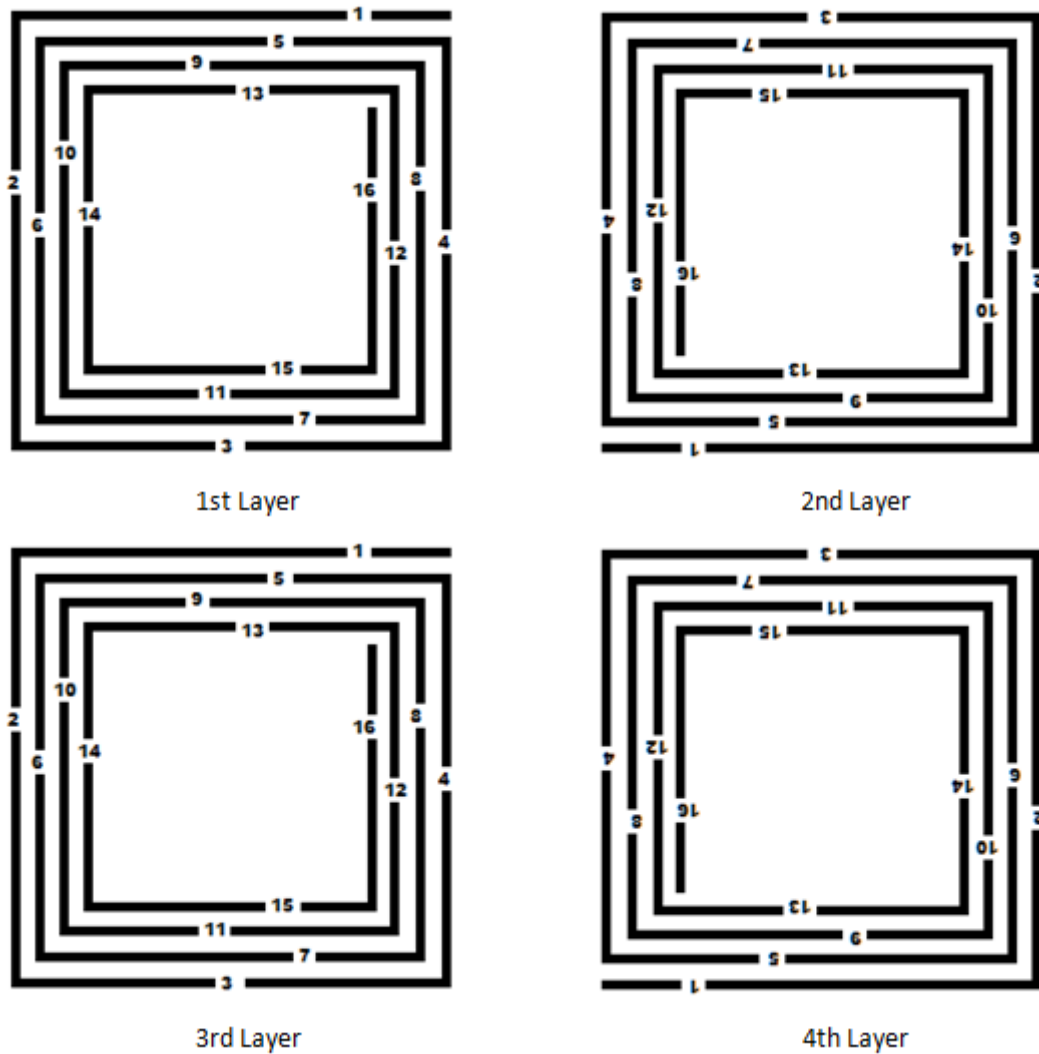


*Fig. 15 Possible scheme of balanced multilayer embedded coil*

### 3.2.3 Magnetic field strength

The magnetic field strength in the center of the spiral can be modeled to perform comparison with experimental results. The procedure is analogue to the one used to define the magnetic moment, exploiting the Biot Savart law for a wire crossed by a current  $I$ .

$$dB_{1.1} = \frac{\mu_0 I}{4\pi} \int_{-l_{1.1}}^0 \frac{\vec{dl} \times \vec{r}}{r^3}$$

Taking in consideration the balanced spiral model each segment can be separated in two parts and the integral can be solved for each of these (Fig. 16).

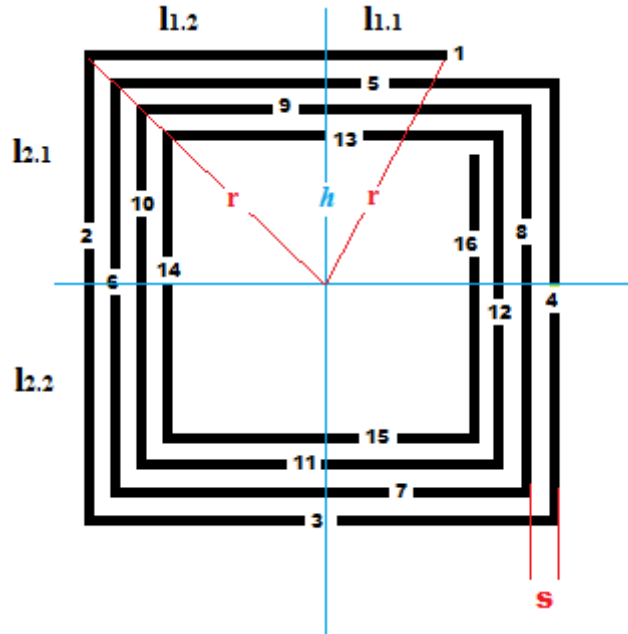


Fig. 16 Square spiral scheme for  $H$  field analysis

The reason of the separation is to consider that at every spiral concentration the second half of the segment is reduced. We consider  $dB_{1.1}$  for the first half and  $dB_{1.2}$  for the second half.

$$dB_{1.1} = \frac{\mu_0 I}{4\pi} \int_{-l_{1.1}}^0 \frac{\vec{dl} \times \vec{r}}{r^3}$$

$$dB_{1.2} = \frac{\mu_0 I}{4\pi} \int_0^{l_{1.2}} \frac{\vec{dl} \times \vec{r}}{r^3}$$

Where 11.1 is the first half of 11 and 11.2 is the second half and so for the other segment.

Defining the relation for r and x:

$$h^2 + x^2 = r^2(x)$$

$$r(x) = \frac{h}{\sin \vartheta}$$

$$dB_{1.1} = \frac{\mu_0 I}{4\pi} \int_{-l_{1.1}}^0 \frac{h}{(x^2 + h^2)^{\frac{3}{2}}} dx$$

Solving the integral

$$B_{1.1} = \frac{\mu_0 I}{4\pi} \left| \frac{x}{h\sqrt{x^2 + h^2}} \right|_{-l_{1.1}}^0$$

Where h depends on the turns considered. Normally is possible to observe that 6 segment lead to the same results for every turns while the first and the last are different because of the spiral structure (Fig. 17).



$$B_{n1} = \frac{\mu_0 I}{4\pi} \frac{1}{\sqrt{2}l^2}$$

Remembering the relation between H and B

$$B = \mu_0 H$$

It's possible to obtain the intensity of the magnetic field H simply eliminating the permeability from the previous expression.

The commonly used simplified model for a square spiral can be evaluated to define the mistakes committed in evaluating the H field with that approximation.

In case of a single square coil:

$$B = \frac{2\sqrt{2} \mu_0 I}{L\pi}$$

Simplifying the spiral with concentric square coils:

$$B = n \frac{2\sqrt{2} \mu_0 I}{L_m \pi}$$

Where  $L_m$  is the medium side dimension between the outer and the inner turn.

As for the magnetic moment, the two models differ more increasing the number of turns (Fig. 18).

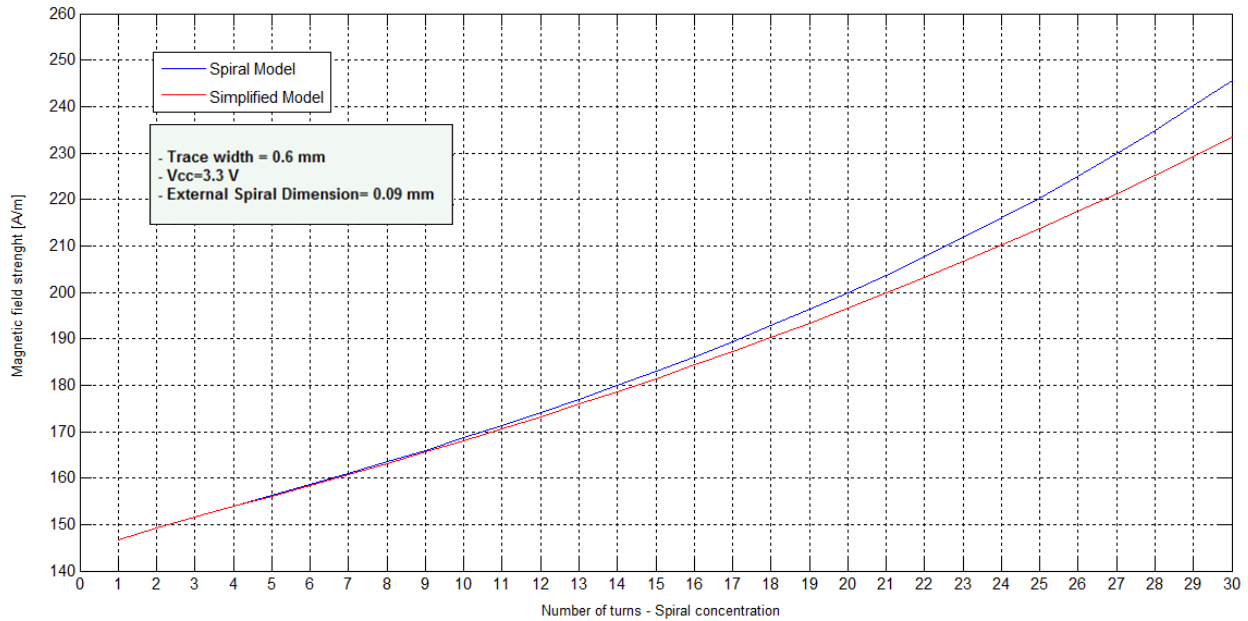


Fig. 18 Comparison between simplified model and spiral model for the  $H$  field estimation

### 3.3 Designing issues

The modelled dipole permits to evaluate the better choice for the designing procedure of the embedded coil. In particular the parameter in which it's possible to operate the most are the copper trace width, the spiral concentration (that somehow represents the number of turns) and the number of layer.

As presented, the procedures will take in consideration the characteristic dimension as input parameter. In case of embedded coil this is absolutely logical solution considering that there would be no reason not to exploit at all the side surface of the satellite with the whole board. The number of layer can be used to determine the thickness of the board thinking a standard value for the insulation layer and the presence of top, bottom and ground layer.

#### Inputs:

- Voltage supply
- Dimension

The copper cross sectional area influences the current reducing the resistance of the whole circuit. In general the thickness of the trace is a quite a standard value for a PCB that is 0.035 mm. However if necessary it can be possible to change also this parameter in the model to observe different results.

The parameter on which it's easy to act is the width of the trace during the designing phase. Several issues limit the possible value: thinner trace consists for a defined current to higher temperature increase of the circuit. Assuming a peak current no bigger than 1.5 A in the circuit and a temperature increase limited to 70° C for the circuit, the minimum value for the trace's width is set as 0.4 mm. In this case a nominal current under the level of 1.5 A will not over heat the board over the level of 70° C.

The power consumption can be evaluated calculating the length of the copper trace and the thickness of the layer to evaluate the total resistance of the coil.

Assuming a defined voltage supply, the power consumption would decrease increasing the number of turns and in that way the total resistance of the trace. This consists in an increase of the trace length and concentration of the spiral, affecting the dipole in two opposite ways: the increase in the resistance reduces the current intensity but on the other side the product Area-number of turns is increased. The total effect would depend on the relation between the increase of Area-Turn product and the decrease of the current. Being the second linear with the number of turns and the first with a logarithmic growth, the general observed effect is a decrease of the dipole. This issue it's really important to understand that there is no advantage to densify the spiral on a layer to increase the dipole strength.

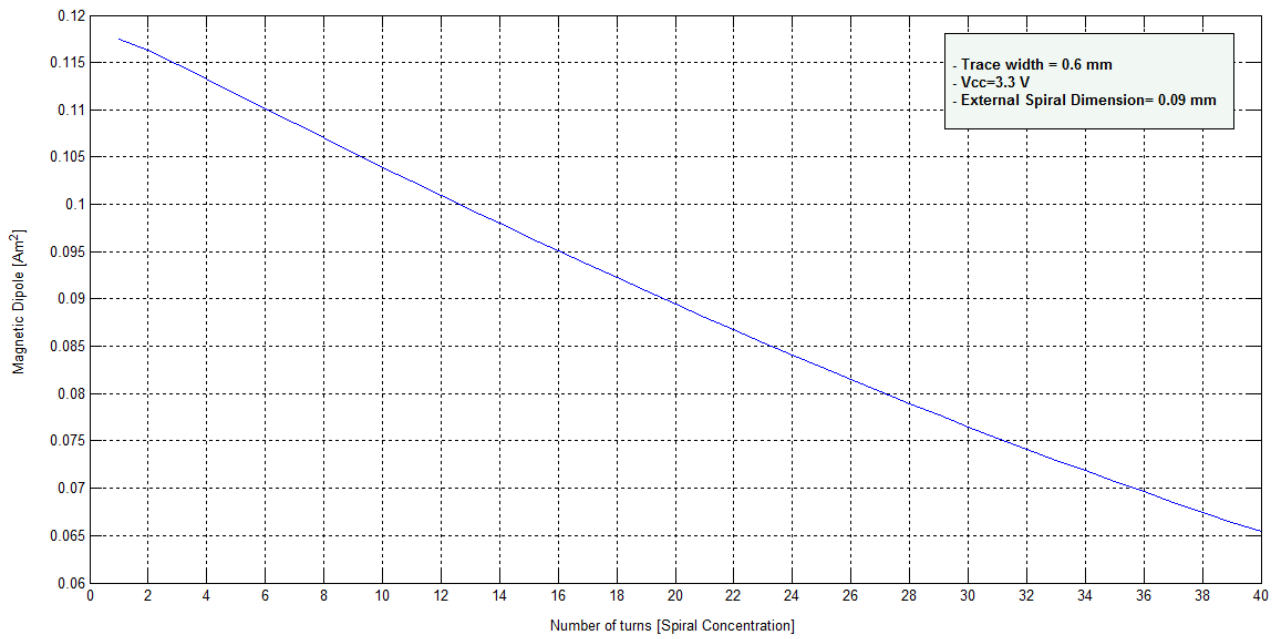


*Fig. 19 Magnetic dipole reduction due to increase of spiral concentration*

On the contrary the increase of the turns it's important to reduce the power consumption. If the required dipole is determined by a specific number of turns, the best way to reduce the power consumption maintaining that value is to increase the number of layers: this would consists in reproducing the same spiral trace in a parallel layer of the PCB (Fig. 20).



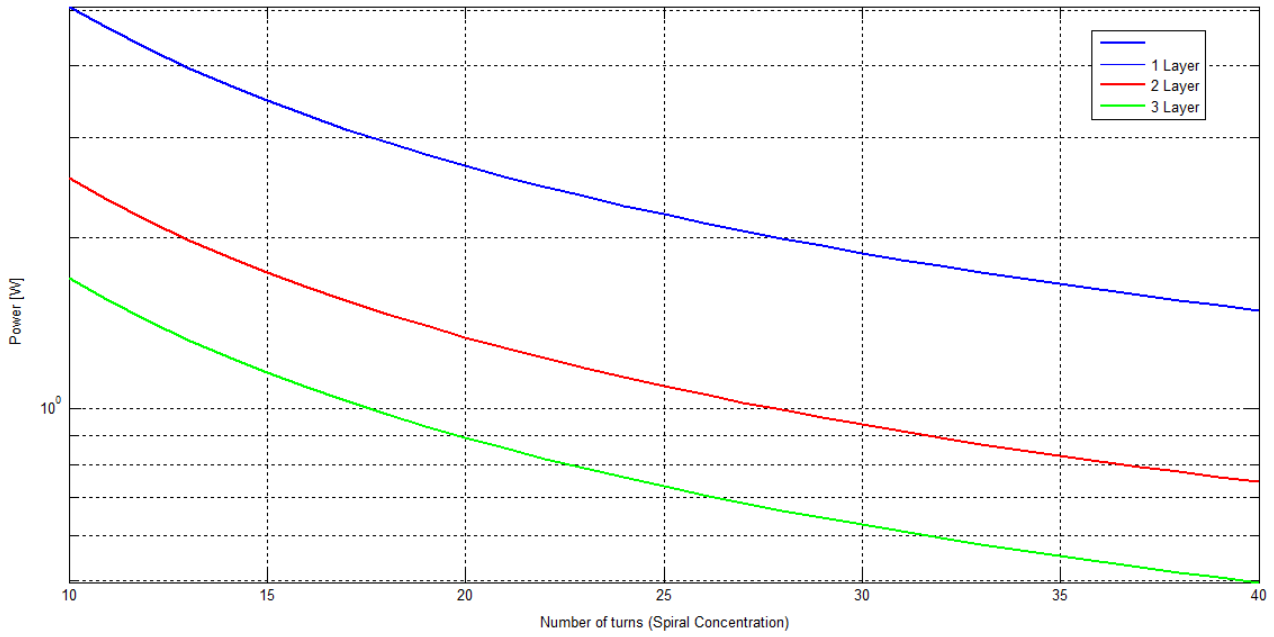


*Fig. 20 Power consumption for a multilayer embedded coil*

Nevertheless two big disadvantages are involved with this solution: first of all the mass of the PCB would consistently increase considering that any layer added requires a layer of insulation. Second, the cost of a multilayer board is many times higher than a single layer one.

The mass of the magnetorquer can be evaluated considering the mass of the copper layer and the mass of the insulating layer. This can be made in several materials even if FR4 is the most used and affordable. The reduction of copper layer could consist in a reduction of the total thickness of the board and in that way the mass. In spite of that, normally, the standard thickness of a 4 layer board is set at 1.6 mm with 0.035 mm copper thickness.

The mass can be evaluated considering the total mass of the copper trace and the mass of the needed insulator that has to be added when multilayer are required.

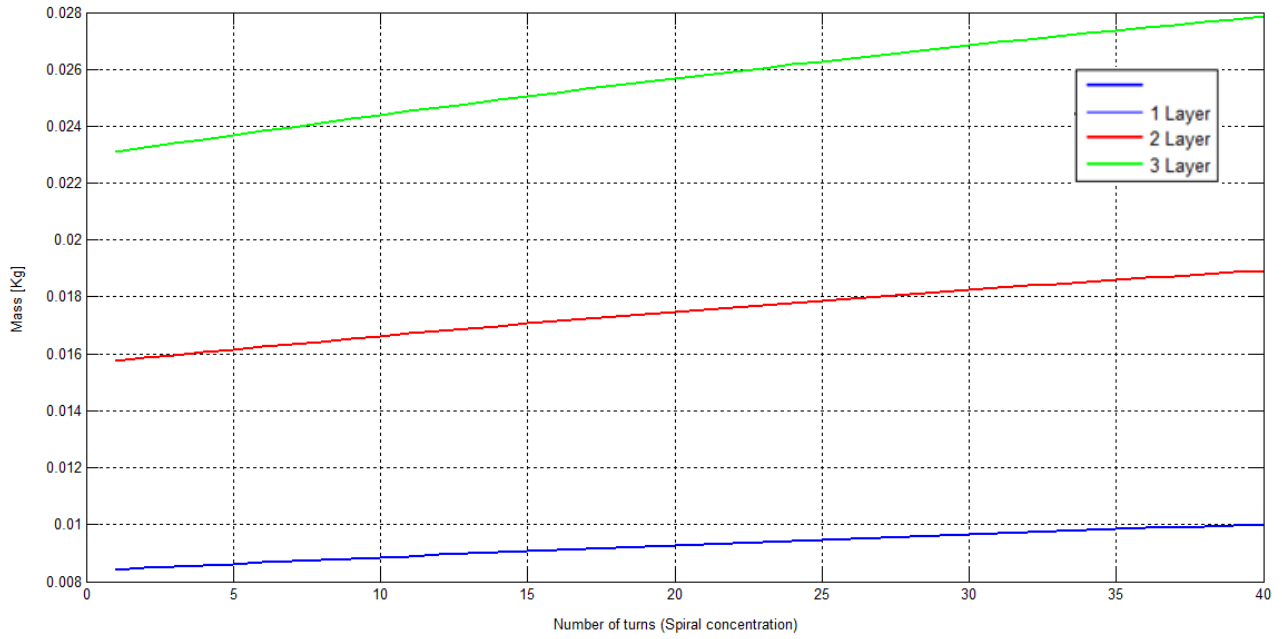


*Fig. 21 Estimated mass increase for multilayer embedded coil*

The mass increase can be observed in the graphs referred to the previous described case (Fig. 21).

The correct design for an embedded coil would be therefore to define the proper number of turns for a defined layer depending to the needed magnetic dipole and then increase the number of layer in order to reenter in the power budget constraints of the system. The general costs of this magnetorquer is pretty high compared to air core magnetorquer because the manufacturing of a multilayer PCB can cost many times more. The advantage of the embedded coil is the volume occupied and the easy integration in the satellite being embedded in the side panels. This is going to reduce the use of screw and other parts that add critical masses and risk during launch vibration.

### 3.4 Experimental measures on embedded coil

Several measures have been led on embedded coil magnetorquer to validate the model and to observe eventual issues not expected for this technology.

In this kind of magnetorquer the coil is "embedded" in a board composed by different material. This material could have a certain susceptibility to the magnetic field induced by the coil and they could affect it according to their magnetic

properties. In general it's possible to define 4 mean layer and parts that are standard for all embedded coil (Tab. 2):

- Insulator layer
- Ground plane
- Solar Cell
- Electronic Components

The insulator layer is the FR4 layer that is between two close copper coils. This is composed by fiber glass in epoxy resin. Glass is in general a diamagnetic material so the expected effect should be a reduction in the magnetic flux density. Though, the glass fibers are disposed on the plane and so perpendicular to the direction of the main applied field (perpendicular to the plane): the preferred direction of magnetic susceptibility should lie in the plane of the coil and in that way affect less the magnetic dipole.

The same concept can be applied to the ground plane that is composed by copper, even if in this case the diamagnetic properties of the material are really weak to determine a not negligible effect on the magnetic flux density.

The solar cell is the only element that could consistently interfere with the magnetic field generated by the coil. This because they are semiconductor material with high electron mobility and in that way high magnetic response. The different material which the solar cells are composed with can't allow to determine empirically a specific effect.

	Material	Relative Permeability	Magnetic Properties
<b>Ground plane</b>	Copper	0.999994	Diamagnetic
<b>Insulator layer</b>	FiberGlass	0.999987	Diamagnetic
<b>Solar Cell</b>	GaAs	?	?
	GaInP <sub>2</sub>		
	Ge		
<b>Electronic Components</b>	Al, Si	?	?

*Tab. 2 Different contributes presents in common nanosatellite side panels [9] [10]*

Even if these materials have really small magnetic quantities individually, the simultaneous presence could lead to a chaining effect whose outcome is not predictable. This thinking also that electronic charging of different components under electronic field leads to magnetic effects.

To evaluate the effect of the presence of different material in the complete board it has been performed an experimental measure. For the test have been studied two different boards with the same identical embedded magnetorquer, one with the mounted solar panel, and the other without. The two boards have been supplied with a defined profile current. The targets of the experiment were the following:

- Determine the average permeability of the whole board and in that way understand the effect of layers of different material on the magnetic flux density.
- Evaluate the difference between the mathematical model and the real case.
- Investigate the presence of eventual residual magnetic field.
- Evaluate the eventual interference of the solar panel on the magnetic flux density.

The experiment has been led exploiting the Helmholtz cage (Fig. 22, Fig. 23): with this device it's possible to compensate properly the earth magnetic field and generate a quasi-zero magnetic field in the measurement volume.

The Helmholtz cage needs to be calibrated before running every experiment. The calibration procedure has been made once the setup was complete and voltage generators turned on (providing zero current). In that way all the disturbance that couldn't be eliminated and could affect the following measures were kept into account in the calibration slope.

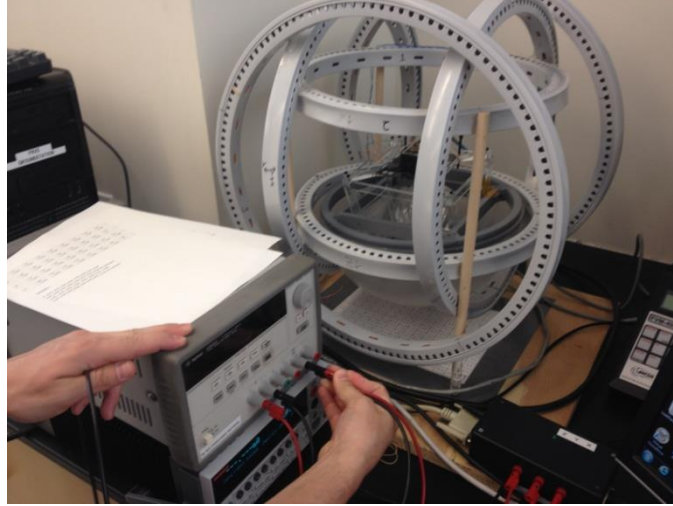


*Fig. 22 Helmholtz cage exploited for embedded coil experimental measurements*

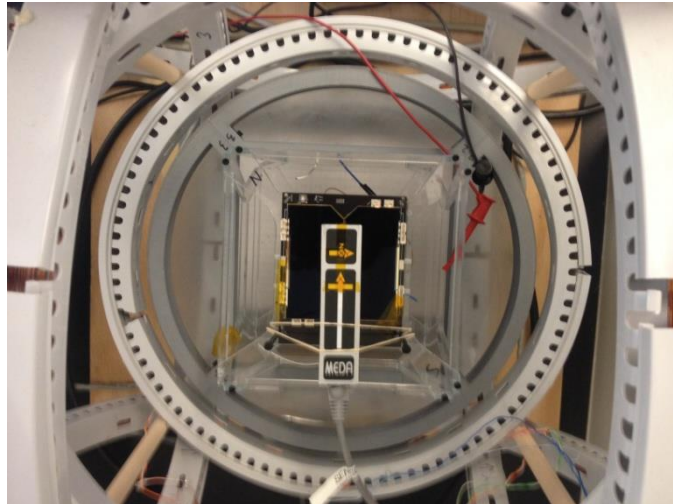


*Fig. 23 Embedded coil experimental layout*

In order to maintain the maximum magnetic field far from the saturation value of the magnetometer (900000 nT) the maximum current provided has been defined exploiting the mathematical model.

The profile provided profile current was a ladder composed of step of different current intensity.

Two profiles have been provided: one stepping 0.001 A from zero to 0.01 A both in positive and negative value (Fig. 24) and the other one equal stepping 0.01 A from zero to 0.1A (Fig. 25). Sampling for certain seconds to each value of current permitted to put on evidence the mean value of the magnetic field affected by

strong fluctuation due to the disturbance of the surrounding. Besides that, the non-continuous current profile avoids the problem connected to inductance of the board that could introduce a delay in the manifestation of the correspondent magnetic field.

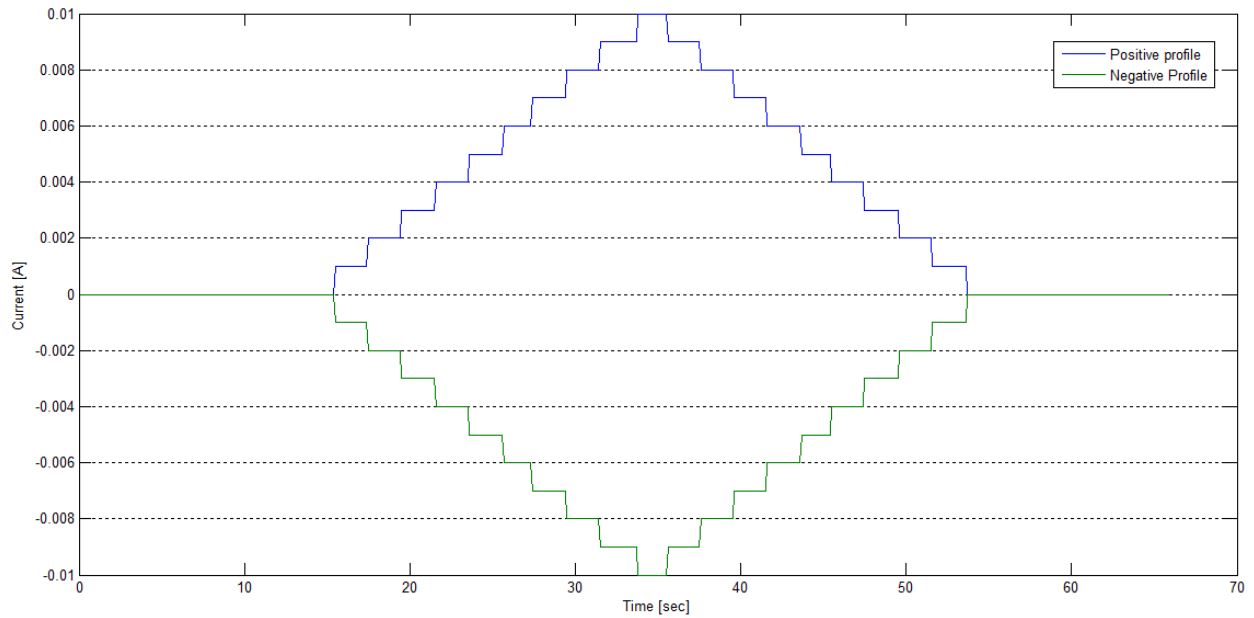


*Fig. 24 Current Profile 1*

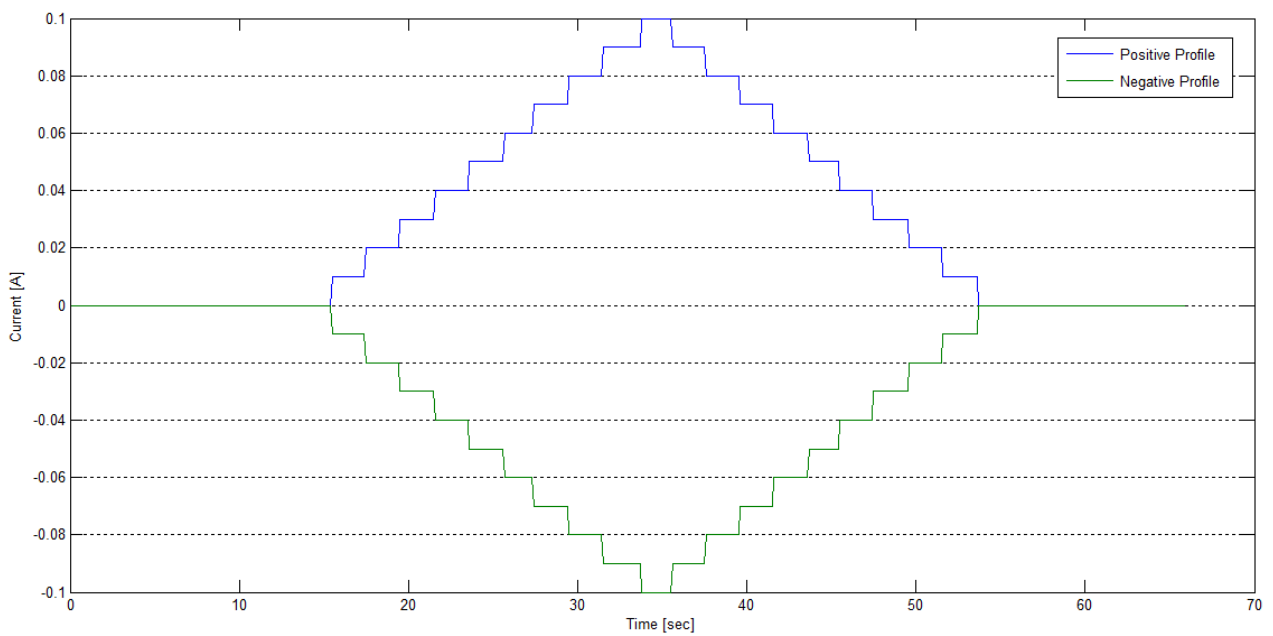


*Fig. 25 Current Profile 2*

### 3.4.1 No Solar cell mounted panel

The first experiment has been lead on a board without solar panels mounted (Fig. 26, Fig. 27). This permitted to eliminate the isolate the effect of the whole board form the effect of the panel and also to put on evidence the main difference between the mathematical model and the measured value.

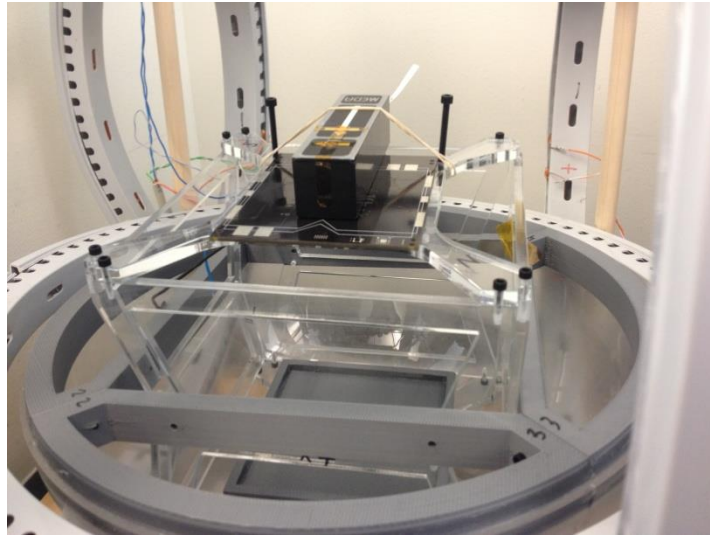


*Fig. 26 No-solar cells mounted panel layout (photo 1)*

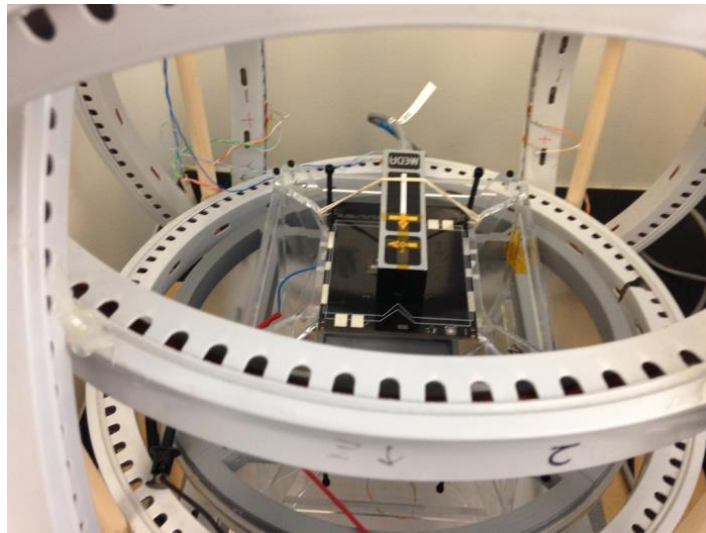


*Fig. 27 N-solar cells mounted panel layout (photo 2)*

In the figure below are presented the two profiles for negative and positive value (red for profile 1 and blue for profile 2). In green the mathematical model for every profile (Fig. 28).

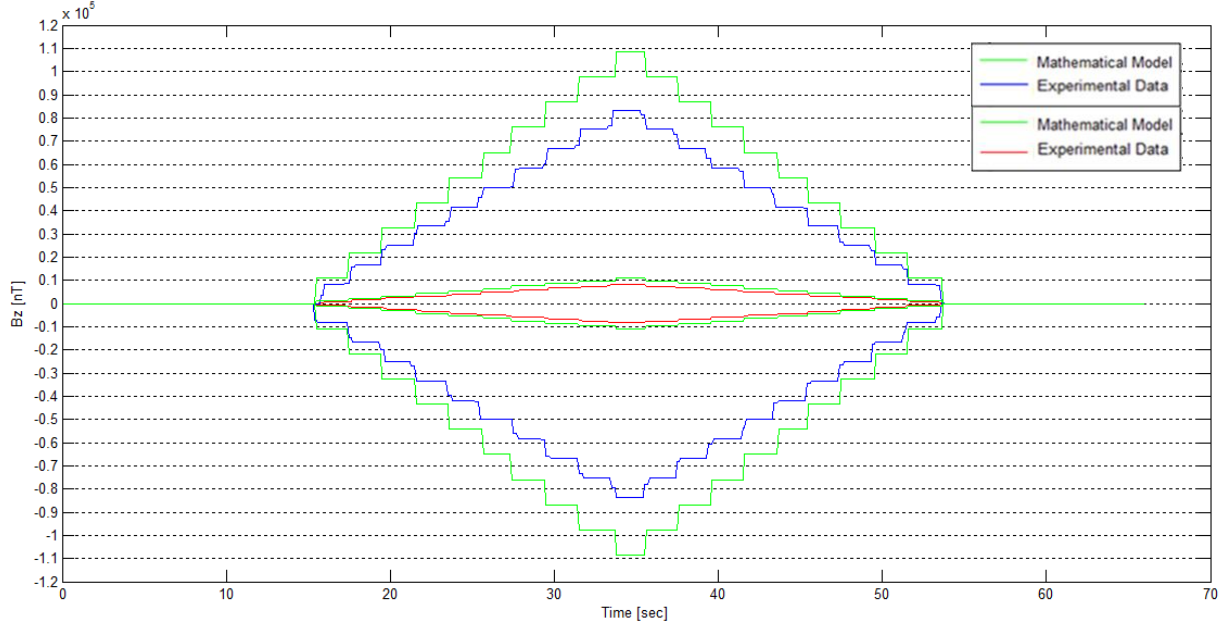


*Fig. 28 Magnetic Flux in z direction for no-solar cells mounted panel*

Because of the experimental setup and the instrument layout the measure is obtained at a certain distance from the center of the coil that, even if really small, leads to a reduction of the field. The idea to compensate the effect of the measurement point for the mathematical model is to evaluate the difference for a circular coil (assuming same characteristic dimensions) for which an exact formula exist to define the magnetic field at a certain distance from the center plane. The ratio between the B field in  $z=5\text{mm}$  (assumed as distance of the measurement plane for the layout) and  $z=0$  is 0.9924.

In a first approximation analysis this could be considered as the corrective factor for the mathematical model.

Looking at the results it's possible to notice a difference between the mathematical model that in general presents higher value for the magnetic flux density, and the difference is proportional to the magnitude of the magnetic field. This effect could be due both to the model itself and both to the presence of diamagnetic effect in the whole board: this because the effect of reduction observed would be too strong to be caused only to the diamagnetism, while it's admissible that the a certain



difference is present for measurement interferences (floating wire and current present in the experimental setup) and model imperfections.

Another important observation concerns the fact that there are no differences between the profiles in the two directions: this suggest that the eventual interference of the board is completely symmetric and equal without a preferred direction (Fig. 29).

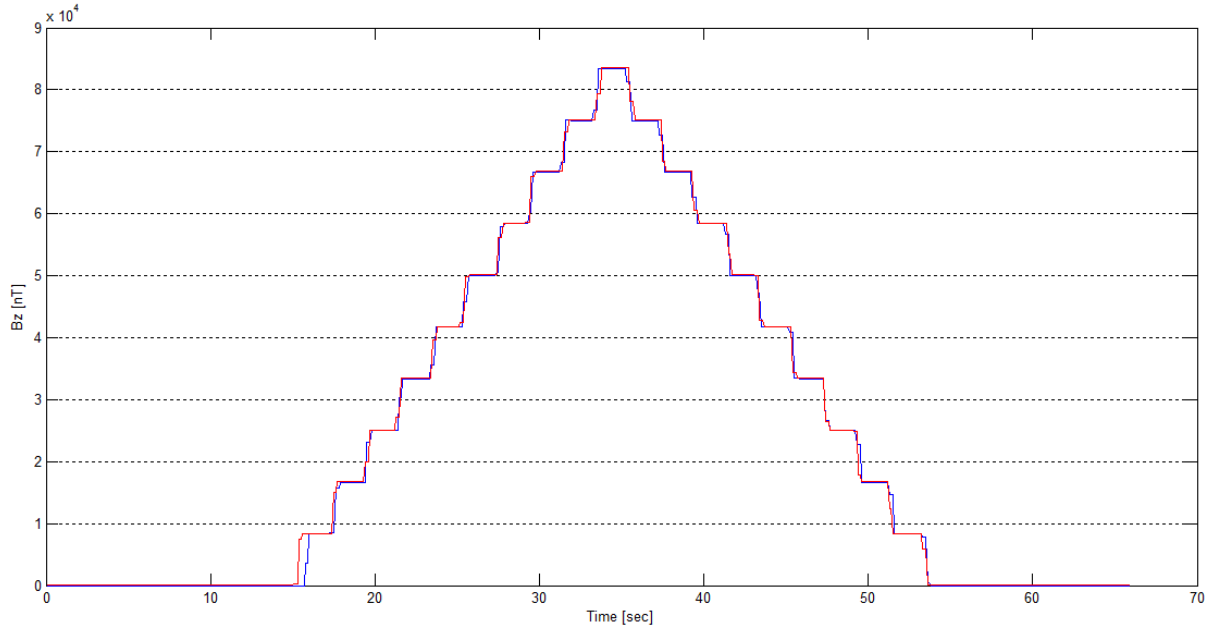


*Fig. 29 Comparison between positive and negative magnetic flux profile*

### 3.4.2 Solar cell mounted panel

The same experiment with the same layout has been led for the panels with mounted solar cells (Fig. 30)

Observing the measure obtained with the panel mounting the solar cells hasn't been observed any characteristic difference. One of the unexpected issues has been the calibration of the Helmholtz cage that has been different in this case (Fig. 31, Fig. 32): even if the procedure was exactly the same the calibration algorithm didn't succeed to set the correct calibration slope and in that way the resulted magnetic field set to zero corresponded to a different real magnetic field inside the Helmholtz cage. The difference with respect to the case of the first panel without solar cell was order of magnitude far from the zero point.

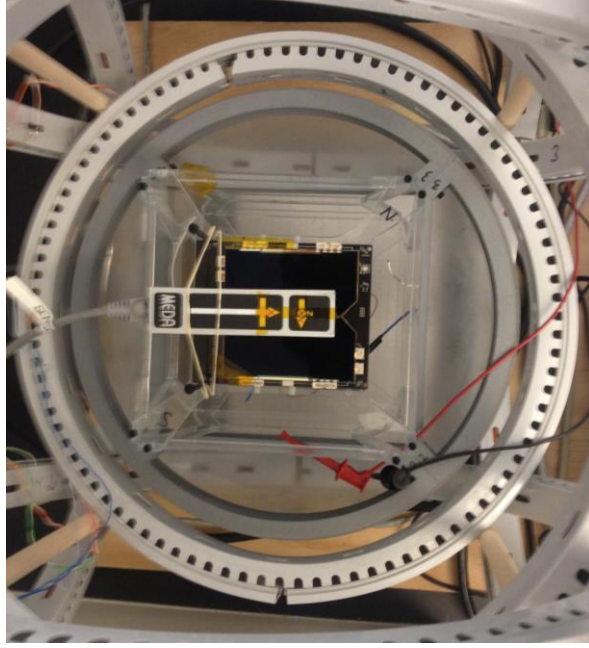


*Fig. 30 Solar cells mounted panel experiment layout*

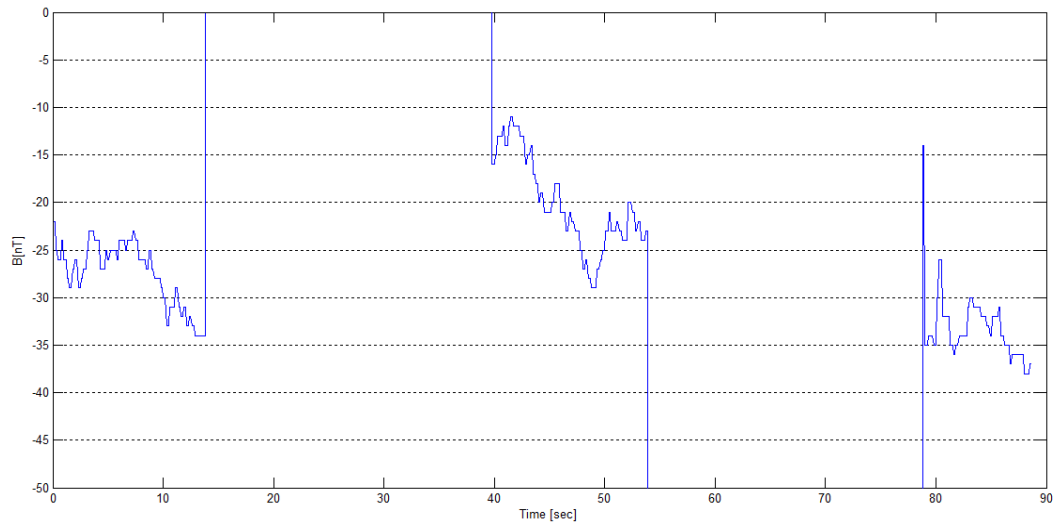


*Fig. 31 No-solar cells mounted panel cage calibration result*

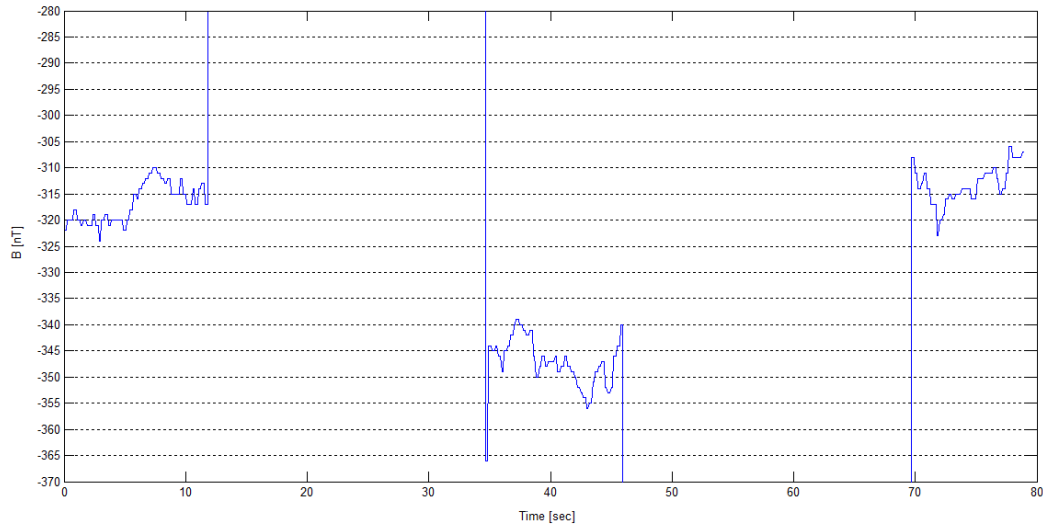


*Fig. 32 Solar cells mounted panels cage calibration result*

The zero level in the panel with the solar cell mounted was set around -300/350 nT while in the first case was quite close to zero being around -20/30 nT (Fig. 31, Fig. 32). This effect suggests that during the calibration phase has been present a behavior not expected by the algorithm that define the calibration slope. This could be related to a sort of hysteresis in the magnetization of the material of the solar cell excited by the field provided by the Helmholtz cage. This behavior could be related to a sort of ferromagnetic properties in the solar cell materials. Even though the difference is negligible suggesting that if present the effect is really small.

This can be observed also considering the profiles obtained: the results for the two current profiles are equal to the first case in term of linearity. The dependence between the current and the magnetic flux doesn't put on evidence any strong non linearity that could be manifested by strong ferromagnetic behavior (Fig. 33).

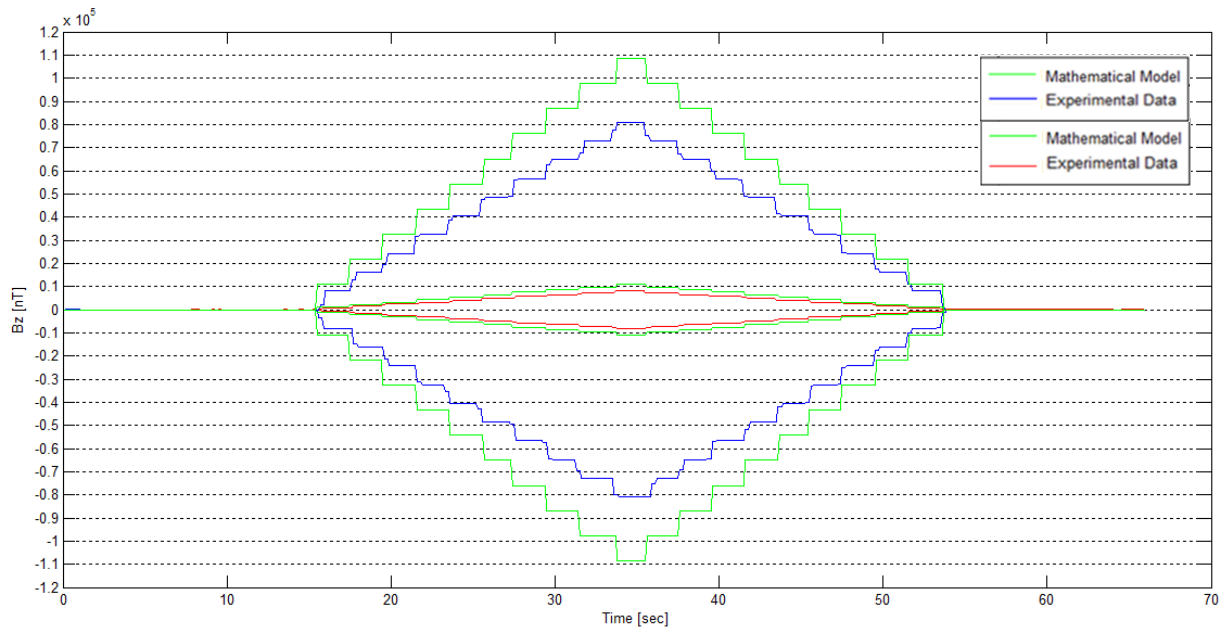


*Fig. 33 Magnetic flux in  $z$  direction for solar cells mounted panel.*

Again also in this case the behavior it's completely symmetric and the profile in the two directions overlaps completely.

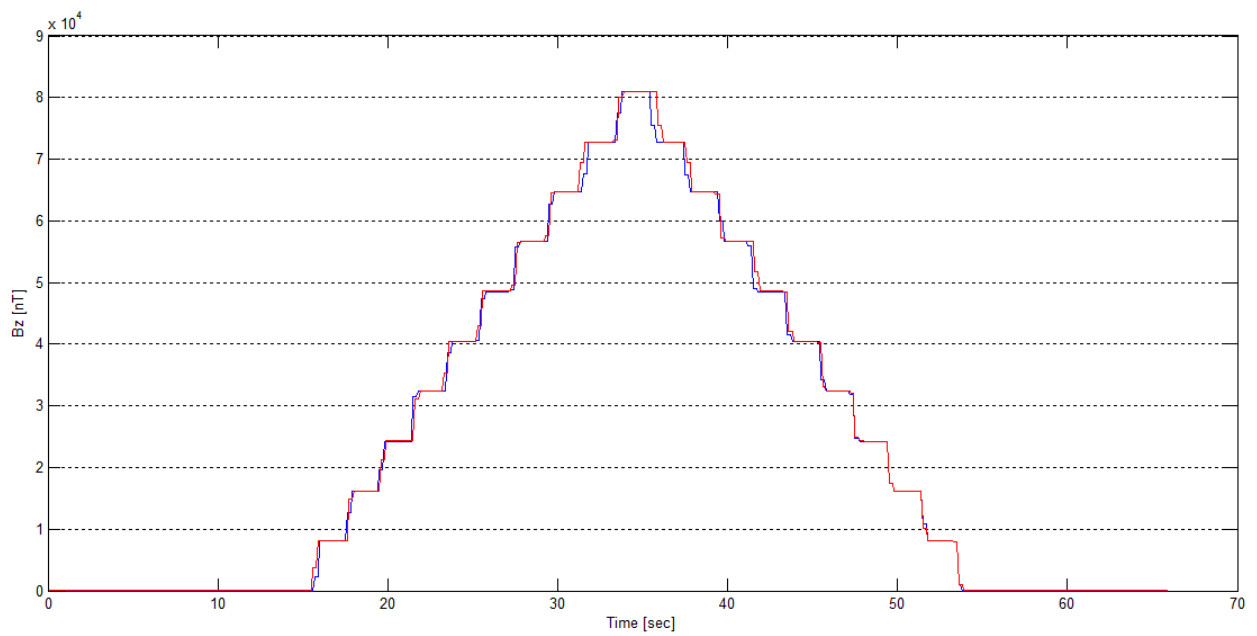


*Fig. 34 Comparison between positive and negative magnetic flux profile for solar cells mounted panel*

To understand the eventual effect of the solar panel it's necessary to compare the two results for the two different boards.

### 3.4.3 Comparison between the two case

Comparing the profile 1 for the board with solar panel and the board without solar panel it's possible to notice a small difference that consists on a reduction of the magnetic flux density (Fig. 35). This effect has to be attributed to the presence of the material in the solar panel.

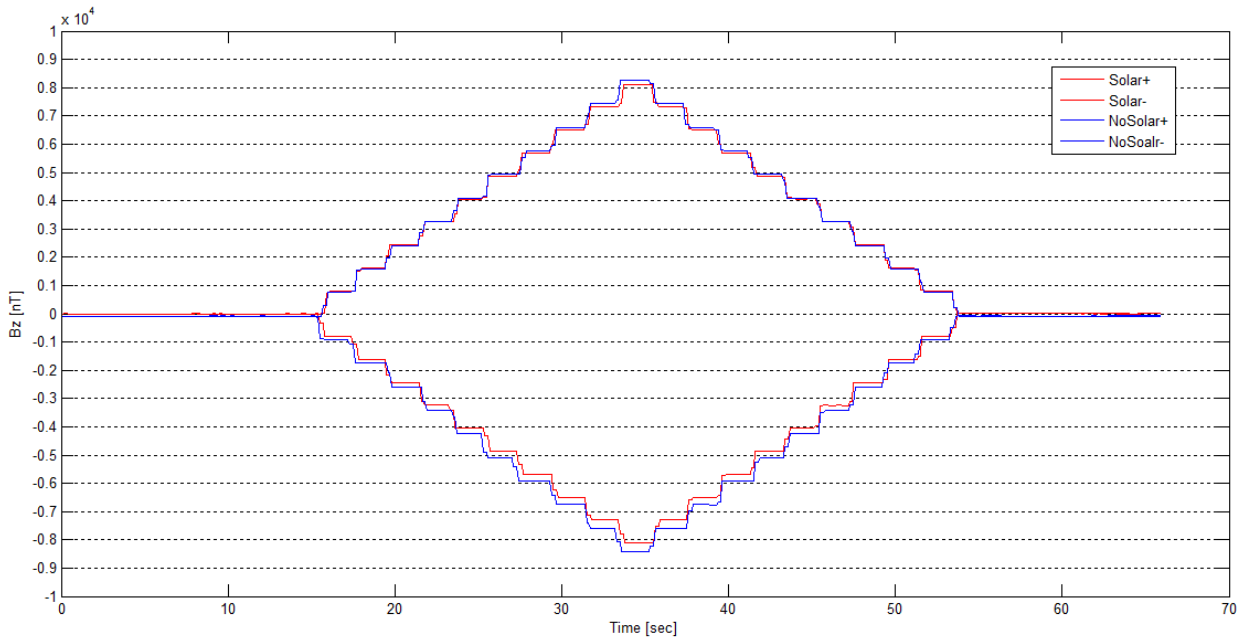


*Fig. 35 Comparison between magnetic flux for solar cells and No-solar cells mounted panel (Profile 1)*

The difference can be put on evidence: for the profile 1 one in in the order of hundred nanoTesla (Fig. 36).

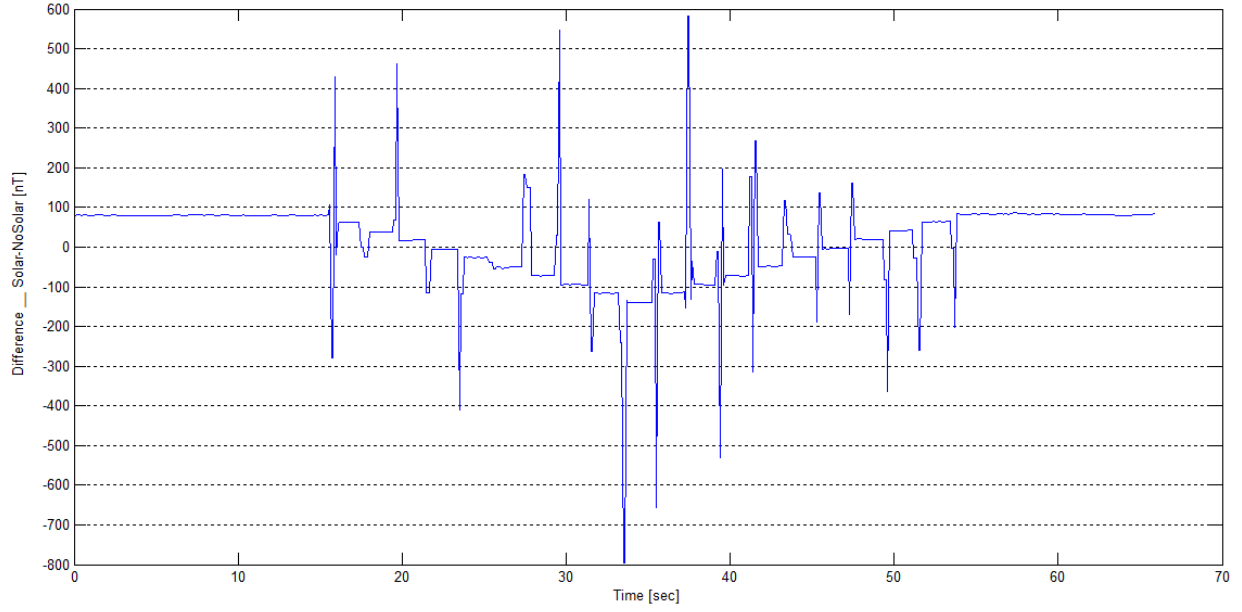


*Fig. 36 Magnetic flux difference between the solar cell case and no solar cells case(Profile 1)*

Comparing the profile 2 the same effect is observed and the difference it's proportional to the magnetic field strength (that it's proportional to the current provided).

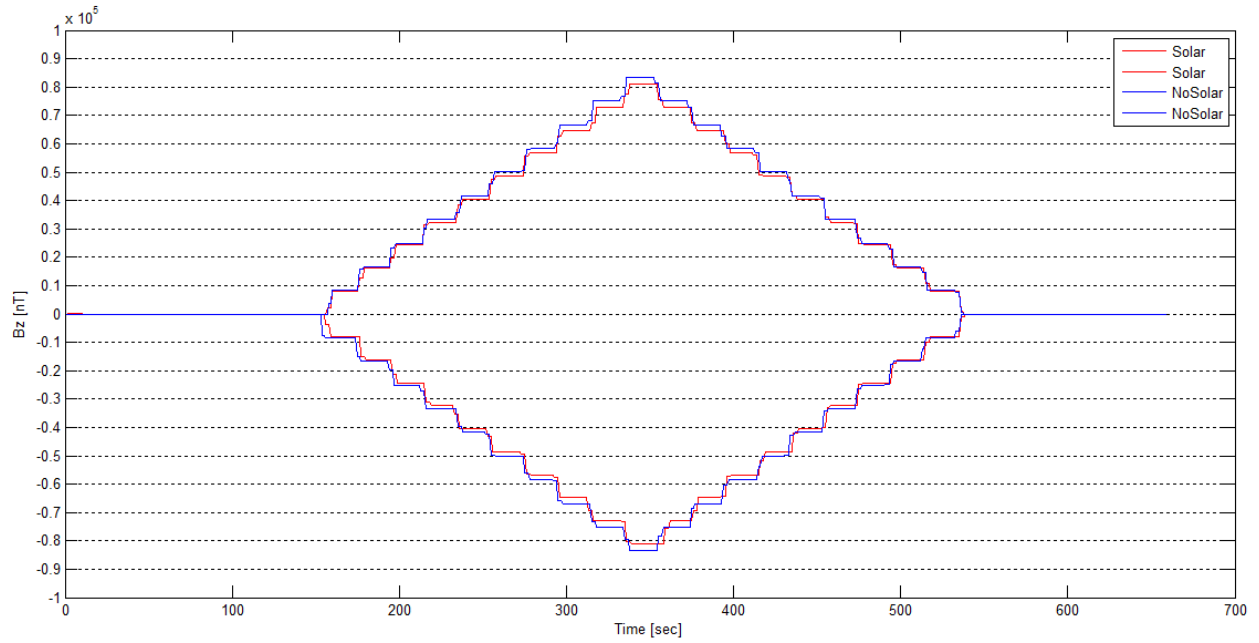


*Fig. 37 Comparison between magnetic flux for solar cells and No-solar cells mounted panel (Profile 2)*

In this case according to the current profile 2 the difference is in the order of thousands nanoTesla.

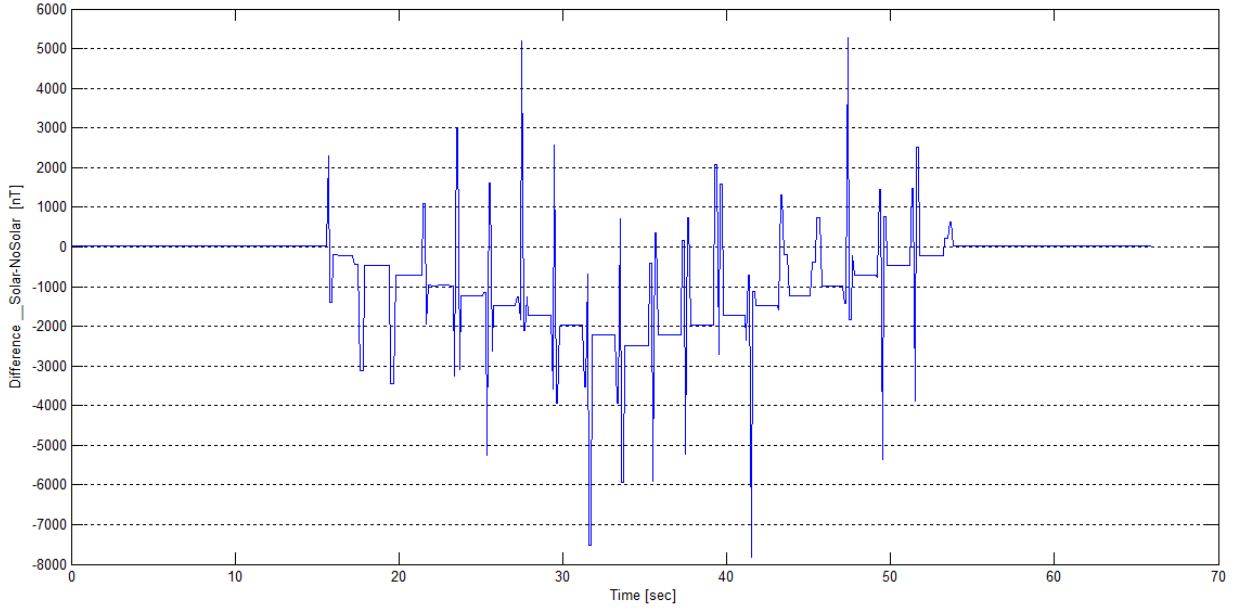


*Fig. 38 Magnetic flux difference between the solar cell case and no solar cells case(Profile 2)*

### 3.4.7 Corrective parameters

The data permits to define some correction value for the model. This correction value will be identified using analogy with magnetic quantities, leading to artificial magnetic quantities that can be easily exploited to correct the model. This quantity will be indicated using apostrophe.

The average permeability for the two samples obtained from the experimental results can be evaluated in empirical way. Assuming exact the model of the magnetic field strength it's possible to obtain artificial permeability that relates the mathematical model to the real case and contains all the presented effects:

$$\mu' = \frac{B_{exp}}{H_{theoric}}$$

This parameter contains all the effect due to model imperfection and board diamagnetic effect.

Assuming empirically  $\mu = 0$  when  $H=0$ , it's possible to observe that the artificial permeability it's constant (Fig. 39).

This artificial permeability results different as expected for the two boards: the presence of the solar cell reduce the permeability.

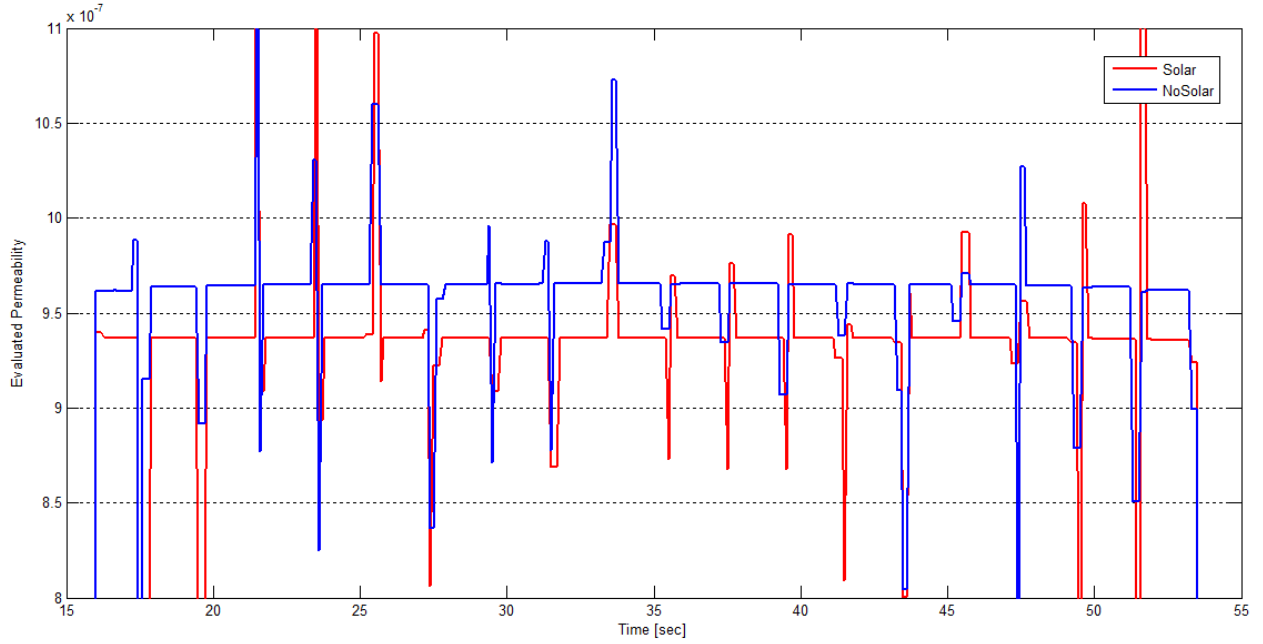


*Fig. 39 Evaluated artificial permeability from experimental results*

Fluctuations and peak are not interesting. These are due to the transient of the magnetic field during the current step (manual) and the consequent manual correlation with the current profile.

The ratio of reduction due to the solar cell can be evaluated around 0.971 (Fig. 40). The value can be obtained relating either the value of the magnetic field or the value of the permeability.

$$\frac{B_s}{B_{ns}} = \frac{\mu_s' H}{\mu_{ns}' H} = \frac{\mu_s'}{\mu_{ns}'} = 0.971$$



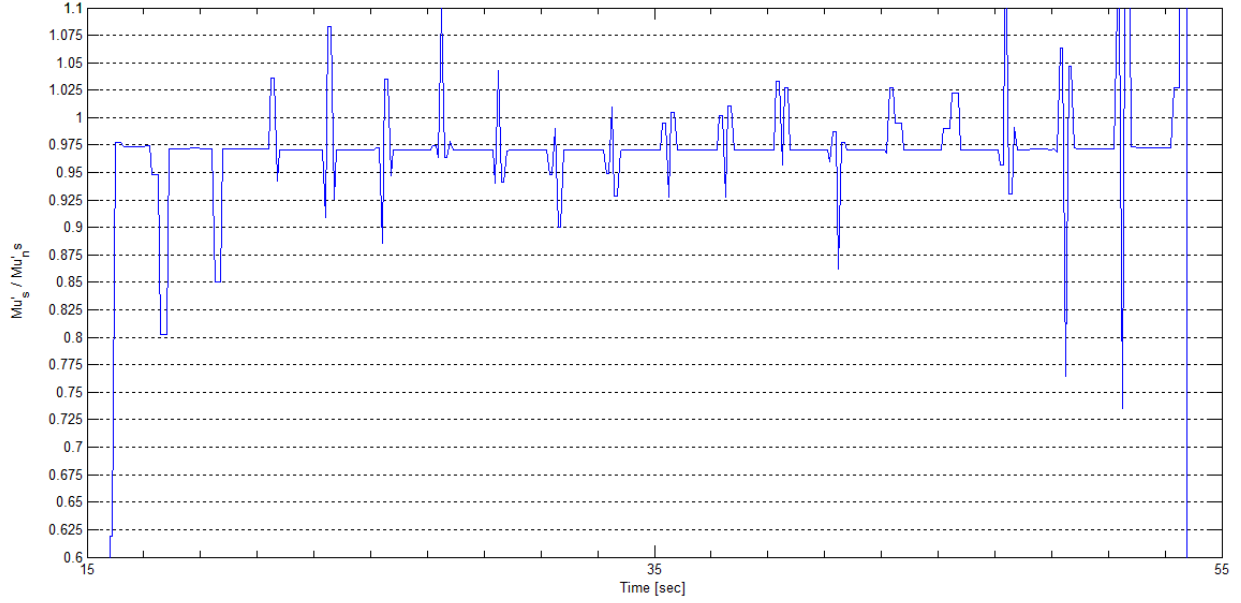


*Fig. 40 Ratio between the artificial permeability in the two case (Solar cells / No-solar cells)*

Considering that all the other effects (disturbances, imperfection) are present in both cases, these do not contribute to the ratio and, assuming  $\mu_{ns} = \mu_0$ , the value can be considered as relative permeability of the solar cell.

$$\frac{\mu'_s}{\mu_0} = \mu'_r = 0.971$$

Considering the relation between the relative permeability and the magnetic susceptibility it's possible to extract an indicative value of the diamagnetic effect of the board. This can be considered again as an artificial magnetic susceptibility of the solar cell applicable to have conservative correction factor to the magnetic field. It can be represented by artificial magnetic volume susceptibility  $\chi'_{vs}$

$$\chi'_{vs} = \mu'_r - 1 = -0.029$$

This value can offer in a first analysis a value that measure the diamagnetic effect of the solar cell on the whole embedded system. As already said, this value doesn't correspond to the real magnetic susceptibility of the single solar cell material in his proper scientific meaning: it represents an empirical value that in a certain way measure the overall effects that different materials with their setup (connections, supports) shows in experimental measures.

The same procedure for the entire panel it can be possible to extract an experimental magnetic susceptibility that allows to redefine the magnetic dipole according to the experimental results (thus comprising not only the solar cell, but also all the differences of model)

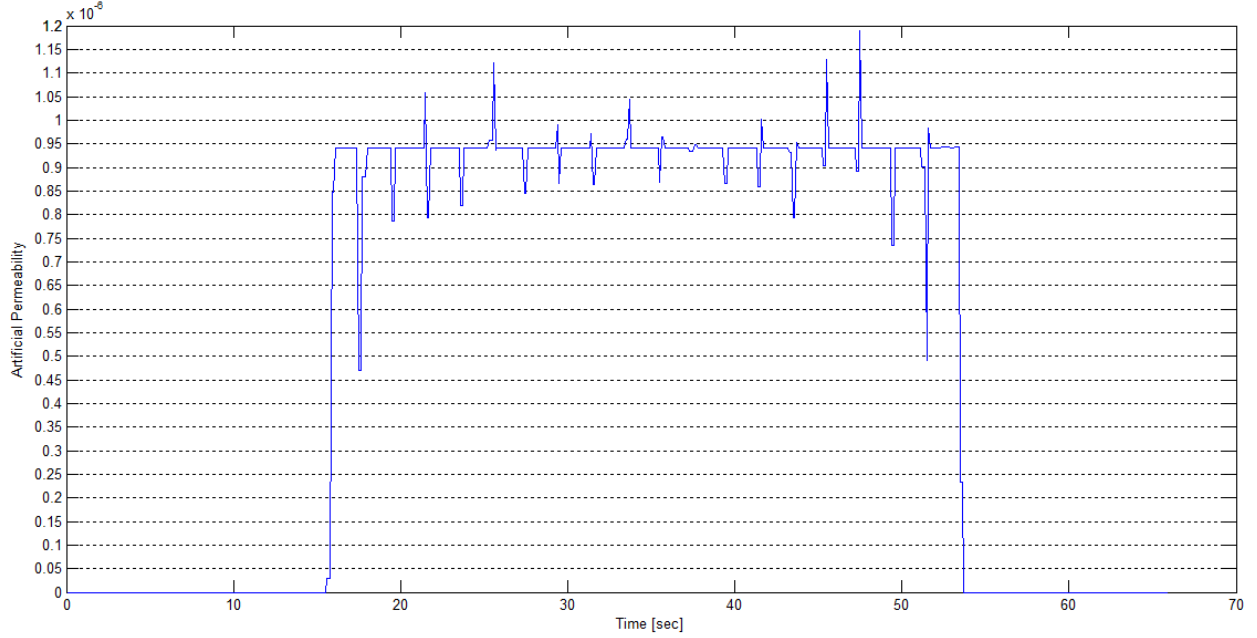


*Fig. 41 Evaluated artificial permeability of the entire panel*

Considering the panel with the mounted solar cell the obtainable permeability it's equal to  $0.9567 \times 10^{-6}$  (Fig. 41). A same result with a difference in the order of 0.1% is obtainable also exploiting the current profile2. Considering the vacuum permeability equal to  $1.2566 \times 10^{-6}$ ,  $\mu_r = 0.7544$ ;

As already said the results give a first idea of the effect of the whole board on the magnetic flux density. The artificial magnetic susceptibility  $\chi_v$ , can be evaluated equal to -0.2456. The value represent an experimental magnetic susceptibility in which are considered both diamagnetic property of the board both model imperfections.  $\chi_v$  is the related to the sum of the artificial magnetic susceptibility that keep into account the board effect and the model error and the evaluated magnetic susceptibility of the solar cell.

$$\chi_v V = \chi_{vs} V_{sc} + \chi_{vb} V_{bd}$$

This value can be interesting to consider in the worst case the opposite magnetization of the whole board materials that contribute to reduce the magnetic dipole produced by the embedded coil.

$$\vec{m}_{tot} = \left( i \sum_{j=0}^{n-1} [2l - (4j + 1) s] \left( \frac{l}{2} - js \right) \right) + \chi_{vs'} HV_{sc} + \chi_{vb'} HV_{bd}$$

Where  $\chi_{vb'}$  represents the artificial magnetic volume susceptibility that corrects the board effects and the model, while  $\chi_{vs'}$  is the artificial magnetic susceptibility attributed to the solar cell. Both multiplied for the respective volumes. The second term because of the sign of  $\chi_v$ , opposes the first then the real total magnetic dipole is slightly reduced. Even though the volume of the board is too small to determine a considerable reduction (Fig. 42).

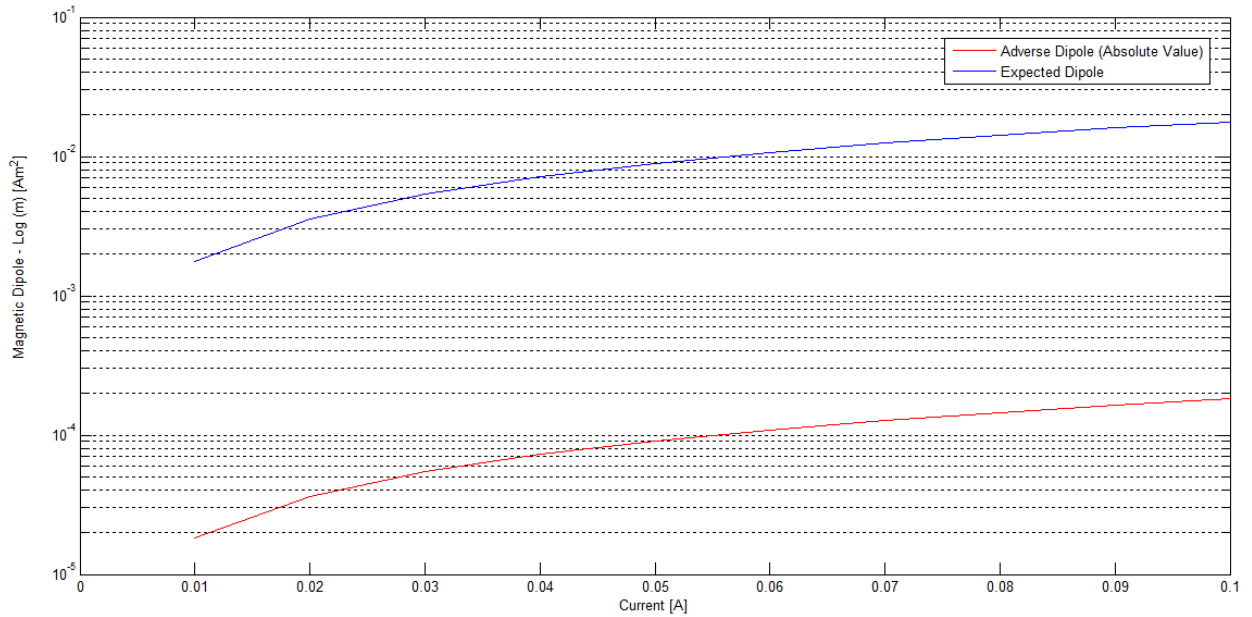


*Fig. 42 Expected dipole and adverse dipole evaluation*

The effect of the reduction of the magnetic dipole in the real case is completely negligible with respect to the mathematical model. The ratio between the real dipole and the theoretic one is 0.98981 that means that there is no issue in assuming the mathematical model as design parameter.

The data can be however exploited in case of different layout or bigger characteristic dimensions.

	Material	Relative Permeability	Magnetic Properties	Artificial Magnetic Susceptibility
Ground plane	Copper	0.999994	Diamagnetic	<b>-0.2644</b>
Insulator layer	FiberGlass	0.999987	Diamagnetic	
Electronic Components	Al,Si	?	?	
Model errors	-	-	-	
Solar Cell	GaAs GaInP <sub>2</sub> Ge	0.971	Diamagnetic	<b>-0.029</b>

*Tab. 3 Model correction obtained by experimental results.*

## 4. Air Core Magnetorquer

### 4.1 Description and Manufacturing

As already presented, an air core magnetorquer consists on a wounded wire with no core inside (air) (Fig. 43 Example of air core magnetorquer).

The winding can be obtained directly on the support or it can be produced separately and then integrated on the support. The winding phase can be done manual or exploiting a winding machine: the manual procedure it's easier and does not require the use of any machine but, if bad made, could lead to a chaotic and not ordered wounded coil. The wounding of the wire has to be made filling layer by layer and positioning every turn as close as possible to the previous. The accuracy and the order of the winding in fact determine the magnetorquer quality ensuring the uniformity of its functional characteristic. In general to manufacture high quality coils, the packing density of the coil needs to be as high as possible. Manual winding can be made keeping attention to maintain as constant as possible the wire's tension: in that way it's possible to fill properly the layer and avoiding the risk of tearing the insulation. This is an important issue above all for square shape coil in which the presence of the corner could cause an overload stretch of the wire.

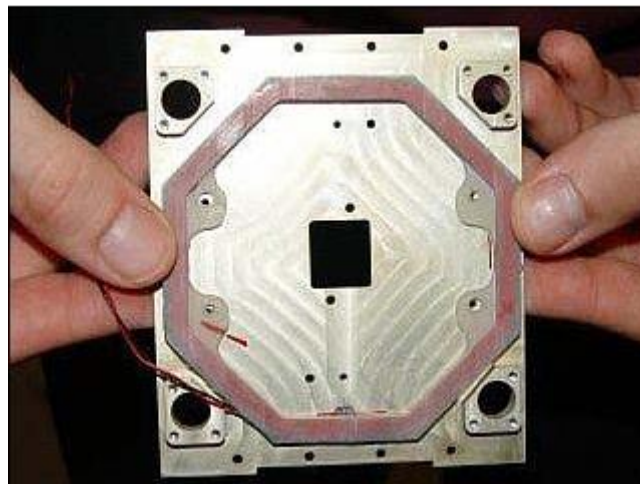


*Fig. 43 Example of air core magnetorquer [11]*

Once the coil has been wounded it's important to ensure its stability: vibration during launch phase could in fact cause the misalignment of the layers affecting

magnetorquer functionality. To avoid that it's used a self-bounding wire for magnetic application: these kinds of wire can be bounded tightly with itself by the heat produced with a current flow through it or it can be warmed up in a thermostatic chamber.

## 4.2 Model

The equation to model the magnetic dipole and the magnetic field for an air core magnetorquer are the classic equation known for the solenoid. In this case the wounded coil can be assumed with a defined area and a defined number of turns, differently than the case of embedded coil. The magnetic dipole moment can be expressed by the well-known formula:

$$m = nIS$$

While for the magnetic field exists a formula for the circular coil and the rectangular shape coil.

Using a circular coil would be not a good solution in general because it presents a higher ratio S/C where S is the surface and C the length of the coil: these two parameters directly are connected to the efficiency of magnetorquer as it will be presented below.

The formula to define the magnetic field for a rectangular shape multiturns coil is

$$B_z = nI \frac{2\mu_0 \sqrt{(l_1^2 + l_2^2)}}{\pi(l_1 l_2)}$$

Where  $l_1$  and  $l_2$  are the dimensions of the coil.

## 4.2 Designing issues

Same procedure used for embedded coil is exploited to define the designing issues of air core. The area is the main parameter that affects more in positive way the magnetic dipole with respect how much affects in negative way the other parameter, that's why the more logical choice is to exploit the most the available

surface. Again, it's a logical choice for the input parameter as well as the voltage supply.

Inputs:

- Voltage supply
- Dimension

We can use the formulas presented to define the mass, and combine to rewrite the magnetic dipole and the power consumption with a different expression:

$$m = \frac{V a_w}{\sigma} \frac{S}{C}$$

$$P = \frac{V^2 a_w}{\sigma C n}$$

$$M = \rho a_w C n$$

It's possible to notice that the number of turns, for the defined scenario of fixed dimension and fixed voltage, doesn't affect the magnetic dipole that, for a defined material, is function of the wire section, as well as the power consumption and the mass. On these in two opposite ways.

The constructive choices presented in the scenario should be made taking into account simultaneously the variations of these 3 quantities that can be easily plotted.

As already said, the magnetic dipole for a fixed size and a fixed voltage is function of the wire diameter (Fig. 44Fig. 1):

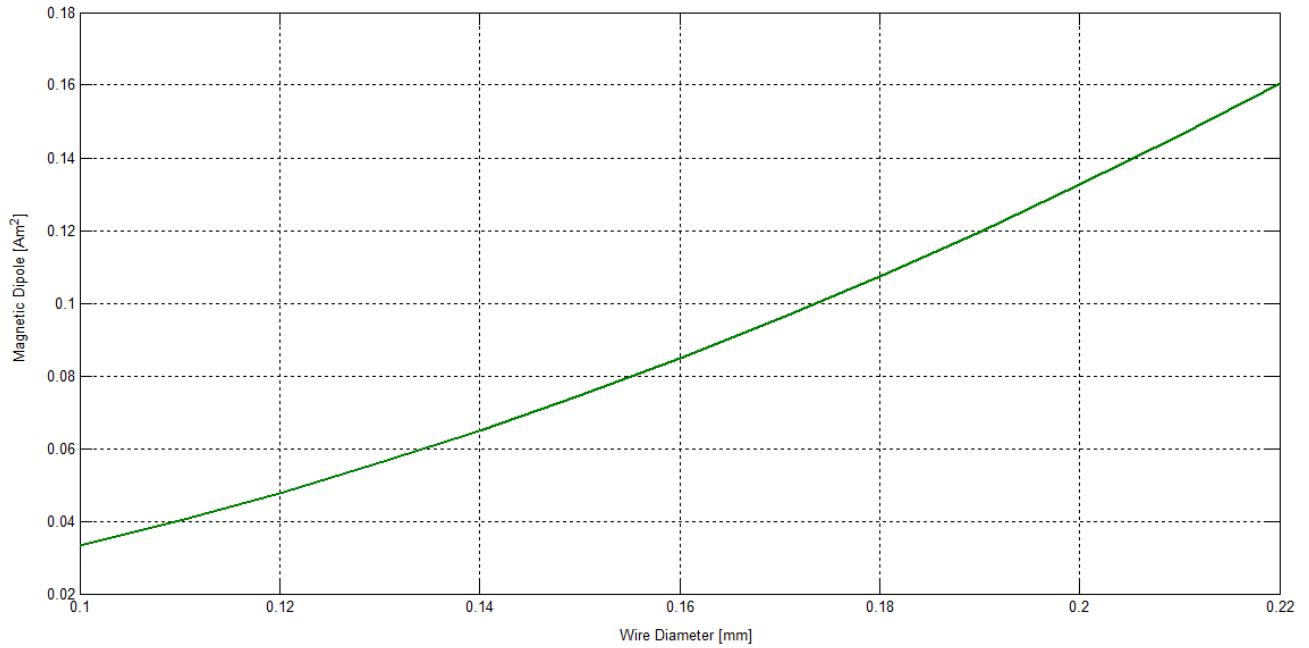


*Fig. 44 Magnetic dipole variation depending on wire's diameter*

As it can be observed in following graphs, the power consumption strongly decreases with the number of turns, while it increase with the wire diameter. It can be assumed a minimum of 100 turns in order to have acceptable power consumption under the level of 700mW that still could be a strong request for a magnetorquer (Fig. 45).



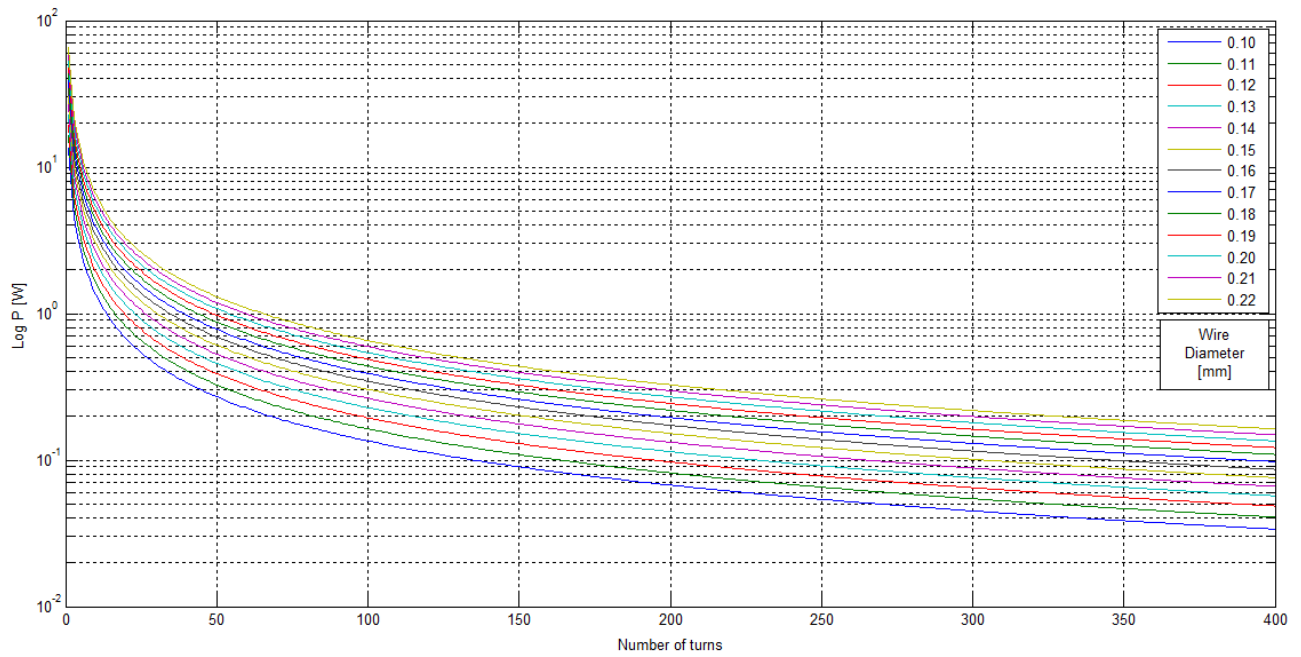


*Fig. 45 Power consumption model*

Choices in terms of number of turns and wire diameter also influence the total mass of the wire. These could be done evaluating the Mass graph (Fig. 46):

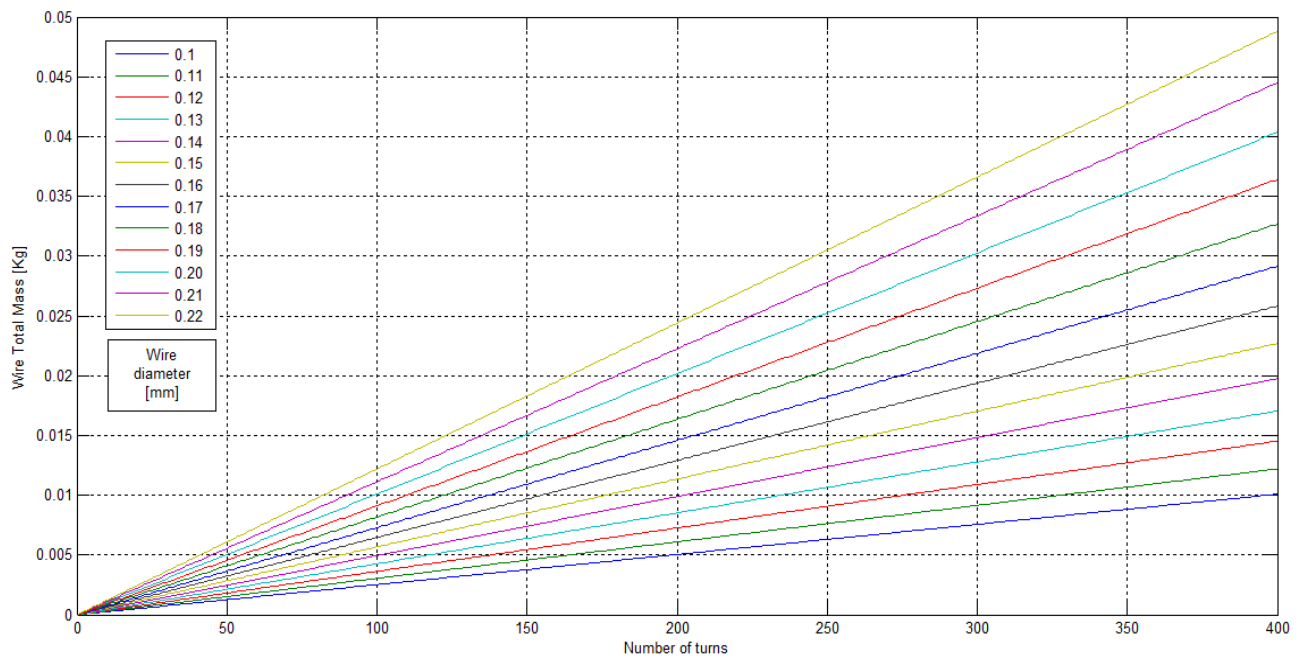


*Fig. 46 Mass model*

In this way it's possible to size the air core magnetorquer depending on mission requirement and mission constraints in term of power and mass. The presented graphs have been evaluated considering a voltage supply of 3.3 V and a dimension of 90x90 mm of the coil as quite realistic for a CubeSat mission. For different scenarios it's necessary to change the input of the voltage supply or change the dimension of the coil.

For example, in case of mass constraints for the system, defining the maximum coil's mass, an example of good compromises could be obtained for the following coil's designs (Tab. 4):

	A	dw	n	P [mW]	M	m
Magnetorquer 1	8100	0.14	200	155	10	0.083
Magnetorquer 2	8100	0.16	150	245	10	0.091
Magnetorquer 3	8100	0.18	125	350	10	0.105

*Tab. 4 Example of possible air core design*

Once the coil has been designed it's possible to evaluate the achievable performance and the operative regime varying the current through it (Fig. 47, Fig. 48, Fig. 49).

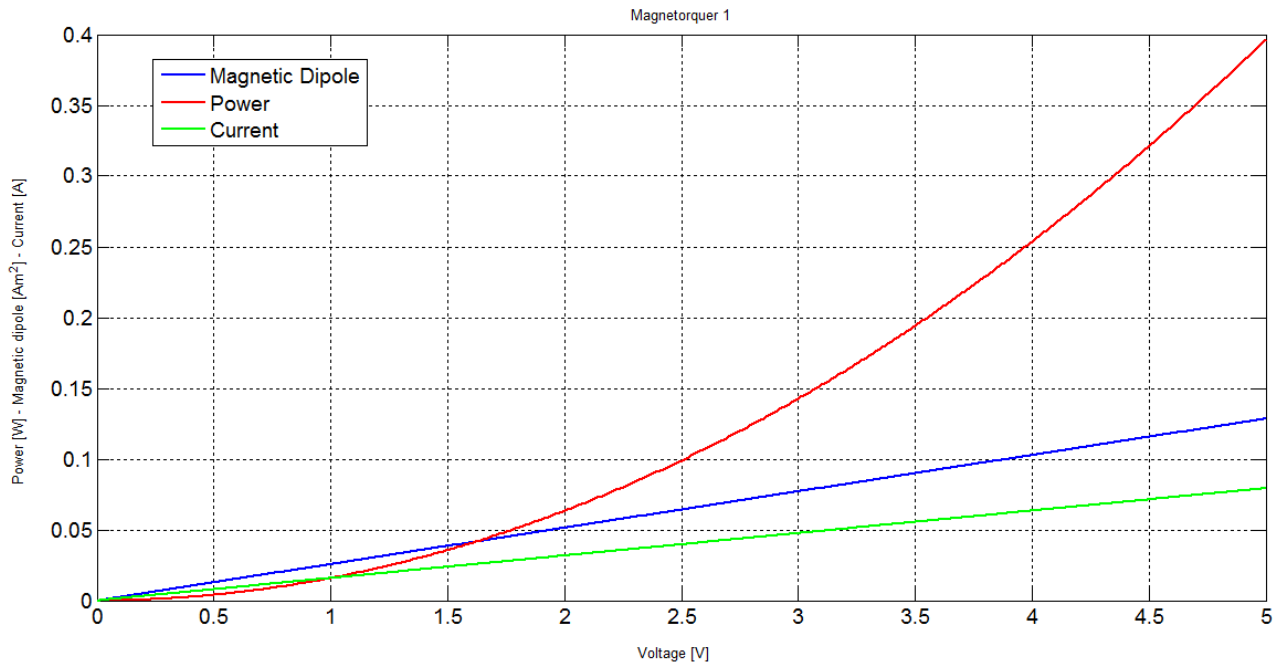


*Fig. 47 Magnetorquer 1 expected performances*

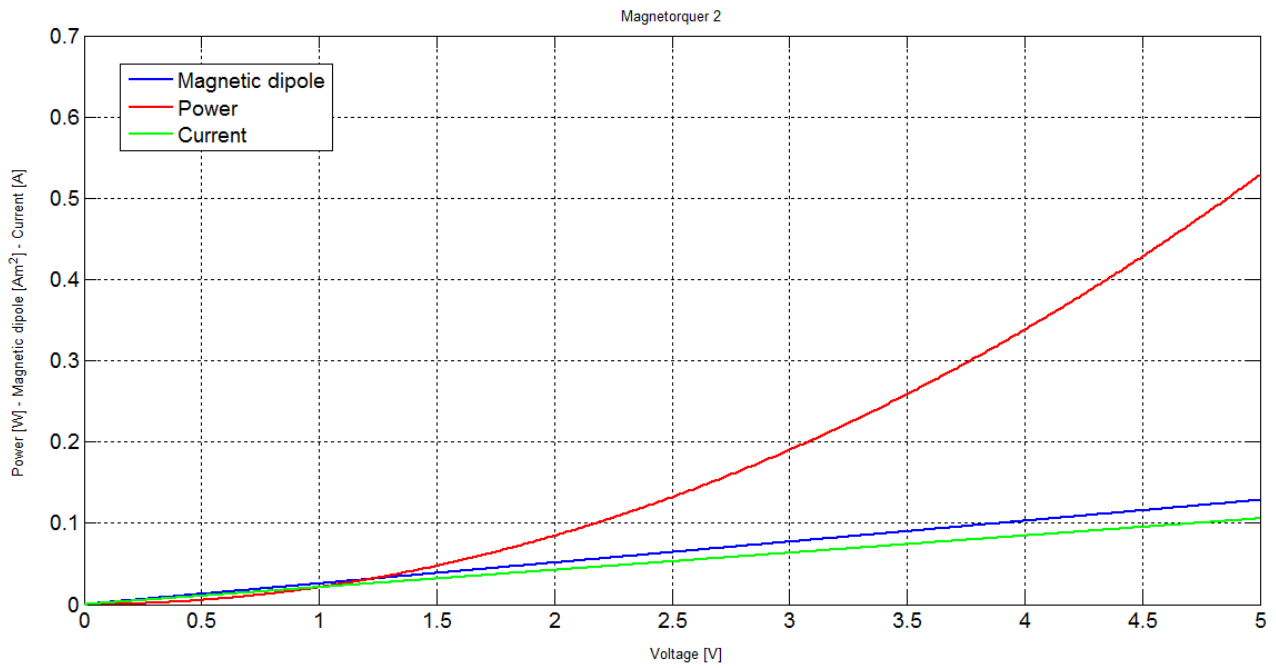


*Fig. 48 Magnetorquer 2 expected performances*

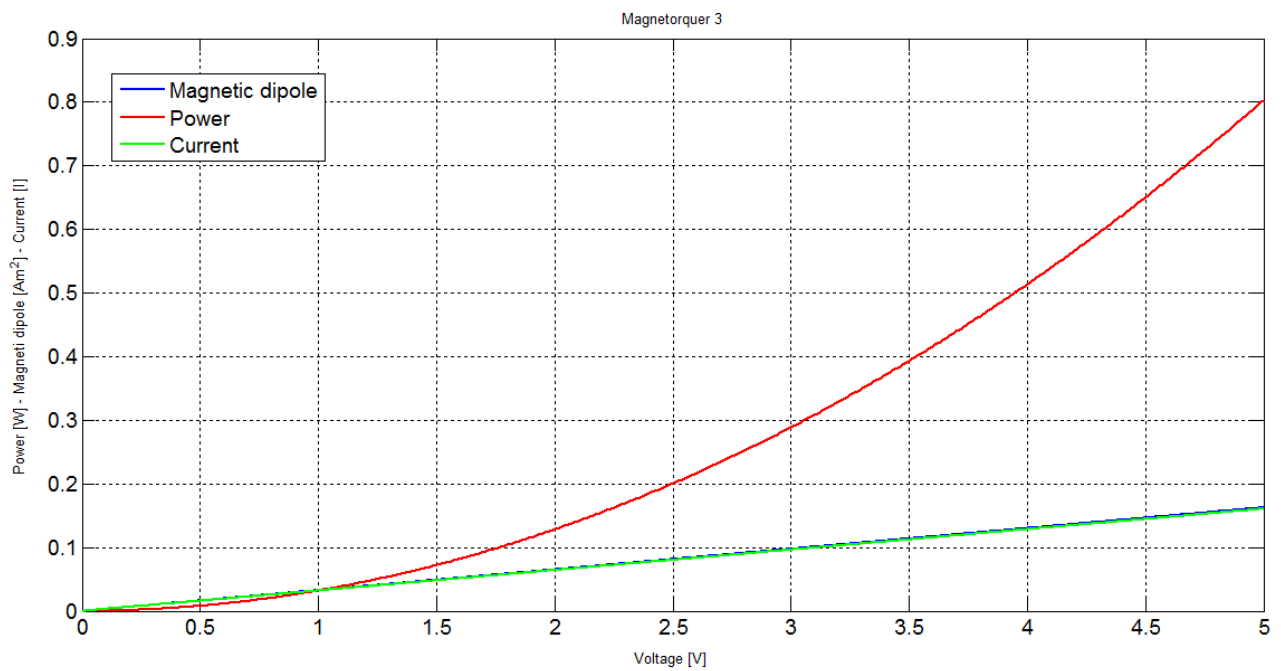


*Fig. 49 Magnetorquer 3 expected performances*

In this scenario of magnetorquer dimensioning we are not assuming the increase in size and dimension due to the diameter of the wire itself: even the wire's diameter is really smaller with respect to the scale of the system ( $10^3$  order of magnitude

less), the fact that it is wounded many time could lead to the condition that the wounded coil arrivals to thicknesses not more negligible. It's possible to estimate an average size of the wounded wire depending on the number of turns and the wire section. To do that it's important to fix at least one of the two dimensions of the section of the loop: usually the coil is wrapped around a support which allows the growth in the radial direction, fixing a maximum instead for the growth in the direction perpendicular to the plane of the loop.

A reasonable size for the maximum thickness in the direction perpendicular to the plane can be considered to be 3-4 mm for a generic air core magnetorquer.

The expected thickness of the coil in radial direction will depend again on the number of turns and the wire's diameter.

For a coil of  $8100\text{mm}^2$ , 400 turns with a 0.22 mm wire's diameter the obtained radial thickness is evaluated to be 6.5 mm that is around the 7-9% of the nominal characteristic dimension.

This evaluation has to be taken into account during the design of the physical support of the coil in order to avoid problems of dimensional incompatibility, properly reducing the support's housing for the wounding.

Besides a mechanical problem it's expected also a difference between the nominal area of the coil and the real area obtained after manufacturing: normally the effective area would be the mean area between the minimal area (defined by the support) and the maximum area obtained. This can lead to a certain mistakes in the evaluation of the magnetic dipole.

If we assume a good design of the support with a final external area of the coil close to the one defined in the project phase we can observe that the effective area will be smaller. It's possible to evaluate the percentage difference that results in an overestimation of the dipole moment (Fig. 50).

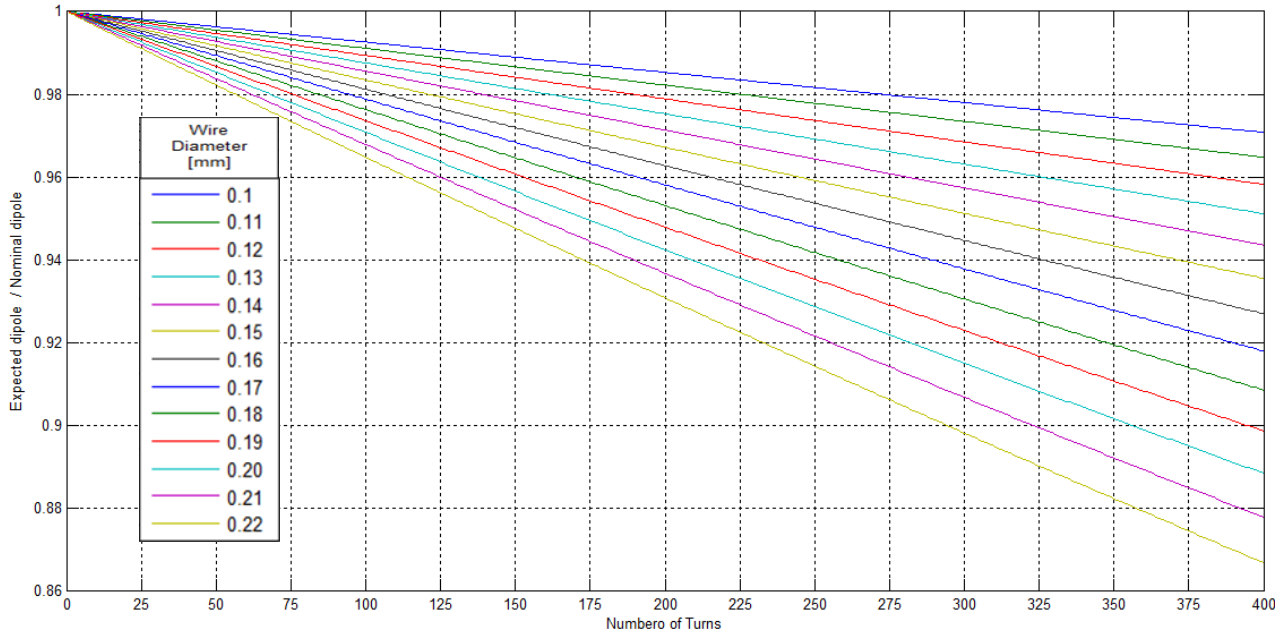


*Fig. 50 Effective dipole corrective factor*

From the graph it is possible to observe that for the considered scenario, the real dipole is evaluated to be 86% of the nominal dipole for 400 turns and 0.22mm wire's diameter (Fig. 50).

This kind of analysis it's important as the design optimization of the magnetorquer presented before, based on the nominal magnetic moment cause, generally leads to a reduction of the real performance. **It's necessary to determine a trade off in which the reduction in term of effective area (or the increase of real dimension) is considered acceptable.**

	A [mm <sup>2</sup> ]	d [mm]	n	P [mW]	M [g]	Nom_m [Am <sup>2</sup> ]	Eff_m [Am <sup>2</sup> ]
<b>Magnetorquer 1</b>	8100	0.14	200	155	9.9	0.083	0.080
<b>Magnetorquer 2</b>	8100	0.16	150	245	9.7	0.091	0.088
<b>Magnetorquer 3</b>	8100	0.18	125	350	10.2	0.105	0.101

*Tab. 5 Possible Air core magnetorquer design (effective values)*

For the magnetorquer designed as example, the reduction ratio expected is quite negligible leading to a difference in the magnetic moment in the order of  $10^{-3}$  Am<sup>2</sup> (Tab. 5)

## 4.7 Experimental measures on air core magnetorquer

The experiment led for the embedded torquer has been conducted also for the air core coil magnetorquer. The coil has been mounted on a side panel similar to inflight configuration (Fig. 53, Fig. 52). The target of the experiment similar to the case of embedded model was to evaluate again the effect of the board and to verify the differences with respect to the mathematical model. The air core magnetorquer exploited for the experiment was a rectangular shape multitrans coil realized in jalopy laboratories (Fig. 51).

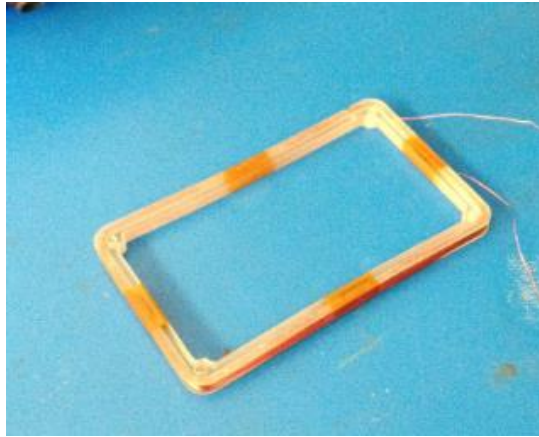


*Fig. 51 Air core magnetorquer prototype exploited for measurements*

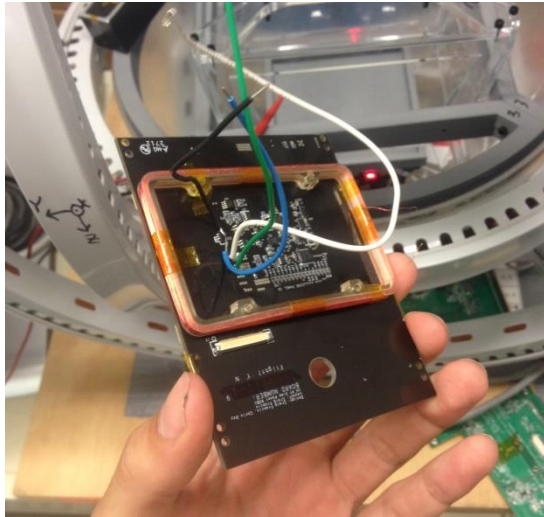


*Fig. 52 Air core magnetorquer mounted on the panel*

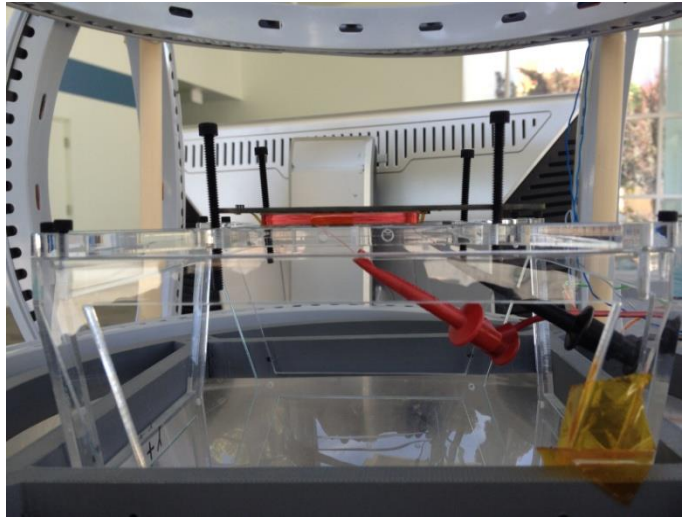


*Fig. 53 Air core experimental setup*

	A [mm <sup>2</sup> ]	Dimensions [mm]	d [mm]	n	P [mW]	M [g]
<b>ExoCube Mag.</b>	3666	78x47	0.16	160	320	10.3

*Tab. 6 Air Core magnetorquer prototype expected performances*

The expected performances (Tab. 6, Fig. 54 ) of the used magnetorquer can be easily evaluated exploiting the model.

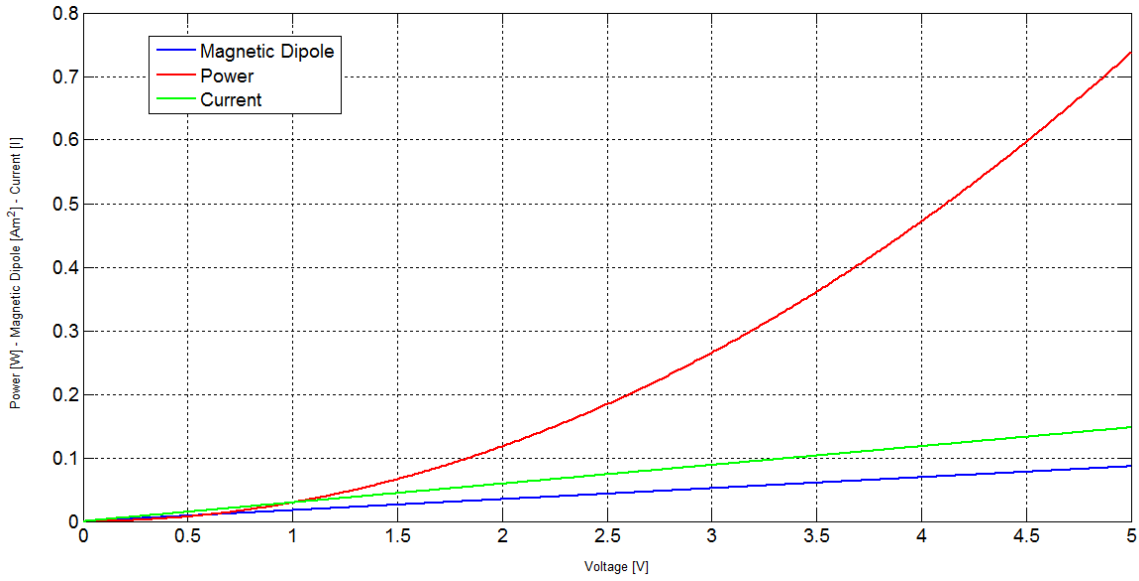


*Fig. 54 Air core magnetorquer prototype expected performances*

While the current profile 1 (Fig. 55) was the same of the experiment on embedded torque, current profile 2 (Fig. 56) for the coil was different, due to the strength of the torquer that led immediately to saturation the magnetometer for value around 0.05 A.

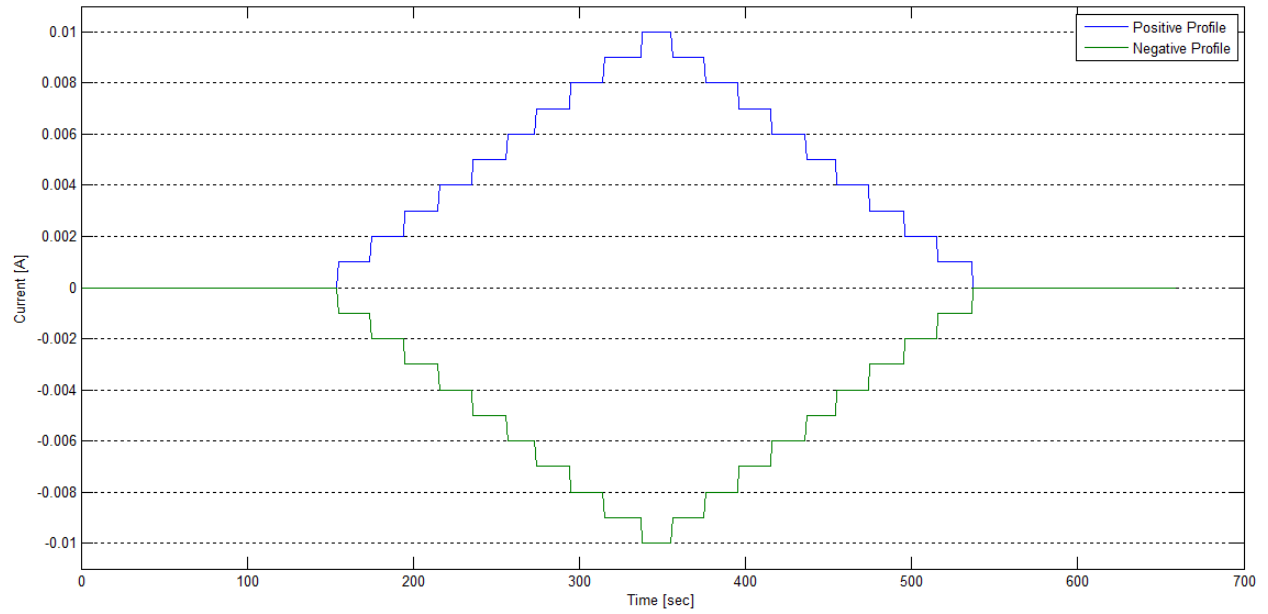


*Fig. 55 Current profile 1 (Air Core experiment)*

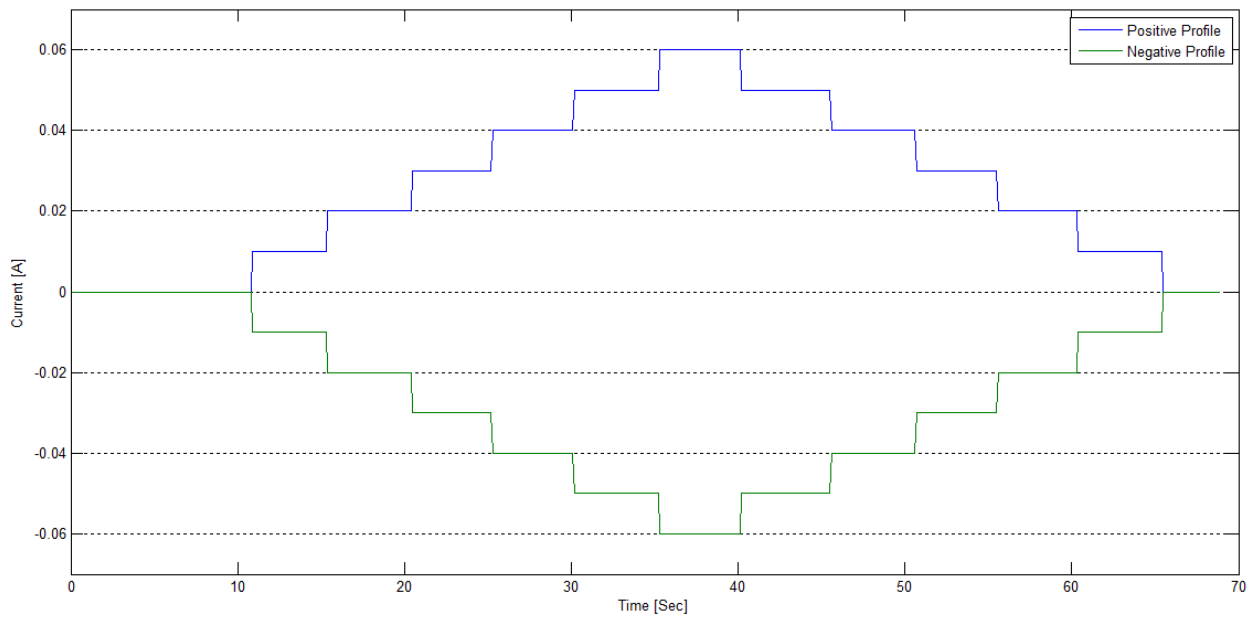


*Fig. 56 Current profile 2 (Air Core experiment)*

#### 4.7.1 No Solar Cell mounted Panel

The air core magnetorquer has been mounted on the board simulating the positioning in a real case application, i.e. behind the board in the inner face.



Also in this case the distance between the central plane in which lie the mathematical magnetic field and the effective measure point needs to be compensated: the model is corrected with a factor 0.868 that again represent the ratio between the magnetic field at  $z=0$  and  $z=0.008$ . In this case being the torquer external to the board the distance is bigger.

Observing the profile 1 it's possible to notice the difference between the model and the experimental data (Fig. 57). Similar to the case of experimental results on embedded coil, this effect contain the error model (the winding it's not ideal and the disposition of the wire is affected by misalignment) and the effect of the board.

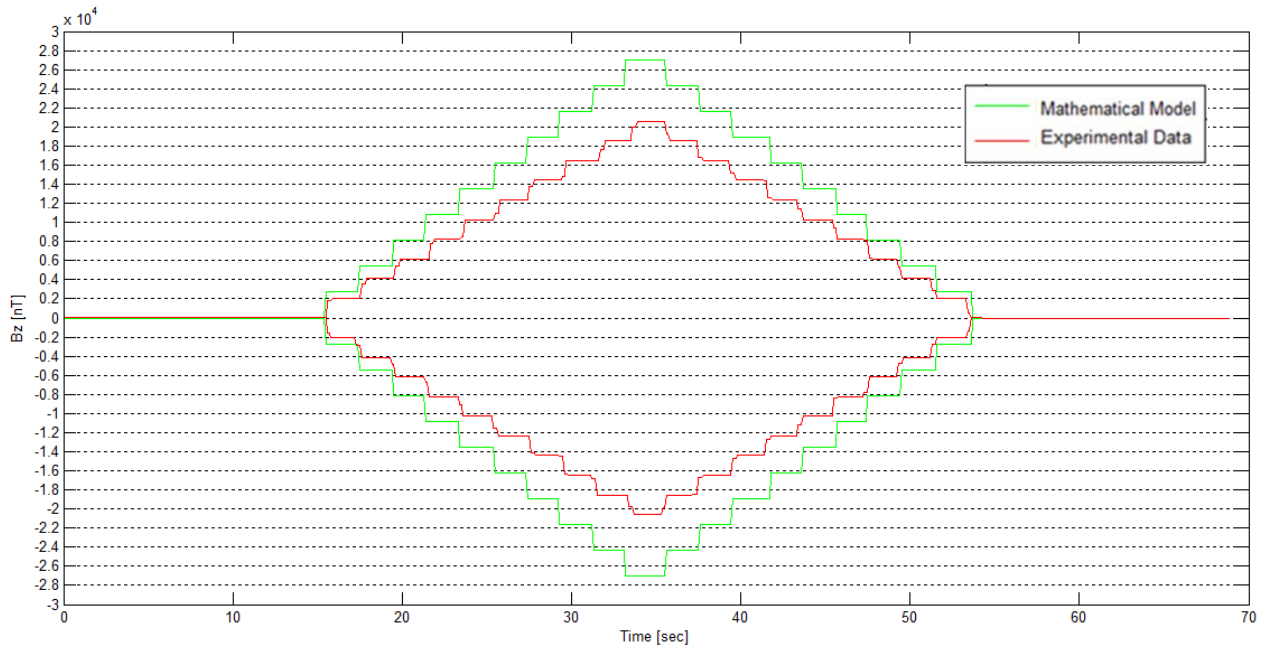


*Fig. 57 Magnetic Flux in  $z$  direction for profile 1 with no solar cells mounted*

Same qualitative data are observed for profile 2 (Fig. 58). In this case for a current equal to 0.6 A saturation in the magnetometer occurs (the "hole" in the magnetic flux density profile between 35 and 40 seconds).

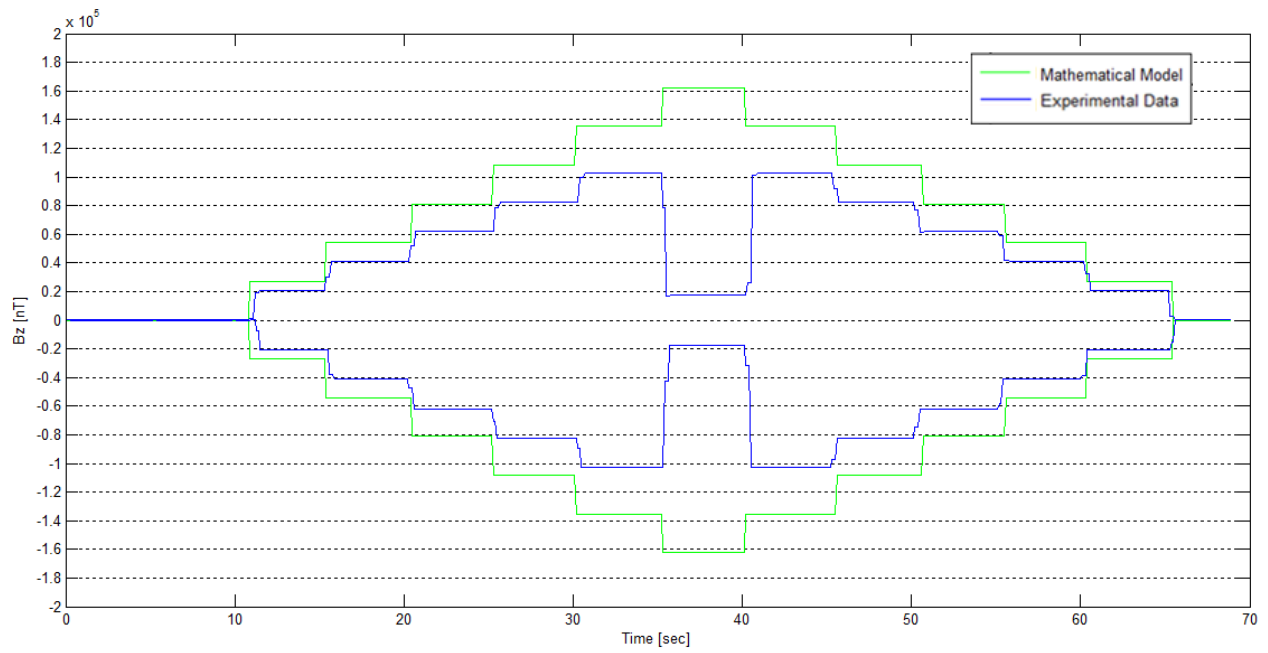


*Fig. 58 Magnetic flux in  $z$  direction for profile 2 with no solar cells mounted. The “hole” between 35 and 40 sec in the experimental data is due to magnetometer saturation*

In both case there is a good symmetry with respect to negative and positive profile.

#### 4.7.2 Solar Cell Mounted Panel

The same consideration can be made for the profile obtained with the panel with mounted solar cell (Fig. 59, Fig. 60).

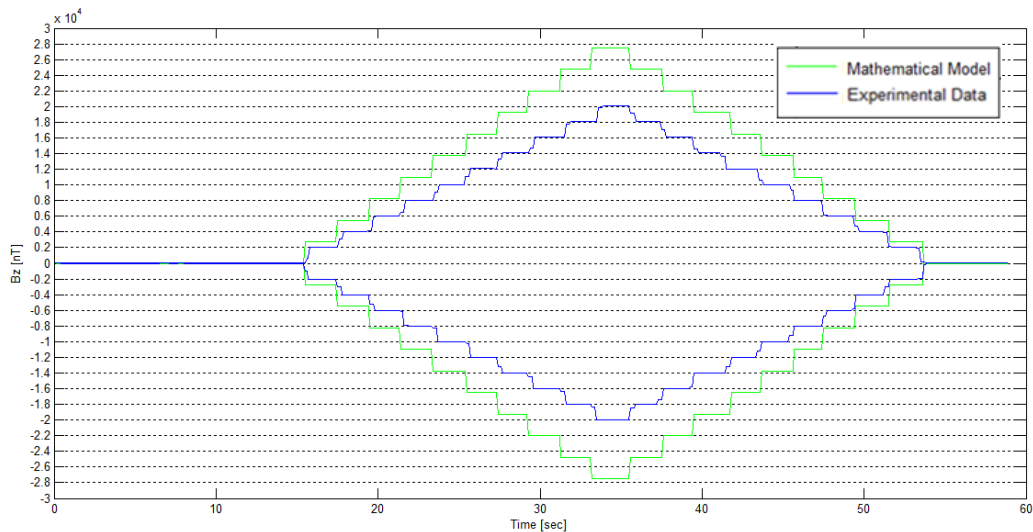


*Fig. 59 Magnetic flux in  $z$  direction for profile 1 with solar cells mounted*

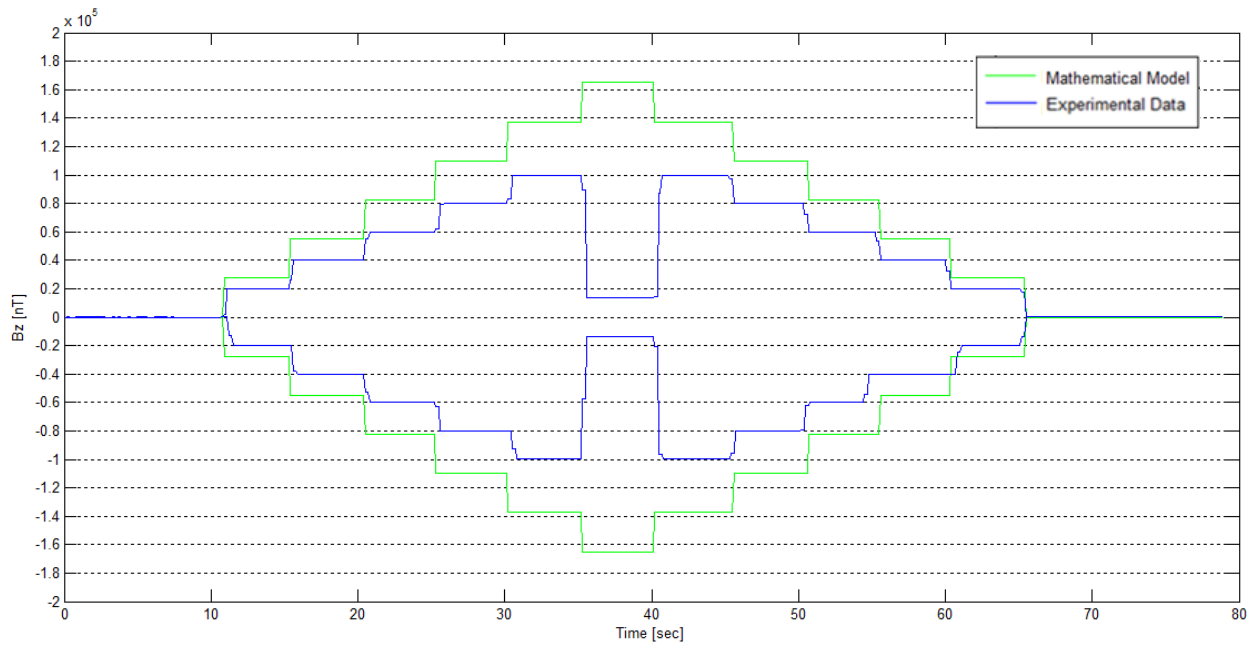


*Fig. 60 Magnetic flux in z direction for profile 2 with solar cells mounted. The “hole” between 35 and 40 sec in the experimental data is due to magnetometer saturation.*

Again the most important results can be obtained comparing the data for the two cases.

#### 4.7.3 Comparison between the two case

Comparing the profile obtained with the solar cell mounted and the solar cell not mounted it's possible again to observe a certain difference proportional to the magnitude of the magnetic field (Fig. 61). Again this effect is due to the diamagnetism of the solar cell.

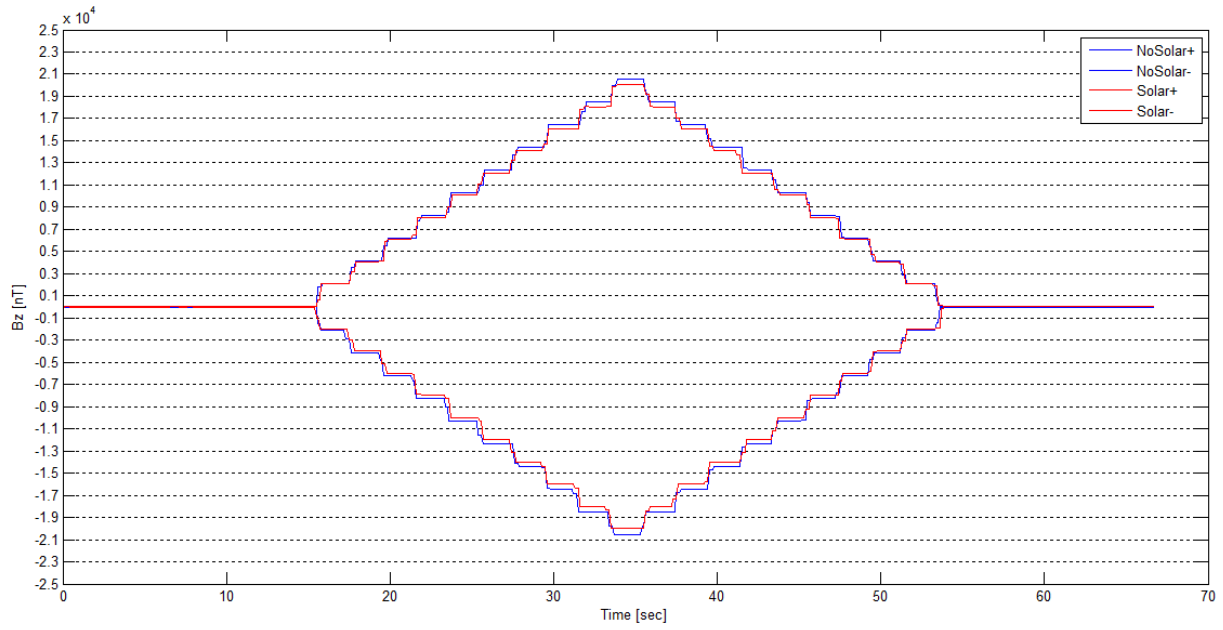


*Fig. 61 Comparison between solar cell and no solar cells mounted (Profile 1)*

The difference for the profile 1 is in the order of hundred nT (Fig. 62).

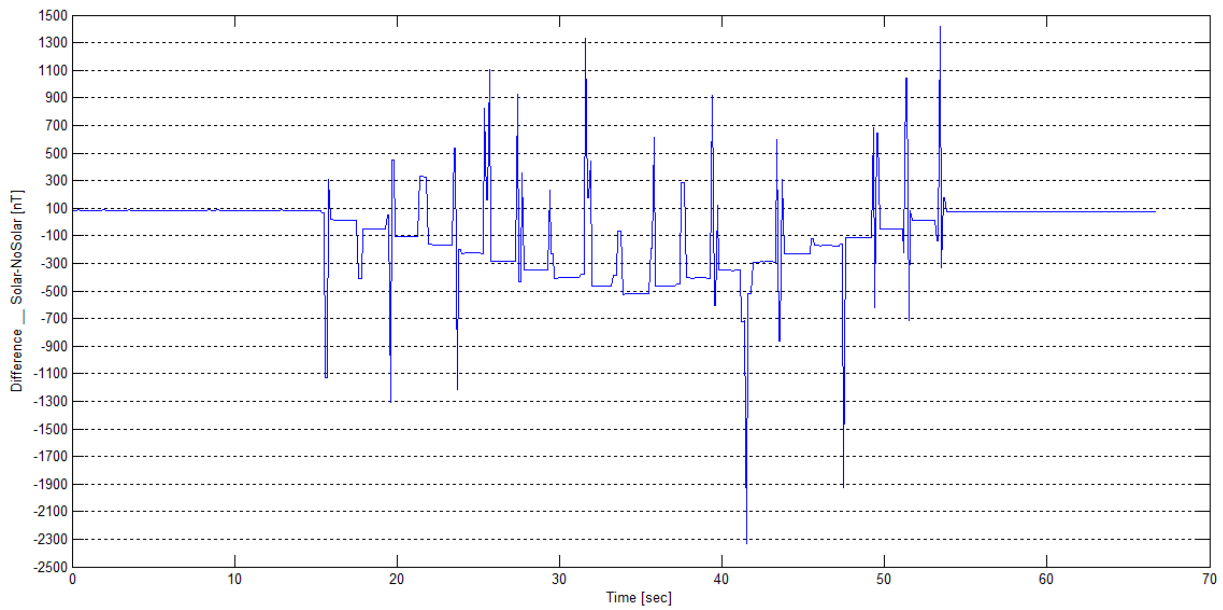


*Fig. 62 Magnetic flux difference between the two case (Profile 1)*

Same results are obtained for the profile 2 in which the difference is in the order of thousand nT (Fig. 64, Fig. 63).

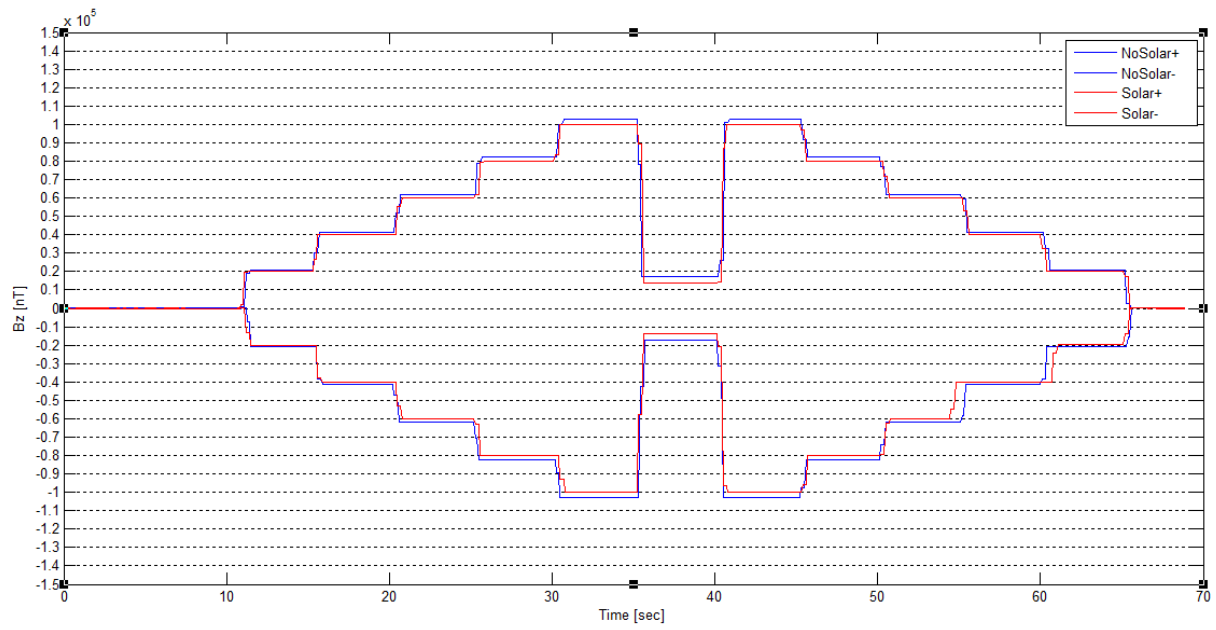


Fig. 63 Comparison between solar cell and no solar cells mounted (Profile 2). The “hole” between 35 and 40 sec is due to magnetometer saturation.

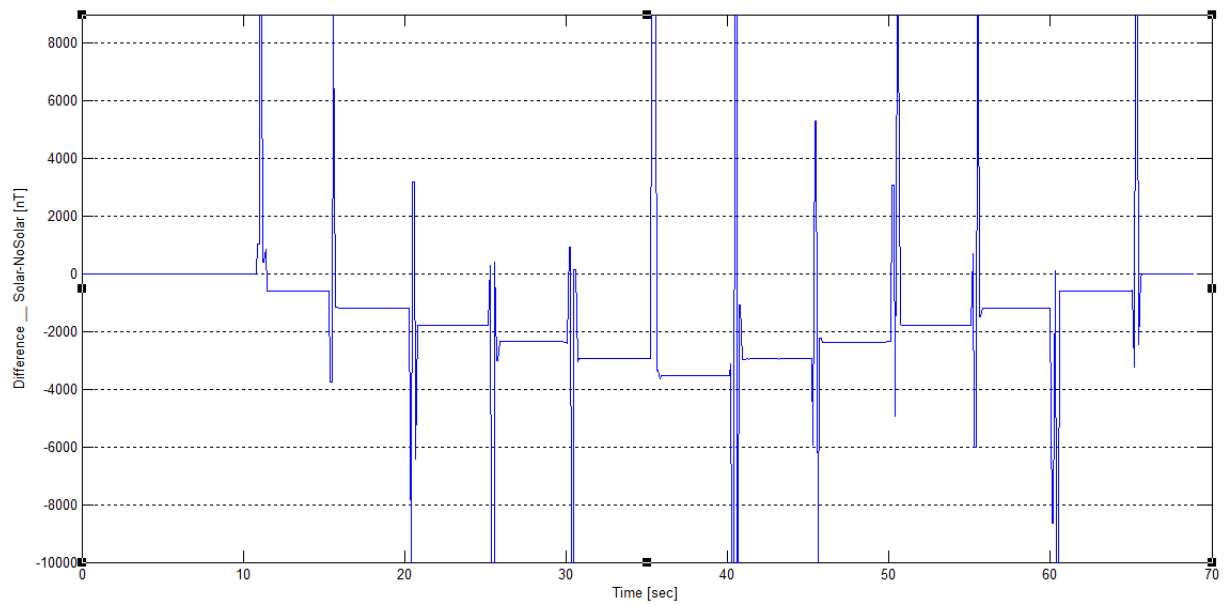


Fig. 64 Magnetic flux difference between the two case (Profile 2)

#### 4.7.4 Corrective parameters

The same procedures used to analyze data for the embedded coil is used to obtain value of the permeability for the case of embedded torquer.

Again appears the diamagnetism of the solar cell that reduces the permeability.

Comparing the artificial permeability for profile 1 it's possible to notice that in the case of solar cell mounted this is not constant (Fig. 65). The effect suggest that in the range of magnetic flux density obtained with the air core torquer (2000-20000 nT) is present a small ferromagnetic behavior of the solar cell in which the permeability slightly decrease increasing the magnetic field strength. This effect could explain the mistakes committed during the calibration procedure. However this effect is not observed in the range between 1000-8000 nT for the embedded coil.

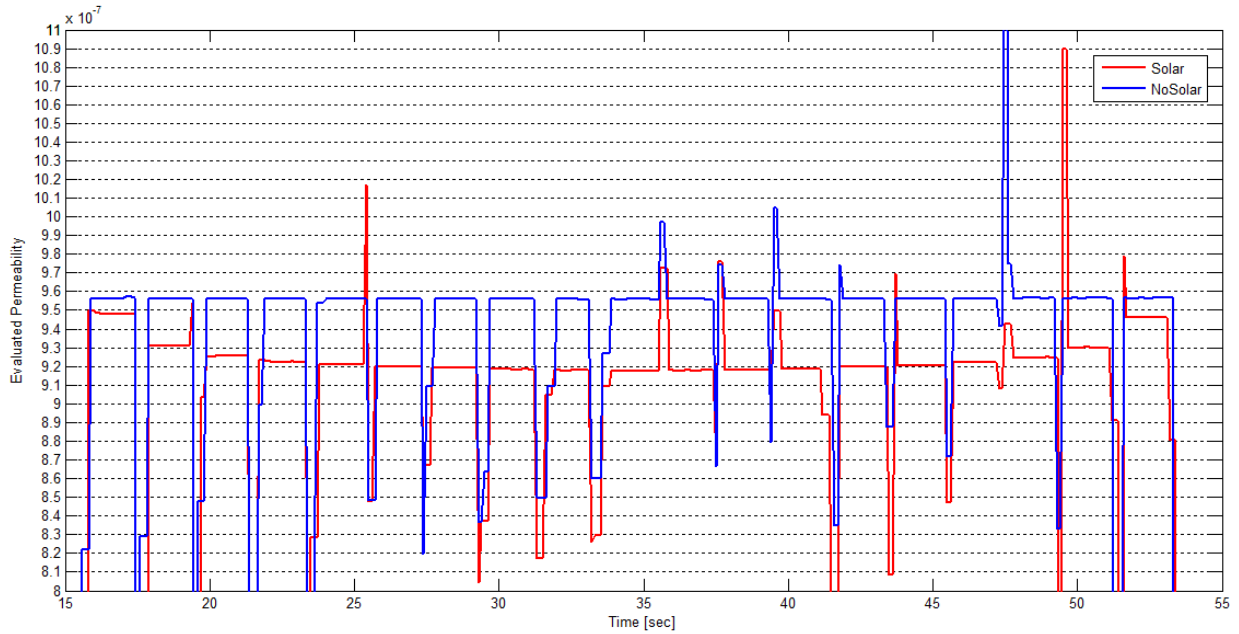


*Fig. 65 Evaluated permeability for air core experiment (Profile 1)*

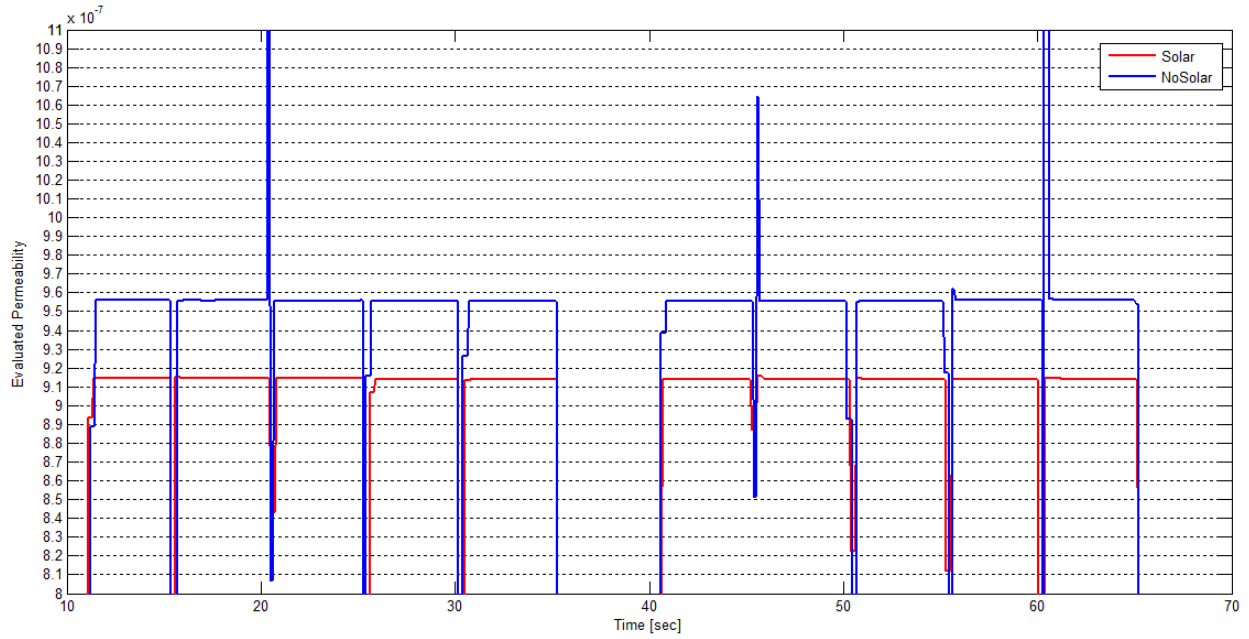


*Fig. 66 Evaluated permeability for air core experiment (Profile 2)*

The ratio between the permeability for profile 2 (Fig. 66, Fig. 67) (constant) is a little smaller than the case of the embedded coil being 0.957 instead of 0.971. Again this is a consequence of the effect observed in the permeability of profile 1 with the solar cell, in which at the lowest value basically corresponds the first step of profile 2 (Fig. 68).

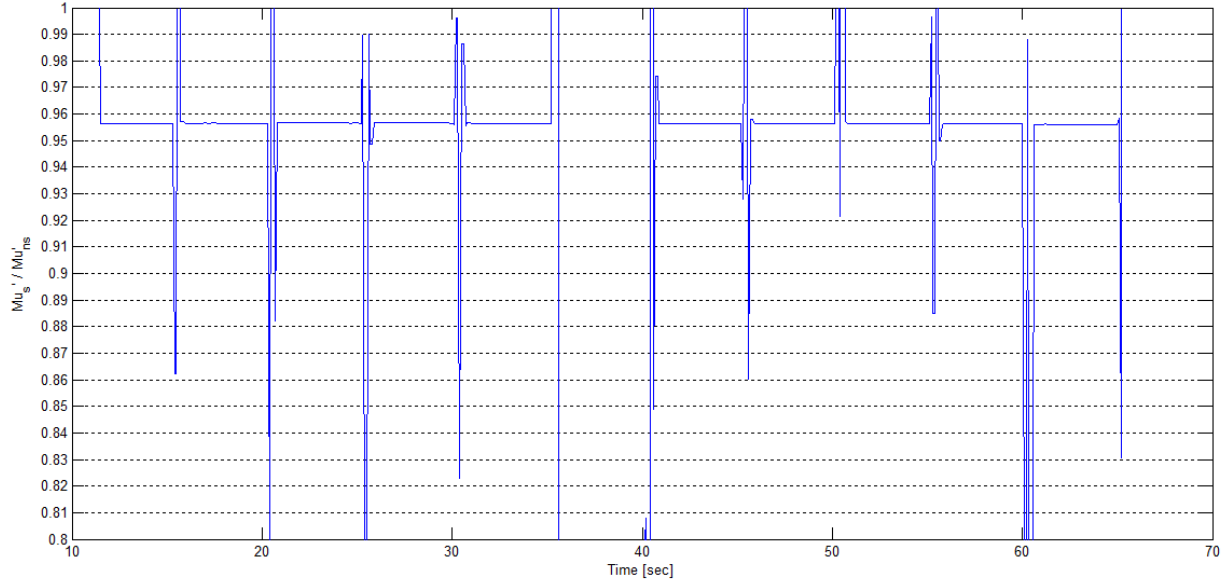


Fig. 67 Ratio between the artificial permeability in the two case (Solar cells / No-solar cells) - profile 2

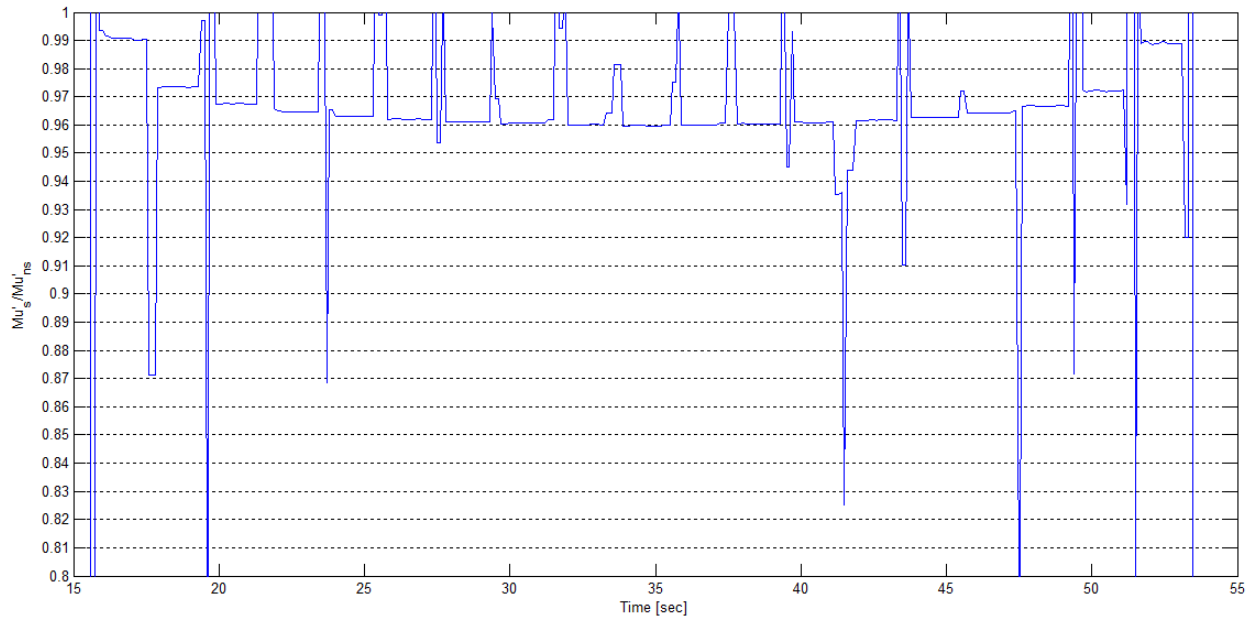


Fig. 68 Ratio between the artificial permeability in the two case (Solar cells / No-solar cells) - profile 1

Exploiting the same procedure used for embedded coil analysis:

$$\frac{\mu_s'}{\mu_0} = \mu_r' = 0.957$$



It's possible to extract an indicative value of the diamagnetic effect of the cell. This can be considered again as an artificial magnetic susceptibility of the solar cell applicable to have conservative correction factor to the magnetic field. Represented again by an empirical magnetic volume susceptibility  $\chi'_{vs}$

$$\chi'_{vs} = \mu'_r - 1 = -0.043$$

The value differs than the value obtained in the first analysis but still confirm the effect of the solar cell. The small difference can be however due to the difference setup and difference interference that were present in this setup: the air core is in general more affected by imperfection being wounded manually and more it's externally connected with the board. This two issues cause that the direction of the B field is less aligned with z axis with respect to the embedded coil resulting in a smaller measured component.

The artificial permeability for the board with mounted solar panels is  $0.915 \times 10^{-7}$  that consists in a relative permeability of 0.728. The value appears smaller than the previous value of 0.7544 for the embedded coil. As already said the difference is can be due to the manual winding of the coil that leads to misalignment of the vector: the value correctly represents that for manual wounded coil the difference between ideal and mathematical model and real case is bigger with respect to the embedded coil (manufactured by a machine). These lead to an artificial magnetic susceptibility equal to -0.272.

## 5. Torquerod magnetorquer

### 5.1 Description and Manufacturing

A torquerod magnetorquer exploits the same principles of an air core coil magnetorquer with two important differences: the shape of the coil is no more a wounded wire but is a solenoid inside which is placed a metal core. This is susceptible to the magnetic field produced by the coil and tends to magnetize itself thus generating an amplification effect on the dipole.

The advantage of this solution is that it's possible to amplify the magnetic dipole by many orders of magnitude to values not obtainable with air core magnetorquer. In spite of that it has to be taken into account the disadvantage of this solution, represented by the increase in mass and dimensions of the system and also by the difficulties introduced in the control law. Therefore torquerod is a convenient solution in terms of power consumption for generated dipole.

To manufacture a torquerod magnetorquer it's necessary to wind the wire around the core in order to create the exciting solenoid. In case of air core magnetorquer this procedure can be done manually due to the geometry of the system that facilitates the procedures. For a torquerod, in which it's necessary to create the spiral along the core, the procedure is much harder the thinner is the used wire: for proper wire section in the order of 0.1 mm the manual procedure is not feasible.

It's necessary to exploit in this case a winding machine.

The winding machine for a torque rod is mainly composed by three parts:

- Axial rotator
- Linear actuator
- Spool

The linear rotator consists in a support on which is mounted the core that rotates along its axis and carries out the operation of winding. The wire is guided by the linear actuator that moves the winding along the axis of the core. The velocity of the winding should be regulated in order to control the procedure and maintain the uniformity of the spiral. Similarly also the velocity of the linear actuator operates by determining the thickening of the spiral. In an ideal winding procedures it would

be necessary to accurately relate the rotation and translation velocity of the two actuators depending on the core diameter.

At the two ends of the core it's necessary to have the support that permits to interface the system with the structure and guide the wire to the input power. Depending on the ratio between the length and the radius of the core it's necessary to consider the possibility of an intermediate support: this because the fact of having a beam supported at the ends may cause excessive vibration and stress of the system. The intermediate support it's important to reduce the buckling length in the case of very elongated systems.

Once the winding has been made it's necessary to bond the wire as well as air core magnetorquer. Again several possibilities can be exploited varying in quality and cost. The best solution is to use self-bonding wire exploiting thermal treatment, or specific space qualified glue. In general could be risky to use kapton tape to wrap the winding because of the possibility to capture air particles in the space between different turns.

## 5.2 Torquerod Designing issues

The core of the torquerod has the key role in defining the efficiency of the system. As presented there are two possible materials to exploit, paramagnetic and ferromagnetic: each one has advantages and disadvantages with the respect to other (Tab. 1Tab. 7).

	<b>Ferromagnetic</b>	<b>Paramagnetic</b>
<b>Advantage</b>	High induced magnetic field	No residual dipole
<b>Disadvantage</b>	Presence of residual dipole	Really low induced magnetic field

*Tab. 7 Possible magnetic samples*

Paramagnetic materials have a really low susceptibility and the benefit in terms of magnetic dipole depends substantially on the volume of the core. The advantage of these materials is presented by the immediate demagnetization when the current is removed: that means that such a torquerod could be easily controlled with the same principles applied for an air core magnetorquer.

To understand the usefulness of a paramagnetic material for this application it is enough to compare for a single solenoid, the balance between the benefits in terms of the dipole generated and added mass. For that reason it's easy to evaluate the effective advantage of this solution with respect to the huge increase of mass.

As example let's took in consideration a solenoid with the following dimensions:

- Length: 80mm
- Radius of the single coil: 10mm
- Number of turns: 500
- Wire diameter: 0.16mm

These can be considered realistic dimensions for such kind of device.

Assuming no core inside, the magnetic dipole with a current of 363mA (5V voltage supply) can be evaluated as  $0.0143 \text{ Am}^2$  while the mass is 2.8 gr.

Inserting a paramagnetic core as a medium will increase the magnetic field as much as the magnetic susceptibility of the material. Assuming to look for the best compromise in term of magnetic susceptibility and density (weight) for the material of the core we can consider  $\chi_m=3.70 \times 10^{-3}$  and  $\rho=3250 \text{ kg/m}^3$  for a manganese sulfate (we do not consider the physical state of the material and it is taken as a rigid bar).

Exploiting the relation presented between the magnetization  $M$  and the  $H$  field and the volume of the sample we can obtain the magnetic dipole induced by the core equal to  $0.0000528 \text{ Am}^2$ . It appears obvious that there is no advantage in using this type of material since it would have a **total increase of the dipole equal to 0.37% increasing the mass of the system 7 times.**

This limit of paramagnetic materials make them not useful at all for the application, while it will be investigated the use of the ferromagnetic material as core of the torquerod.

Due to the wide range of ferromagnetic materials available it's important to analyze all the aspects connected to the operational use of torquerod. These are related to the problems of demagnetization, of control modes and mass.

### 5.2.1 Demagnetization Issues

One of the main problems in the use of a ferromagnetic core for a torque rod is the presence of the residual  $B$  field in the core. This feature creates many problems in

the controlling law of the system leading to the design of a specific circuit whose scope is to "turn off" the torquero.

While for an air core coil is enough to remove the current through it and eliminate the magnetic dipole and the magnetic flux, for a torquero the process is more complicated: it's necessary to reach the condition in which both the H field applied (controlled by the current through the device) and the B field in the core are restored to zero.

The complete demagnetization of the core occurs when the temperature is brought over curie temperature, clearly not feasible in this kind of application. A quite similar demagnetization could anyway be obtained alternating different H field with decreasing intensity creating multiple cycles like in Fig. 69 [12]. This process could be quite hard and not cost effective in terms of power consumption. It would be in fact necessary to reverse the current many time reaching the negative value of the saturation to obtain the complete demagnetization of the core.

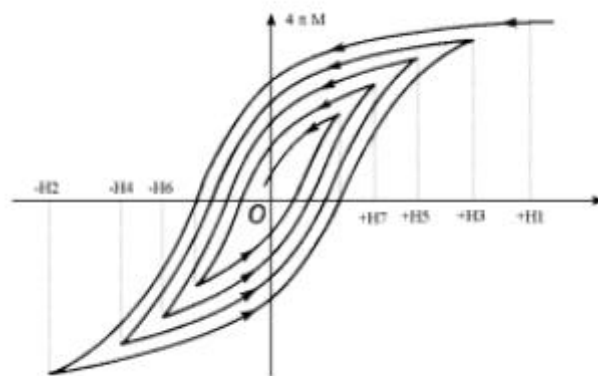
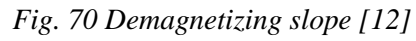
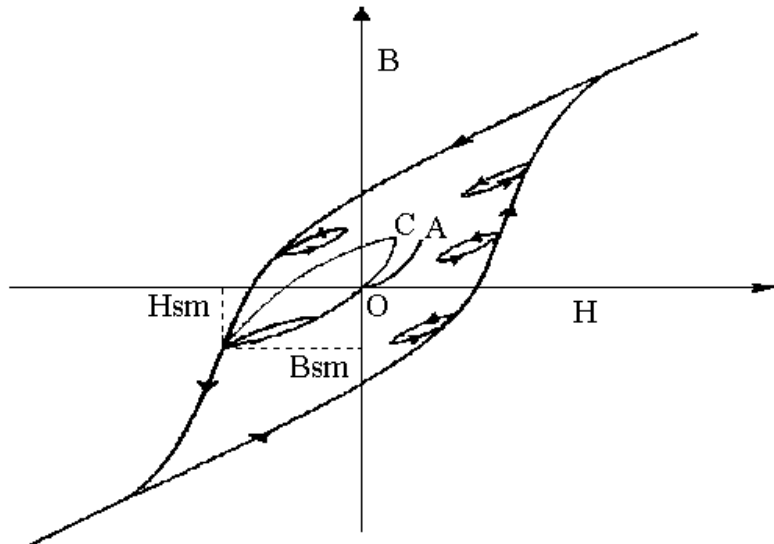


Fig. 69 Example of minor hysteresis cycles [12]

The idea to resolve this issue is to exploit the minor hysteresis cycle. Taking in consideration the demagnetization slope of a ferromagnetic material it's observed that varying the H field properly it's possible to obtain small cycles contained in the main one.



As obvious the idea is to define a specific Hsm to which bring the ferromagnetic core and then move on the minor cycle Bsm-O reaching the condition of  $H=0$  and  $B=0$  (Fig. 71);



*Fig. 71 Example of apparent demagnetization exploiting minor hysteresis cycle [12]*

This procedure for demagnetizing the torquerod lead to a macroscopic demagnetization and it doesn't correspond to a correct and complete demagnetization obtainable with the other methods. The main problem consists in the fact that a further magnetization would follow a different slope that is the slope OC bringing eventually to unexpected behavior of the device. Nevertheless, using a soft magnetic material, this issue can be reasonably neglected since the magnetic behavior is reestablished every time the core is lead to saturation: using the torquerod always in saturation regime it's possible to have a replicable hysteresis curve even after the incomplete demagnetization process. Soft ferromagnetic materials are the best solution because of their low coercivity and high permeability that consists in easy magnetization and demagnetization.

The presence of residual dipole can be acceptable if it's in the order of the total residual dipole of the complete satellite.

### 5.2.2 Mass

In a torquerod the core represents the element with the greatest impact on the mass of the whole device. For a fixed geometry defined by the requested performance this aspect could be improved choosing a low density material. In general soft ferromagnetic sample are composed the most by NiFe alloys and CoFe alloys with

a density that can vary from  $7500 \text{ Kg/m}^3$  to  $8700 \text{ Kg/m}^3$ , showing therefore few margin for mass reduction: for this reason, this issue affects less the considerations that must be made for the choice of the core.

### 5.2.3 Control mode

Among soft ferromagnetic materials there are different alloys that present different characteristics depending strictly to their composition.

Choosing the proper core depends on many factor related to the control mode of the torquerod.

To maximize the generated dipole and so the efficiency of the device it has to be as high as possible the induced B field for a defined H field. Apparently this means to have a material with the highest relative permeability. In general this aspect is not sufficient to find the best solution because there are many issues related to the operating modes of the devices that could lead to completely different choice.

Depending on its operative method (DC or AC, saturation) there are several aspects to be considered.

To justify the increase in mass and dimension due to the choice of the torquerod instead to an air core torque it's reasonable to think that this device has to be used the most in saturation region. In this way it's possible to maximize the advantage in term of magnetic dipole obtainable with the minimum current provided. This operative method also simplifies the controlling law as the device is controlled in similar to ON-OFF regime. There are also other important issues that lead to this consideration connected to the problem of demagnetization procedure. As already said, to demagnetize the core in an easy and fast way it can be brought it to a specific H field that generate the slope OC to reach the condition  $B=H=0$ . The problem of this method is that the further magnetization would not follow the nominal magnetization slope. This problem is greater when the further magnetization is in the opposite direction of the previous as the generated dipole could not correspond to the expected one. The way to reestablish an almost well-known behavior is to bring again the magnetization to saturation. It's clear that using the torquerod always in saturation significantly reduces the uncertainty on the working points of the core in the B-H loop.

Another important issue that drive the choice of the material depending to its operative method is connected to the provided current: for DC applications the



main consideration for material selection is most likely to be the permeability and the saturation induced magnetic flux. In this case the material is kept magnetized by a constant current in the solenoid for a defined time, while demagnetized at the end of the operation. In this case we can consider negligible the time in which the magnetic flux change with the respect to the time it's kept fixed at the saturation level, and for that reason, the frequency loss has less importance then the consumption during the activation. Having high permeability drastically reduces the power consumption for a requested dipole.

For instance, for AC provided, the important consideration is how much energy is lost in the system as the material is cycled around its hysteresis loop. The energy has already said is originated from three different sources:

- The hysteresis loss related to the area contained in the loop.
- Eddy current loss, which is related to the generation of electric currents in the magnetic material and the associated resistive losses
- Structural loss, which is related to the movement of domain walls within the material.

Hysteresis losses can be reduced exploiting materials with really thin loop area that consists in a low coercivity. Eddy current losses can be reduced by decreasing the electrical conductivity of the material and by laminating it. And then structural losses can be reduced by having a completely homogeneous material, within which there will be no hindrance to the motion of domain walls.

In spite of that the permeability strongly decreases increasing the frequency of the exciting H field. This issue could get really significant in case of really high frequency. Even though the AC supply for a magnetorquer is not very common and, also in the case of PWM supply, frequencies are sufficiently low to consider the system in DC.

#### **5.2.4 Choice of the core material**

As it can appear obvious, soft ferromagnetic materials are the best solution for the core. Among these it's important to find the one satisfy the following requirements (Tab. 8) in order to have great flexibility in the operative method and best performances:

Maximum dipole generated	High relative permeability High induced magnetic field saturation
Minimize hysteresis loss	Thin hysteresis cycle area B-H relation as much possible similar to linear function
Easy demagnetization/magnetization	Low coercivity value High relative permeability

*Tab. 8 Core's choice requirements*

By conducting a thorough search among the various suppliers of these materials has been observed that hardly it's possible to find complete data on the hysteresis curve. The producers provide as evaluation parameter the major point of the loops as saturation B field, coercive force and initial and maximum permeability.

One of the first observations that can be made concerns the relation between relative permeability, saturation magnetic field and coercive force depending to the alloy composition.

NiFe alloys present higher sensibility, represented by the higher permeability, but lower saturation magnetic field. The opposite happens for CoFe alloys where the strength of the magnetic flux it's higher at the expense of a lower global permeability (Fig. 72).

	<b>Sensitivity (permeability)</b>	<b>Strength (flux density)</b>	<b>Cost</b>
<b>Highest</b>	Nickel-Iron	Iron-Cobalt	Iron-Cobalt
	Silicon Iron	Iron	Nickel-Iron
	Iron	Silicon Iron	Ferritic Stainless
	Iron-Cobalt	Ferritic Stainless	Silicon Iron
<b>Lowest</b>	Ferritic Stainless	Nickel-Iron	Iron

*Fig. 72 Resume table for main ferromagnetic materials [13]*

Different supplier has been examined in order to collect the most available data on material's magnetic properties (Tab. 9). Among the suppliers have been taken in consideration only the ones which provide bar with proper diameter for the application in a torquerod.

The shape of the material is one of the most critical problems because the magnetic properties vary depending on it. All the data acquired by experimental procedures are based on toroidal strip-wound cores with defined thickness.

Name	B <sub>sat</sub> [T]	H <sub>c</sub> [A/m]	μ <sub>i</sub>	μ <sub>max</sub>	ρ [Kg/m <sup>3</sup> ]	T <sub>c</sub> [°C]	σ [Ohm m]
EFI ALLOY 50	1,450	4,770	NA	100000	8165,000	450,000	4,821E-07
EFI Alloy 79	0,870	1,190	NA	230000	8746,000	460,000	6,550E-07
Hiperco 50A	2,400	32,000	NA	15000	8110,000	940,000	4,006E-07
RdioMetal 4550	1,600	8,000	6000	40000	8250,000	450,000	4,489E-07
Magnifer 7904	0,800	1,100	180000	350000	8700,000	410,000	5,802E-07
Magnifer 50	1,550	8,000	10000	50000	8250,000	470,000	4,655E-07
Mumetall	0,800	1,500	60000	250000	8700,000	400,000	5,500E-07
Vacoper100	0,740	1,000	200000	350000	8700,000	360,000	6,000E-07
Permenorm 5000H2	1,550	5,000	7000	120000	8250,000	440,000	4,500E-07
Permenorm 5000V5	1,550	4,000	9000	135000	8250,000	440,000	4,500E-07
Permenorm 5000S4	1,600	2,500	15000	150000	8250,000	500,000	4,000E-07
Permenorm 3601 K5	1,300	10,000	4000	50000	8150,000	250,000	7,500E-07
Megaperm 40L	1,480	6,000	6000	80000	8200,000	310,000	6,000E-07
Trafoperm n3	2,03	20,000	1000	30000	7650,000	750,000	4,000E-07
Vacofer s1	2,15	6,000	2000	40000	7870,000	770,000	1,000E-07
Mumetal	0,75	0,400	na	470000	8700,000	420,000	6,000E-07
Supra 50	1,5	5,000	na	200000	8200,000	450,000	4,500E-07

*Tab. 9 Commercial soft ferromagnetic samples [14] [15] [16] [17]*

Observing the table it's possible to put on evidence the relation between the parameter described above: higher magnetic saturation field corresponds to higher coercivity and lower permeability. In order to have a core easy magnetizable and demagnetizable and more flexible it's good to look for the lower coercivity and higher permeability that means higher sensitivity of the device.

Nevertheless it has to be considered that the value of coercivity generally tends to increase for bar shape of the material.

When the exiting current vary with a certain frequency it's possible to observe a general decrease of the permeability and increase of the coercivity. The loop tends to get wider and increasing the hysteresis loop.

This behavior can be observed in the following graphs referred to Magnifer 7904 (Fig. 73, Fig. 74).

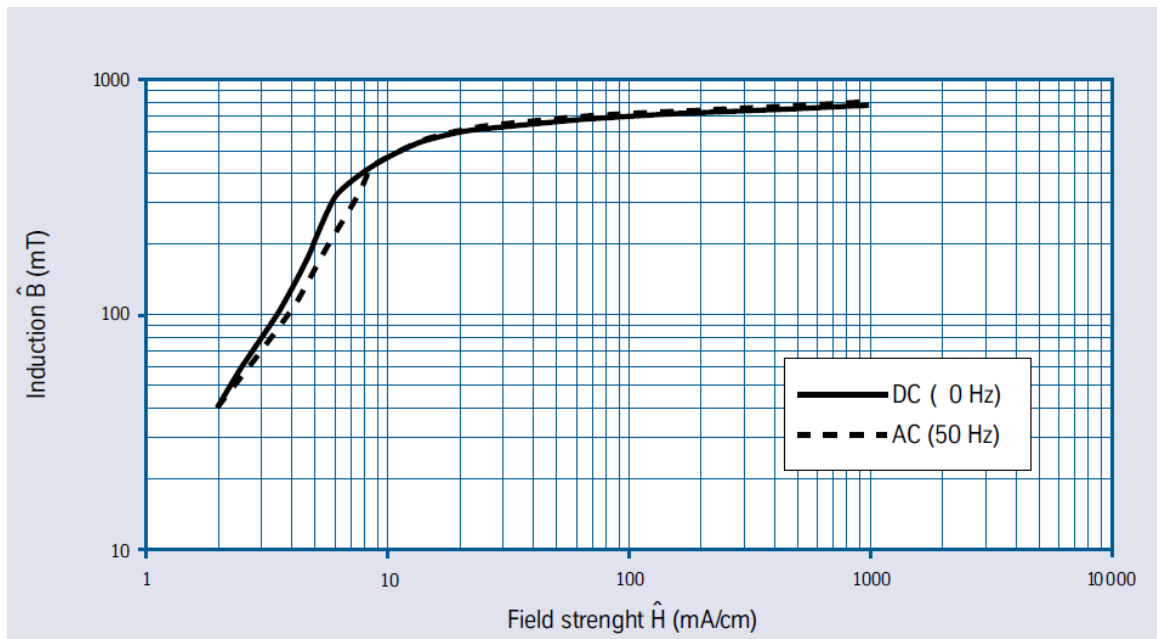


Fig. 73 Magnifer 7904 characteristic slope [16]

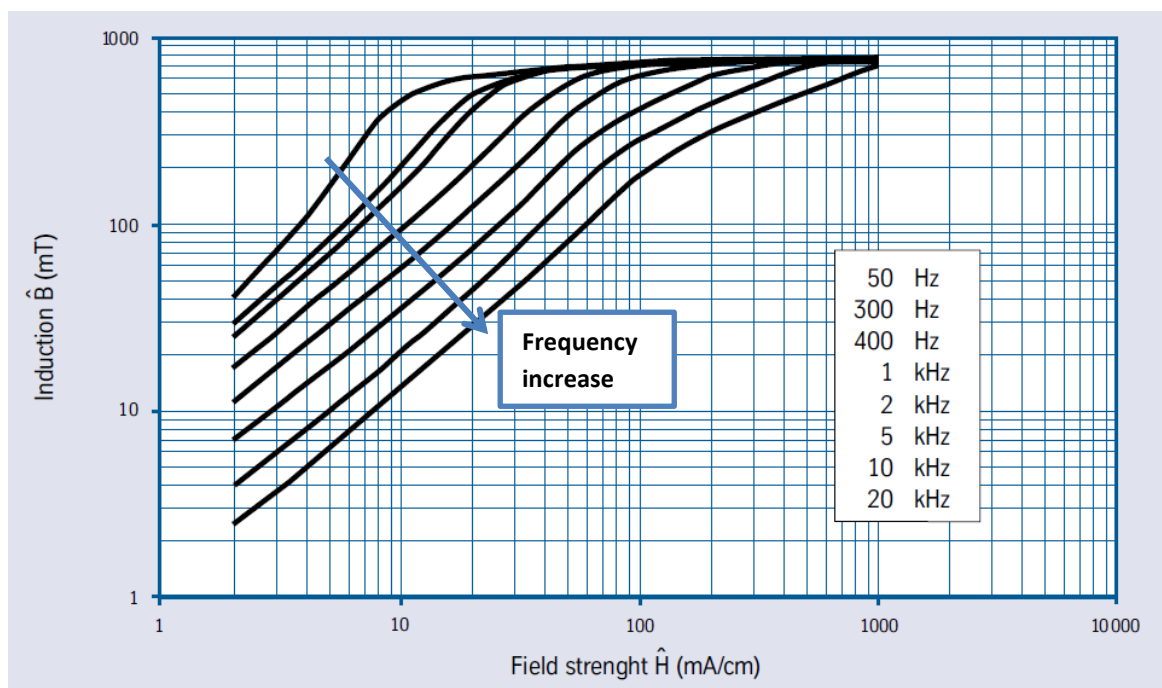


Fig. 74 Magnifer 7904 permeability variation with respect to frequency [16]

This issue has to be taken into account if the torquerod works at AC where the slope relaxation consists in general in higher power consumption. As already said, for most of nanosatellite applications, is not practical to consider AC for electronic devices. The magnetorquer are in general driven with direct current in ON/OFF operative regime. The supply exploiting PWM for a magnetorquer has generally a frequency lower than 44 Hz: as it's possible to see there is no significant effect on the hysteresis curve for this range of frequency, thus the assumption of DC can be maintained.

The variability of the hysteresis curves shows that it is generally very difficult to obtain accurate data for sizing the torquerod. Some values that allow the quantitative estimates of the maximum in the design phase can be taken from the datasheet of the supplier. However it must always to carry out tests on the prototype to be able to characterize the behavior for the desired operating mode.

### 5.3 Dimensioning equation for torquerod

Designing a torquerod involves more difficulties with respect to the design of an air core magnetorquer.

The introduction of the core leads to an increase in mass and magnetic dipole depending to its volume and not linearly to its shape. The same issues presented for an air core magnetorquer design are always presents because the fundamental parameter are still dependent to the coil winding around the core. To this it must be added the constructive parameters of the core that, as already said, introduce additional variables.

In this case therefore becomes even more important to set the maximum number of constraints and performance requirements in order to optimize around this requested operative condition.

The magnetic behavior of samples does not only depend on its intrinsic properties but also on its shape and dimensions connected to the demagnetizing factor.

The magnetic dipole can be expressed as the sum of the dipole due to the solenoid and the dipole introduced by the core's magnetization:

$$m = NIS + V_c M$$

Where  $V_c$  is the volume of the core,  $S$  the area of the solenoid,  $N$  the number of turns,  $I$  the current and  $M$  the magnetization of the core. Assuming the thin wire negligible with respect to the dimension of the core  $S$  is equal for the solenoid and the core.

Then the  $V_c$  and  $S$  can be rewritten:

$$m = \pi r^2 (lM + NI)$$

Increasing the efficiency of the torquerod is related to the increase of  $M$  for a defined  $H$  field, i.e. a defined current.

For a cylindrical core  $N_d$  can be evaluated [18]

$$N_d = \frac{4 \left[ \ln \left( \frac{l}{r} \right) - 1 \right]}{\left( \frac{l}{r} \right)^2 - 4 \ln \left( \frac{l}{r} \right)}$$

Where  $r$  and  $l$  are the radius and the length of the core.

The magnetic flux strength is:

$$H_c = \frac{NI}{l} - N_d M$$

Where  $\frac{NI}{l}$  is the  $H$  field generated with the solenoid.

$M$  is equal to:

$$M = \frac{\frac{NI}{l} - H_c}{N_d}$$

The geometry of the core it's important thus it affects its magnetization. To reduce the demagnetization effect it has to be defined the proper  $l/r$  factor of the core.

Increasing the  $l/r$  ratio the demagnetizing factor will decrease tending to zero (Fig. 75).

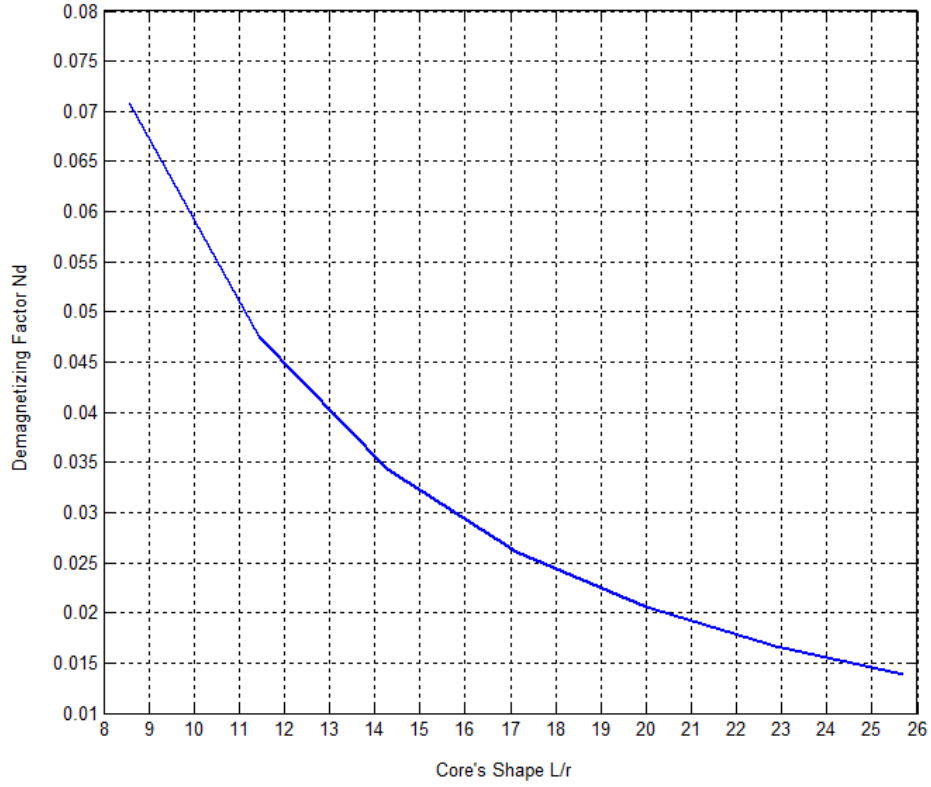


*Fig. 75 Demagnetizing factor dependence on L/r ratio*

Assuming a linear relation within B and H it's possible to write:

$$H_c = \frac{B}{\mu_0 \mu_r}$$

This idealization can be made to find a linear relation useful to define the performance of the system.

B can be rewritten as:

$$B = \frac{\mu_0 \mu_r NI}{l(1 - N_d + \mu_r N_d)}$$

The formula permits to relate the magnetic field induced with the current provided and the shape of the core. Taking in consideration the fundamental relation:

$$B = \mu_0 (H_c + M)$$

It's possible to obtain M as function of I,  $N_d$  and the properties of the material.

$$M = \frac{NI(\mu_r - 1)}{l(1 - N_d + \mu_r N_d)}$$

Through that it's possible to obtain the final expression for the magnetic moment of the solenoid with the core rod:

$$m = NI\pi r^2 + \frac{\pi r^2 NI(\mu_r - 1)}{(1 - N_d + \mu_r N_d)}$$

The formula is fundamental to relate the efficiency of the rod to the material properties, the core's shape and the provided current of the solenoid.

Thorough that formula is easy to put on evidence the geometric parameters that affect the magnetic dipole: the volume of the core and the shape are directly involved in the equation, the first determine the magnitude of the magnetic dipole effect due to the core, the second affects the magnetization of the core for a defined current, that can be considered similar to the efficiency of the core.

For a defined volume of the core it's possible again to observe the global effect of the geometric choices in the efficiency of the device: isolating the core effect in the equation appears the term in parenthesis:

$$m = NI\pi G$$

Where G can be assumed as a geometric parameter that contains the shape of the core and its magnetic properties.

$$G = \left( r^2 + \frac{r^2(\mu_r - 1)}{(1 - N_d + \mu_r N_d)} \right)$$

Considering a defined volume for the core, r can be expressed as function of l/r as well as  $N_d$ .



$$r = \sqrt[3]{\frac{V}{\pi \left(\frac{l}{r}\right)}} \quad N_d = \frac{4 \left[ \ln \left( \frac{l}{r} \right) - 1 \right]}{\left( \frac{l}{r} \right)^2 - 4 \ln \left( \frac{l}{r} \right)}$$

The relation is quasi-linear, suggesting that in order to increase the efficiency of the core it has to be longer and thin (Fig. 76). This issue is really important because put limits to the use of this device. In order to have higher dipole it's necessary to have bigger volume but, maintaining a high value of  $l/r$ , the limit is due to the dimension of the satellite. For a CubeSat the total length can't be bigger than 80/85mm considering the dimensional constraints of the inner volume of the satellite.

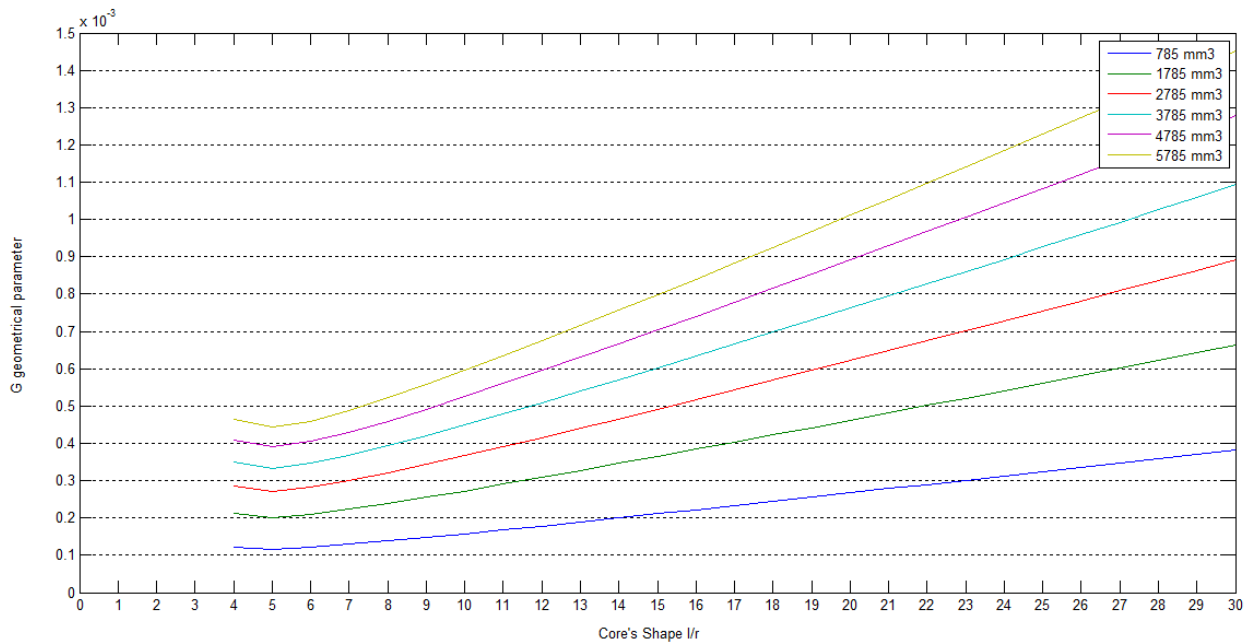


*Fig. 76 Geometric parameter for different volumes of the core*

The first analysis would take in consideration the effect of the core's shape on the performance in order to define the guideline for the proper dimension and size to look for.

To do that it's not a bad assumption to exploit the data obtained for sizing the air core magnetorquer to define the best compromise for wire's diameter regarding power consumption and magnetic dipole. In that way it's possible to eliminate a

variable from the problems and observe the different solution obtainable varying the core's shape and the provided current.

The material considered is an alloy 79 characterized by the lowest coercivity. There is an important issues related to the material properties: contacting the material providers has been underlined that the data provided are obtained through experimental measures lead on toroidal thick wounded core. The data strongly differs when the shape of the core changes as well as the hysteresis curve. For that reason it's important to understand that the data obtained represent an indication of the performance of the system from a quality point of view. Unfortunately there are no possibilities to obtain magnetic property for a material for a defined geometry without carrying on experimental measures.

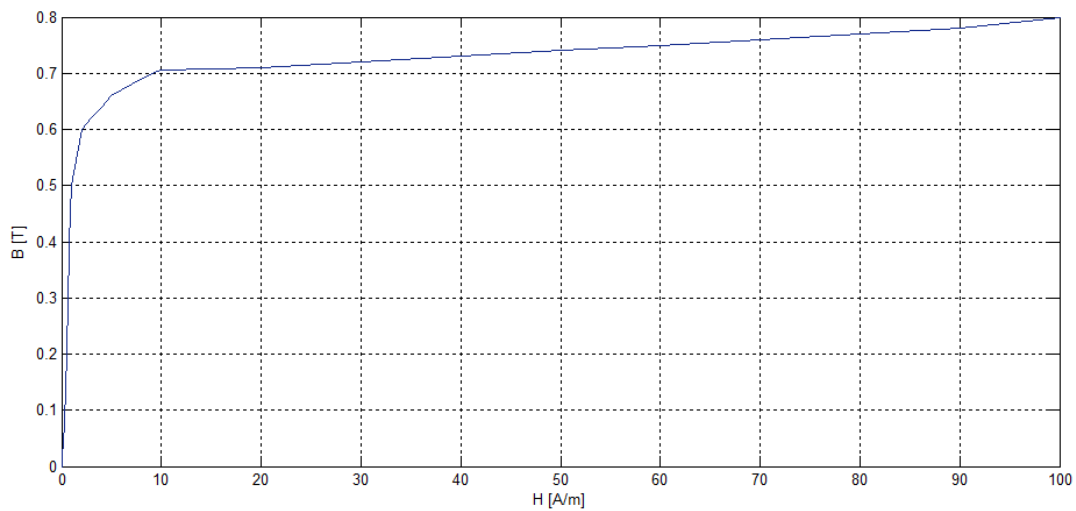


*Fig. 77 Alloy 79 first magnetization curve [16]*

From the datasheet it's possible to obtain the curve of first magnetization of the material (Fig. 77). Because of the choice of a soft ferromagnetic material, the initial part of the slope that represents the range of interest is can be simplified: assuming the magnetorquer to work in this region the relation between B and H can be assumed linear and the permeability for the equation (that represents the angular coefficient) can be obtained graphically.

The idea is to define the core and turning the wire in order to cover the whole surface of the core, in that way the number of turns would be automatically determined depending of the core's shape and dimensions reducing to this as the only observed variable.

Solving the equation for different voltage supply provided it's possible to observe the different effect of the design choice for the torquerod (Fig. 78). The data are related to a fixed radius of the cylindrical core equal to 7mm and a variable length compatible with CubeSat dimensions.

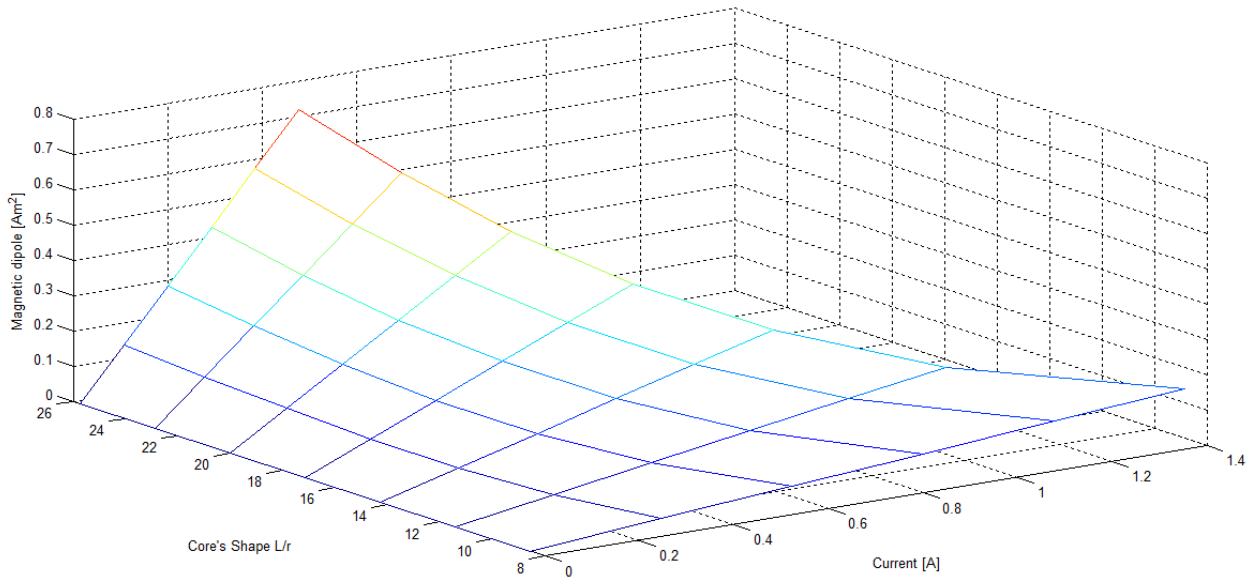
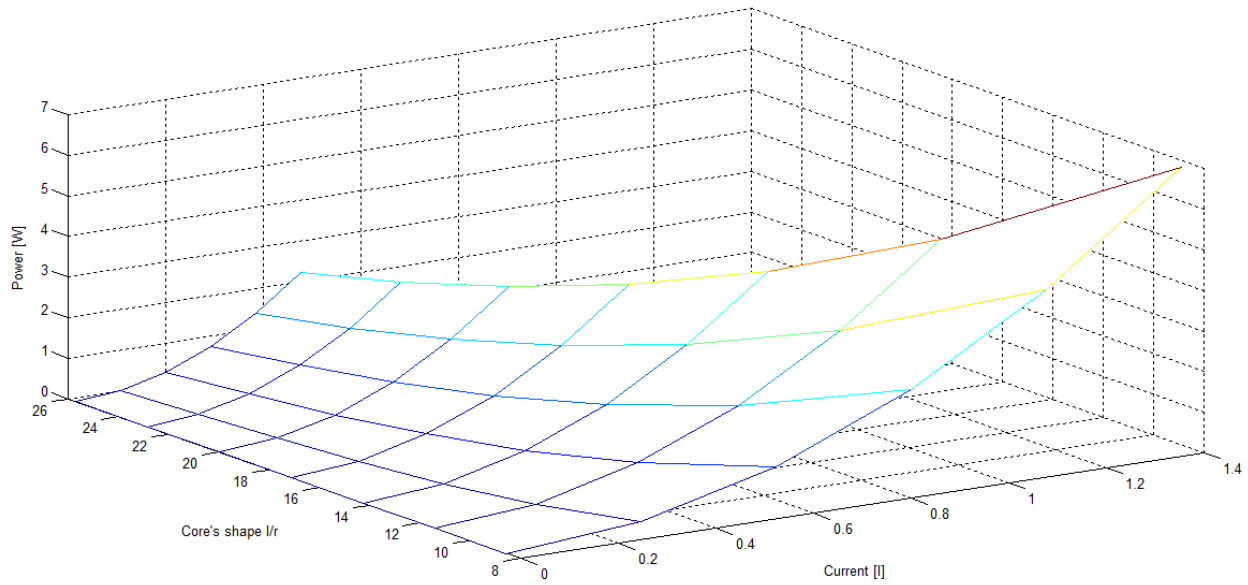


Fig. 78 Magnetic dipole dependence for different core's shape

As obvious the magnetic dipole increase with the current but the effects of core's shape is not negligible: a thin core characterized by high  $l/r$  ratio improves the performance of the rod reducing the demagnetizing factor. The values of the dipole are in general higher than the typical values of an air core torquer as expected. Nevertheless, higher values of the dipole are related to higher values of the power consumption: also in this case the shape of the core strictly determines the power consumption curve depending on the current (Fig. 79).



*Fig. 79 Power consumption dependence for different core's shape*

The core's ratio  $L/r$  has to be maximum in order to reduce the Power consumption and increase the magnetic dipole. Once the proper dimension has been defined it's possible to rescale the system for different satellite standards. The limits are due to the available maximum length for the core. **It's important to observe the magnetic dipole depends on the volume of the core that's why the shape of the core has to be defined according to a proper volume that permits to achieve a specific dipole moment.**

The relation between power consumption and magnetic dipole depending to the core's shape and the provided voltage is showed in the graph below where the full line represents the power and the dotted line represents the magnetic dipole (Fig. 80).

**The target is to minimize the gap between the two curves by acting on the geometry of the core.**

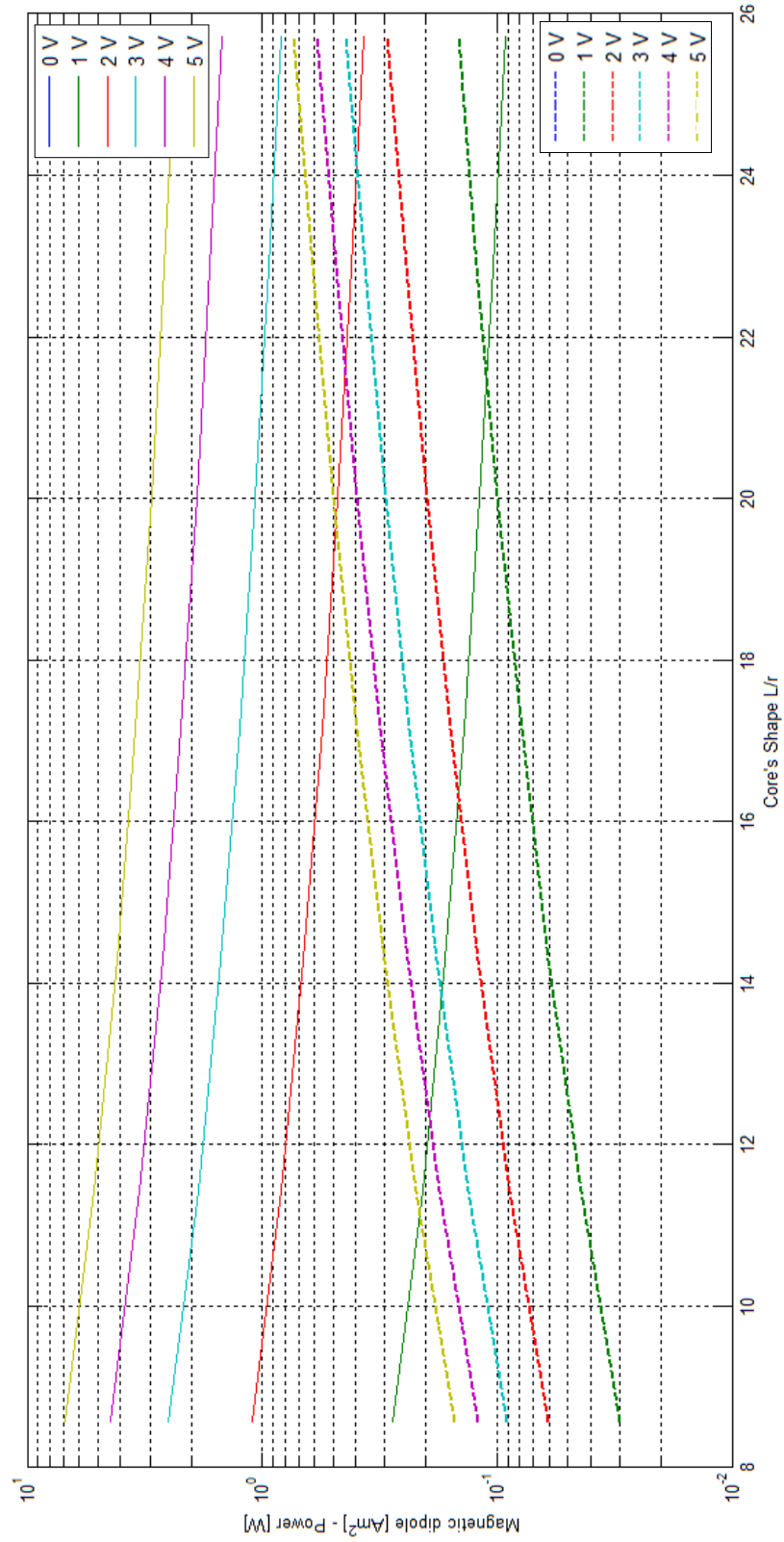
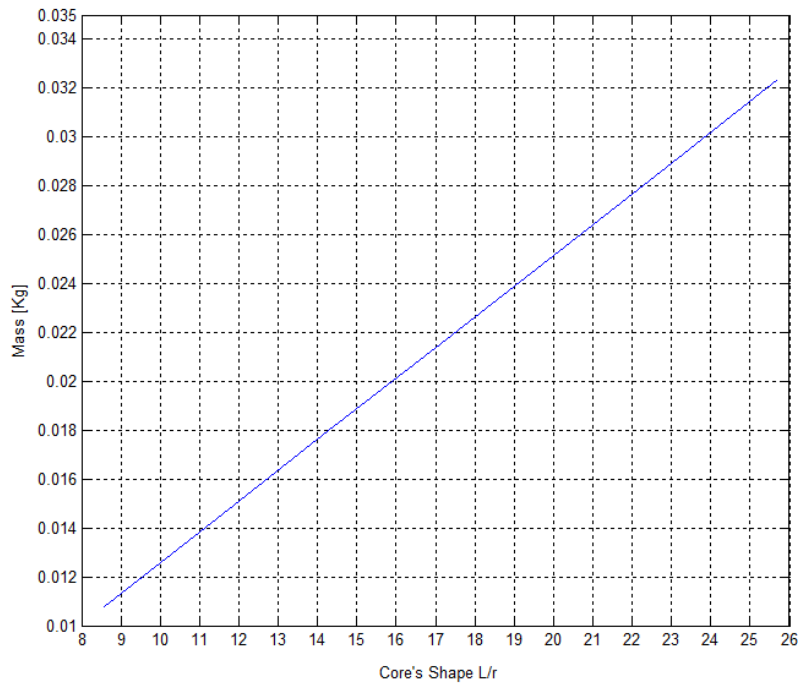


Fig. 80 Magnetic dipole and power consumption magnitude for different core's shape: the dotted line represents the magnetic dipole while the continuous line represents the power consumption, both according to different voltage supply.

As obvious the volume of the core determines the increase of volume of the system rod+solenoid. Referring to the case of fixed radius of 7mm, the mass would increase linearly (Fig. 81). The higher contribution is related to the high density material of the core.



*Fig. 81 Mass relation depending on core's shape*

Observing the previous equation and graphs it appears clearly the function and the main geometrical parameter that the core has to satisfy:

- Increase the volume to increase the strength of the system
- Increase the L/r ratio to reduce the demagnetizing factor

Both this aspects are strictly related to the constraints the system has to satisfy in terms of mass and dimension. As already said for air core magnetorquer, normally in CubeSat application there is not much flexibility for this 2 parameter and consequently for core's dimensioning. Besides that, the shape and the size of the ferromagnets are limited from the supplier: standard measure of cylindrical core available on the shelf reduces the possibility to decide a specific shape and dimension.

Whether possible the core's choice should respect the following guide line:

- NiFe alloy with low coercivity and high sensibility.
- Proper volume to maximize the magnetic dipole depending on mass and volume constraints
- Elongated shape to reduce demagnetizing factor

The result of this consideration is that, again, the parameters that can offer the highest flexibility in determining the system performances are (besides the choice of the material) the wire size and the manufacturing in terms of number of turns.

This reconfirms the design procedure of a torquerod to the same procedure used for air core and embedded coil, in which the starting parameter where the dimensions and the voltage supply.

The difference with these has to be researched in the operating region of the core not present for the previous magnetorquer: in this case, for certain combination of dimensions and power provided the core could get working in not linear region and saturation region with consequent behavior to determine.

Considering the same ferromagnetic core exploited for the previous analysis it is possible to fix the dimensions and shape considering both available products both realistic constraints in a CubeSat application.

Assuming a core of 10 mm as radius and 80mm long, it's studied the resulting magnetic flux density exploiting the equation presented above. The current is determined automatically setting the voltage supply for the system: in order to look for maximum reachable value of the B field this would be 5 V, realistic value in case of constant supply or PWM.

With this assumption the magnetic flux density it's not determined by the number of turns that is canceled in the equation being in I

$$B = \frac{\mu_0 \mu_r N \frac{V}{NC}}{l(1 - N_d + \mu_r N_d)}$$

For defined core, the magnetic flux density is function of the wire only (Fig. 82):

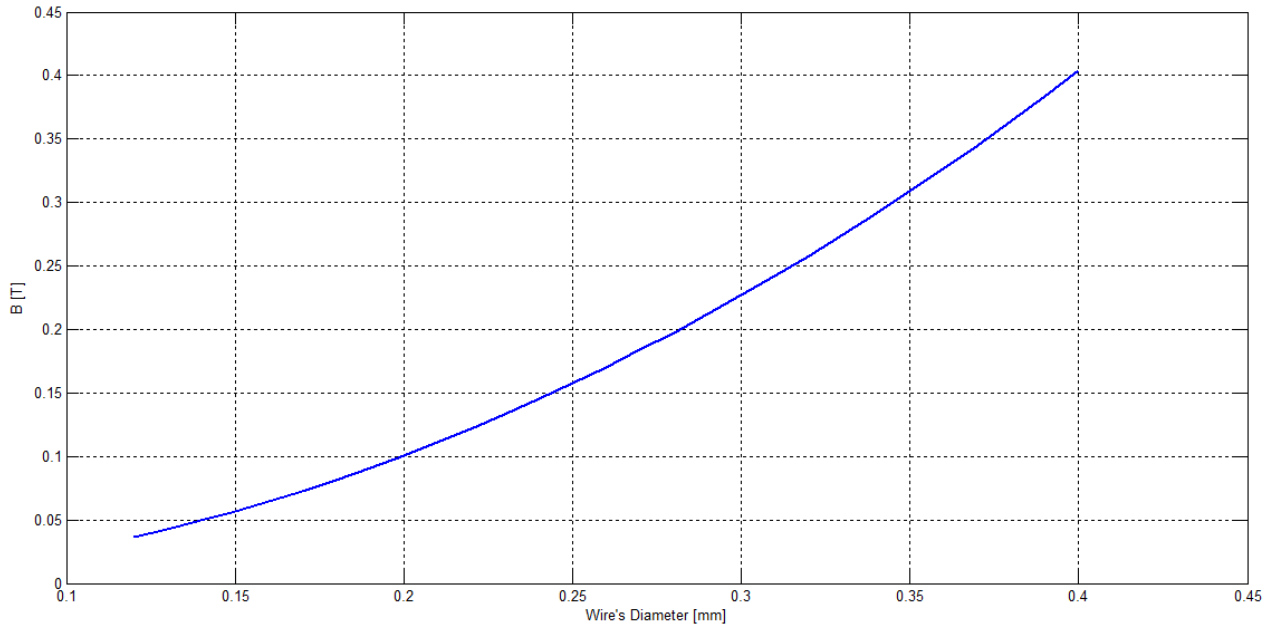


*Fig. 82 Example of magnetic flux density for a defined core (10x80mm)*

For the presented case the operating magnetic flux region would be in worst case (really thick wire) half of the saturation region, keeping the linear relation between B and H.

Increasing the size of the wire would be reached the region of non-linearity and saturation. Nevertheless this condition could be hardly realistic because increasing wires thicker than 0.4-0.45 mm would lead to current bigger then 1.3-1.4 A. More, this would happen in the unrealistic case of more than 1000 turns, not negligible in terms of size with such a thick wire. In a practical case, that means with less turns, the resistance would be lower and the current would be much higher than the previous value. The limit of 0.4-0.45 mm as wire diameter for a torque rod can be assumed as limit to avoid enormous current with realistic number of turns also in case of lower voltage (600 turns with a 0.4mm wire would consists in more than 2A).

The results in change if the  $L/r$  is increased. Reducing the diameter of the core to 7mm and maintaining the same length it's observed that the reduction of the demagnetizing factor it's sufficient to bring to saturation (Fig. 83).



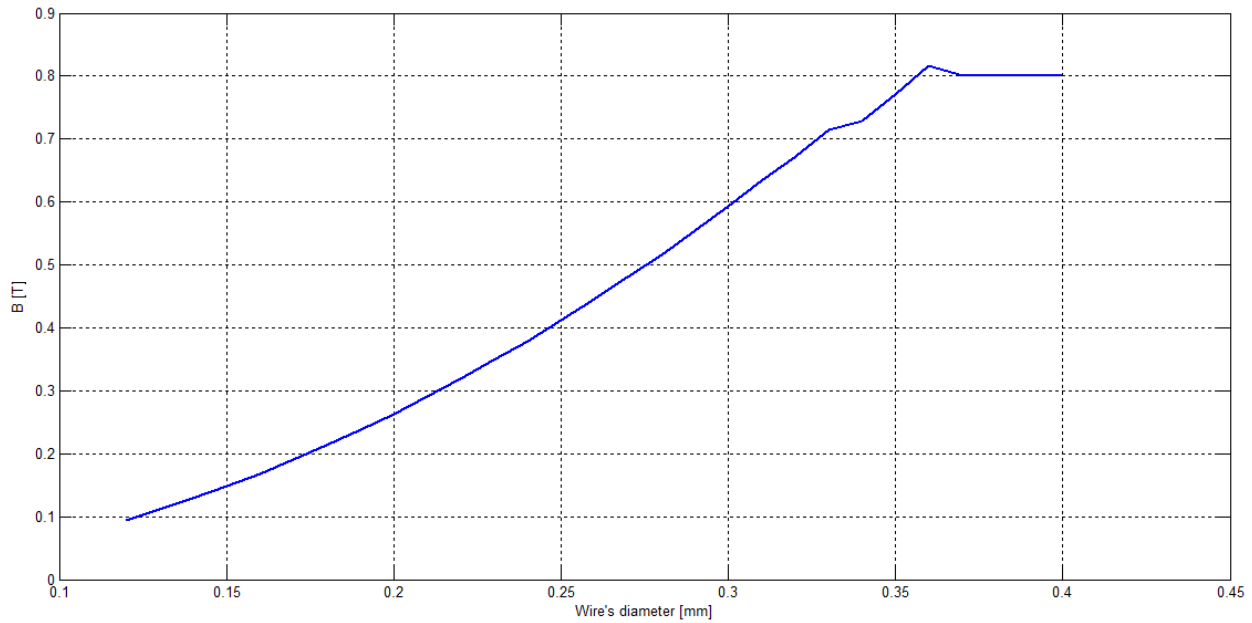


*Fig. 83 Example of magnetic flux density for a defined core (7x80mm)*

In the graph the step at 0.74 T is due to the change of the permeability according to the material datasheet. The peak over 0.8 is due to the model and it's not part of the results.

This example shows that for a defined geometry there could be a limit in the wire section that would bring to the saturation condition. Oversizing the system beyond this limit would consist in a not optimal use of the core (the effect doesn't increase more) and waste of mass. Consequently the same should be evaluated varying the voltage or fixing the wire diameter and defining the proper shape that guarantees to be in the optimal operating region. Nevertheless as already said between these three parameters the voltage can be assumed fixed and the less flexibility is in the core's dimension rather than the wire section.

So that for each core the choice of the wire would not only determine the power consumption and the magnetic dipole as well as the other torquer but also the operative region of the core and in that way several issues related with the system.

For a defined volume of the core and a defined material (so permeability) exists a combination  $L/r-dw$  (Length over radius and wire's diameter) that lead the core to saturation at a defined operative voltage. This analysis could be interesting considering the condition in which the core is defined: in this case it can be

important, knowing the voltage supply to choose the correct wire diameter that permits to exploit the core over or below saturation region.

Taking as example a core of defined volume  $3.07 \cdot 10^{-6} \text{ mm}^3$  it's possible to evaluate the minimum wire's diameter for which depending to the  $l/r$  ratio the core reach saturation with a certain voltage supply (Fig. 84).

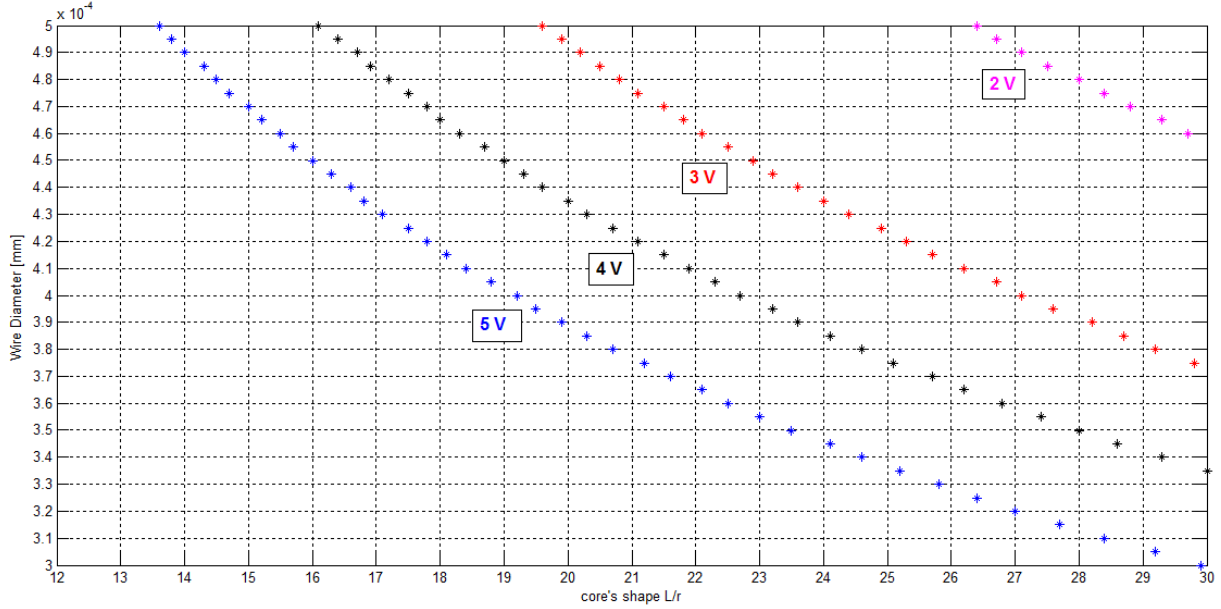
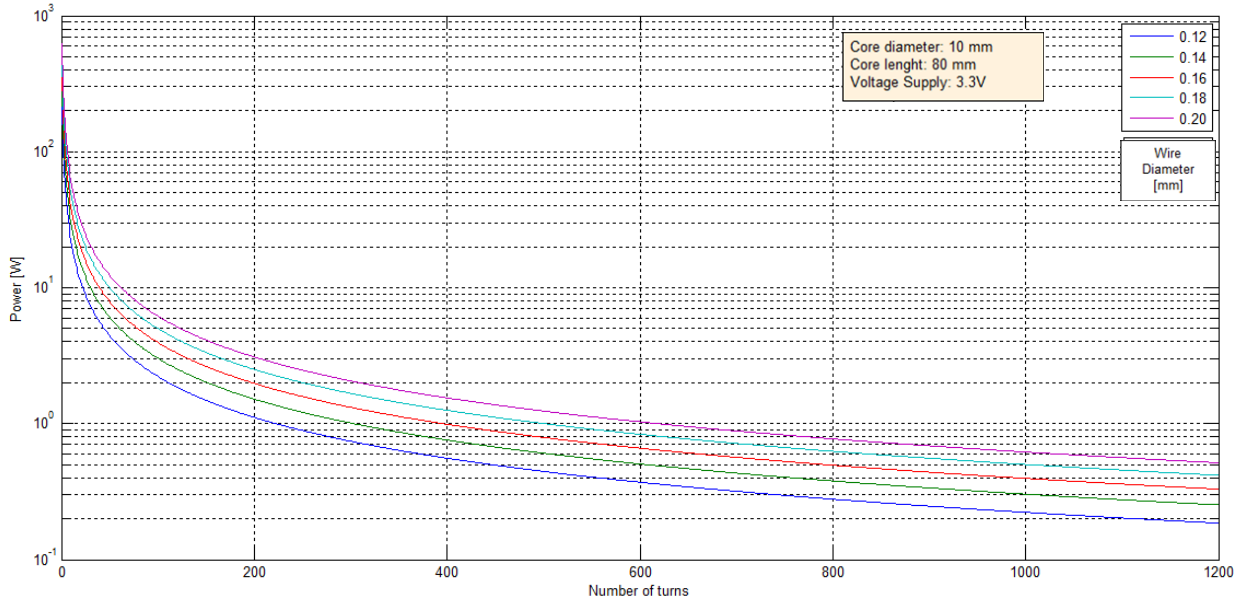


Fig. 84 Minimum wire's diameter to reach saturation for a defined core ( $3.07 \cdot 10^{-6} \text{ mm}^3$ )

Choosing the correct wire once the core is defined can permits to optimize the operating region and in that way the control law. The number of turns can be then adjusted to reduce the power consumption without affecting the magnetic dipole.

This can be observed in the previous example of a 10mm core diameter. The results are qualitatively exactly the same obtained for the air core magnetorquer. The power consumption is affected by both the number of turns and the wire diameter while the magnetic dipole is function only of the second (**Error! Reference source not found.**).



*Fig. 85 Power consumption relation for different wire's diameter (10x80mm)*

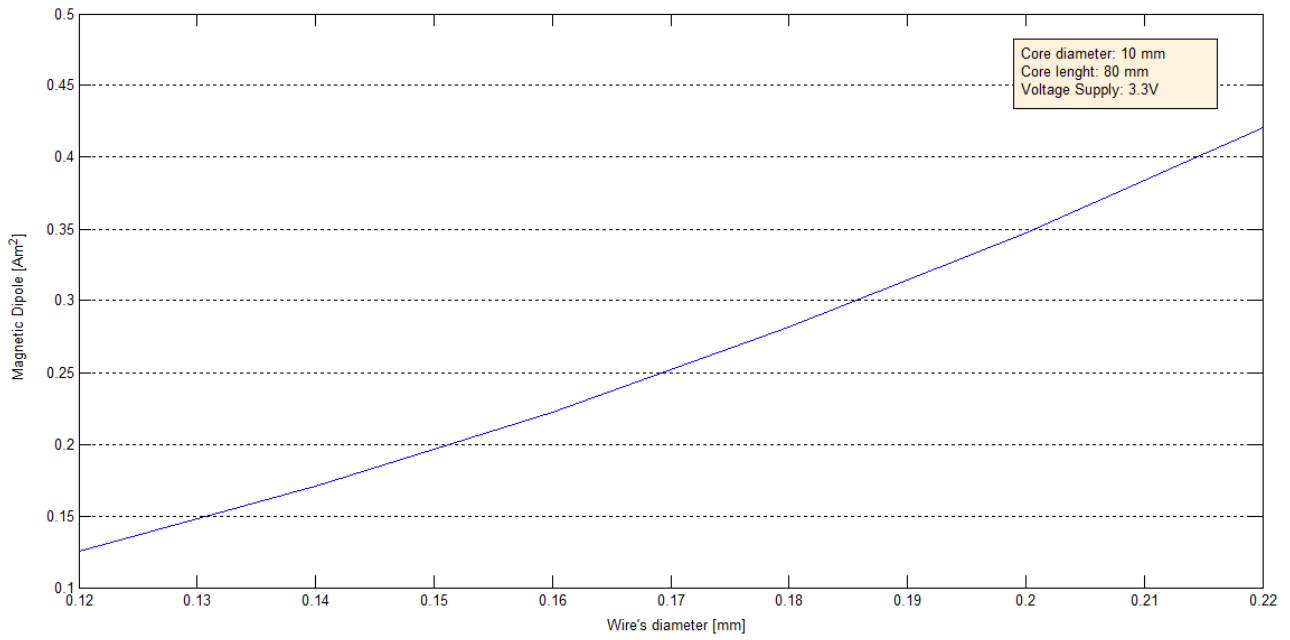


*Fig. 86 Magnetic dipole relation (10x80mm)*

In general it's possible to obtain with a torquered a magnetic dipole that is order of magnitude bigger than the one obtainable with previous torquer. The number of turns in this case is more critical to reduce the power consumption due to the fact

that the length of each coil is much shorter and every turn increase less the resistance with respect to air core. Trying to isolate the different contribute it's possible to follow the previous step as design flow chart for a torquerod, starting with the choice of the core, then defining the needed wire's diameter and then rearranging the properly the number of turns (Tab. 10).

Core →	Wire's diameter →	Number of turns
Affects operative region Affects magnetic dipole	Affects magnetic dipole Affects power consumption Affects magnetic dipole Affects operative region	Affects power consumption

Tab. 10 Torquerod design main steps

Important considerations have to be made concerning the residual magnetization expected once the current is removed.

The residual magnetization can be evaluated empirically referring to different formulas.

Referring to intrinsic magnetization [12] (Fig. 87) cycle residual magnetization can be expressed as function of the residual magnetic flux density:

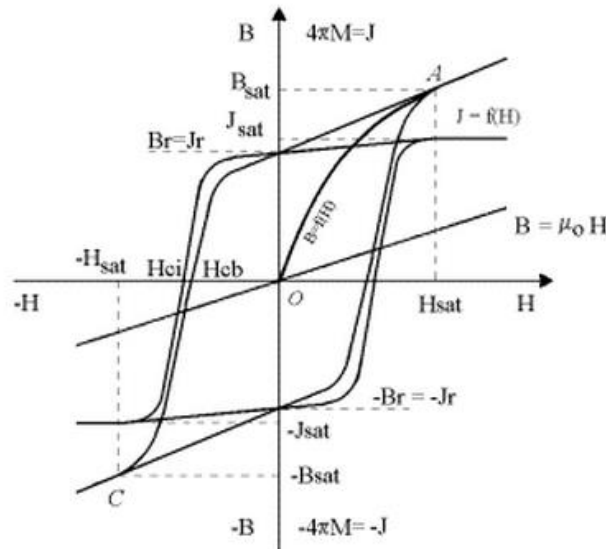


Fig. 87 Relation between magnetic flux and intrinsic magnetization [12]

Where  $J$  is the slope of intrinsic magnetization that represents is the contribution of the magnetic material to the total magnetic induction  $B$ . It is the vector difference between the magnetic induction in the material and the magnetic induction that would exist in a vacuum under the same field strength,  $H$ .

$$J = B - \mu_0 H$$

$$J = 4\pi M$$

The evaluation of the residual dipole is connected to the knowledge of remanence of the core being:

$$J_r = B_r$$

$$M_r = \frac{B_r}{4\pi}$$

This value is not normally provided in the datasheet of the different supplier analyzed and also in bibliography there are many different data. One interesting formula found seems to agree with the most of the typical hysteresis cycle of soft ferromagnetic materials, and specifically is referred to NiFe alloy (50%-80%) [19]. According to this, the theoretical value of remanence can be expressed as function of the saturation intrinsic magnetization:

$$\frac{J_r}{J_s} \cong \frac{2}{\pi}$$

$$\frac{M_r 4\pi}{M_s 4\pi} = \frac{J_r}{J_s}$$

$$M_r \cong 0.64 M_s$$

Other text refers to a typical residual magnetization in the order of:

$$B_r \cong 0.8 B_s$$

Exploiting the first formula that seems to be closer to the typical property of soft ferromagnets (low remanence and low coercivity).

The uncertainties in this value suggest that also in this case it's necessary to directly measure this value in the manufactured torquerod. Obtaining the value of  $J_{\text{sat}}$  from the material first magnetization graph it's possible to obtain the value of  $M_s$  and consequently the value of  $M_r$ .

The residual magnetic dipole is evaluated considering the effect of the core alone.

$$m_r = NI_{(=0)}S + V_c M_r$$

This can lead to the result, for the defined material with 0.8 T as saturation flux, of a residual magnetic dipole in the order of  $0.0026 \text{ Am}^2$ .

This value it's close to the value reported in some commercial products and can be easily equated to the total residual magnetic dipole of the entire satellite.

The value would change according to the properties of the material and the volume of the core. In the case of NiFe50 alloy this value would be approximately double due to the higher saturation flux and the lower permeability that determines higher saturation H field.

For bigger satellite in which the volume of the core increase it's probably obtainable a higher results.

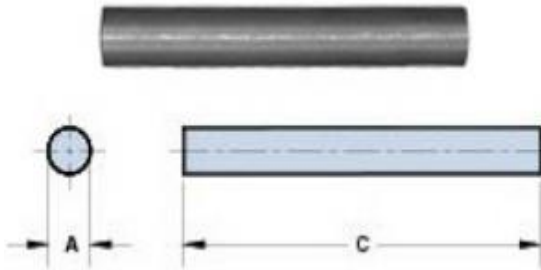
The residual value of the magnetic dipole it's also strictly connected to the operative region of the core: In those cases in which the core isn't led to saturation it's expected a lower value of remanence and consequently lower value of residual magnetic dipole. This issue could be important in the design of a torquerod knowing the requested global performance of the system: it's always necessary to perform experimental measure to determine the hysteresis cycle of the material when this operates below saturation condition.

If the remanence is not negligible it will be necessary to design a demagnetizing circuit: this circuit has to provide alternating voltage in order to reduce the hysteresis loop converging to  $B=0$  until the requested value of remanence is reached: the circuit design is again strictly connected to core's properties.

## 5.4 Experimental measures on torquerod prototype

Exploiting a material sample available as been prototyped a small torquerod in order to perform some measures.

The material used for the core was a Ferrite 77. This kind of material is not suitable for torquerod application because of the low permeability: the advantage of this material is basically in the low hysteresis loss at high frequency (>10KHz) due to the high resistivity of the core. As said these frequencies are completely not compatible with torque rod operative range. Typical values of permeability for these materials are in the order of 1000 to 10000 while the saturation magnetic flux is typically under 0.6 T. An overview of the material properties can be obtained from the datasheet (Tab. 11): again the data refer to high frequency application leaving in that way some uncertainties.

Magnetic Properties			
	Unit	Value	Symbol
Initial Permeability @ B<10 G	-	2000	$\mu_i$
Flux Density @ Field Strength	Gauss Oersted	4900 5	B $H_c$
Residual Flux Density	Gauss	1800	$B_r$
Coercive Force	Oersted	0.3	$H_{co}$
Physical Properties			
	Unit	Value	
Diameter (A)	Millimeters	9.45	
Length (C)	Millimeters	50.80	
Weight	Grams	17.00	
Specific Gravity	Kg/m <sup>3</sup>	4700	

Tab. 11 Ferrite core exploited for the prototype: magnetic and physical properties [20]

An idea of the hysteresis loop and average permeability can be obtained also exploiting the data provided remembering that these are referred to 100 KHz frequency. As already said for lower frequencies the permeability tends to increase.

The hysteresis loop can be schematized as follow (Fig. 88).

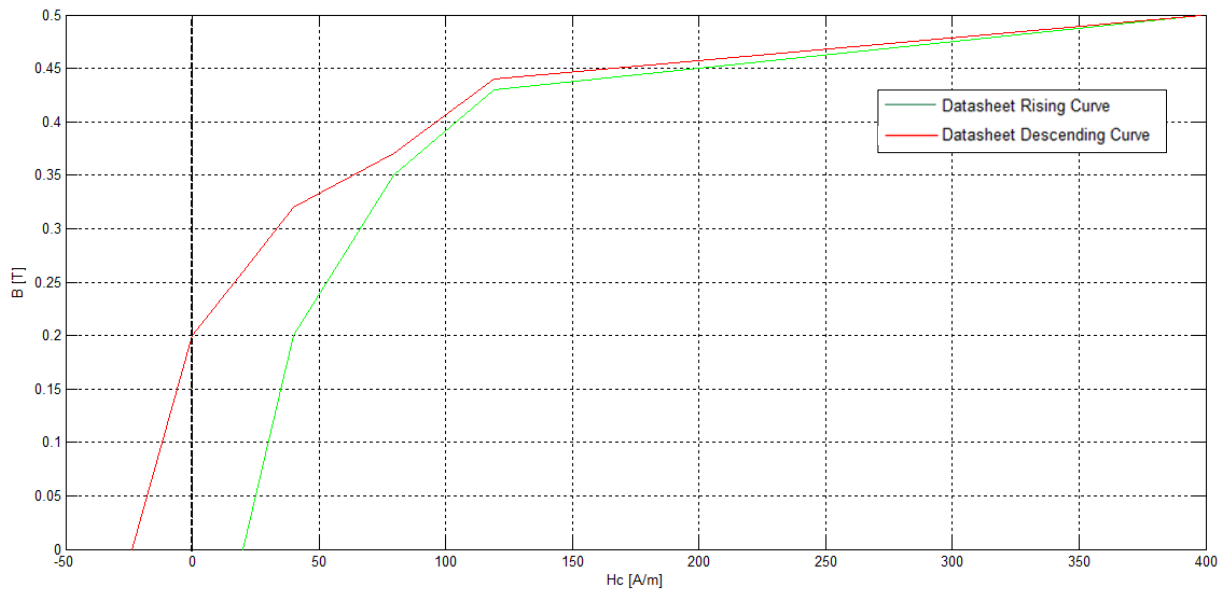


*Fig. 88 Ferrite core hysteresis loop reconstruction at 100 KHz*

Graphically it's possible to evaluate an average permeability for the first part of the slope equal to 0.058. This consists in a relative permeability  $\mu_r=4615$ .

To realize the prototype has been designed two small support with proper geometry to guide the wire in firsts loops of the winding (Fig. 89, Fig. 90). These have been made in rapid prototyping technique.

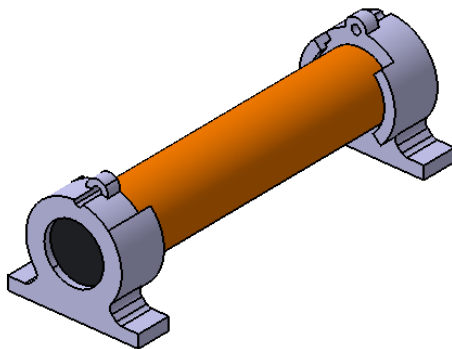


*Fig. 89 Torquerod prototype design (1)*

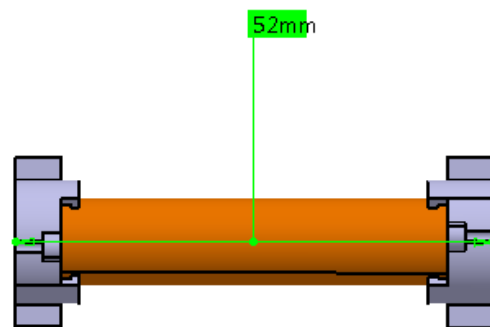


*Fig. 90 Torquerod prototype design (2)*

The rod has been wound manually with a 34 awg magnetic wire (0.16 mm diameter). On the two edge of the rod have been integrated the two support. In this



way it would have been possible to maintain the rod on horizontal plane during the measure. The whole wounded wire has been fixed with kapton tape in order to maintain the solenoid wounded. This solution could be risky for a real space application because of the possibilities of trapped gas particles between the tape and the winding.

The realized prototype has resulted in 258 turns with a total resistance of the wire of  $6.7\ \Omega$ . (Fig. 91, Fig. 92)

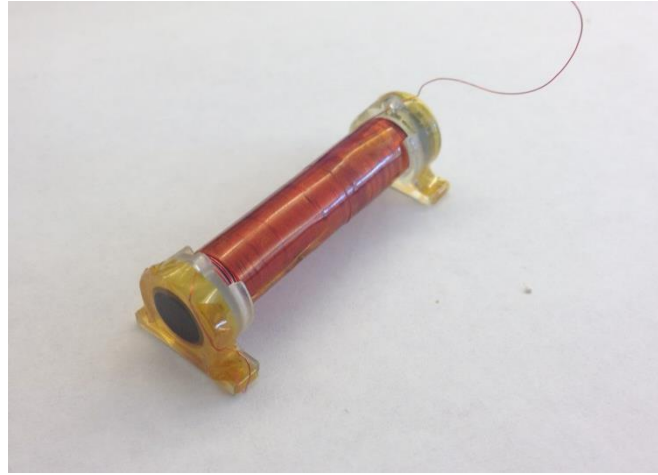


*Fig. 91 Realized prototype (1)*

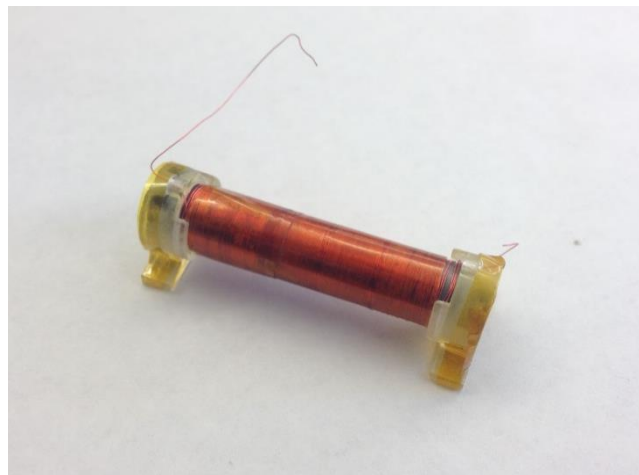


*Fig. 92 Realized prototype (2)*

Two several issues affects the experiment on torquerod prototype: first of all, differently than the air core, the mathematical model offers the exact formula for the magnetic field in the center of the solenoid, point in which is impossible to take the measure (Fig. 93, Fig. 94). Due to the edge effects, the measure taken outside

the core can significantly differs more than the 50% then the real value. Second important issues are related to the strength of the magnetic core that, immediately can lead the magnetometer to saturation. For that reason it's necessary to keep the measure at a certain distance from the edge in order to obtain enough data point.

This second important problem introduces the need to define a law to reduce the magnetic flux according to the distance from the edge.

Concerning the first issue, the magnetic flux density at the edge of the solenoid can be obtained considering the entering and exit flux equal and leading to the result

$$B_e = \frac{\mu_0 IN}{2L}$$

Assuming the same relation for the magnetic field expressed taking into account the demagnetizing factor:

$$B_e = \frac{\mu_0 \mu_r NI}{2l(1 - N_d + \mu_r N_d)}$$

Concerning the distance reduction law it's well known that the magnetic field decrease as  $d^3$  where  $d$  is the distance from the source. Reducing simply in this way is not possible because it would admit that is possible to observe exactly the source point.

The idea is to exploit the analogy with the exact solution for a single coil: in this case the magnetic field on the  $z$ -axis at distance  $z$  from the coil plane it equal to

$$B_z = \frac{\mu_0 I r^2}{2(r^2 + z^2)^{\frac{3}{2}}}$$

While on the plane at  $z=0$

$$B_0 = \frac{\mu_0 I}{2r}$$

Combining the two equations it's possible to explicit  $B_0$  in  $B_z$

$$B_z = B_0 \frac{r^3}{(r^2 + z^2)^{\frac{3}{2}}}$$

$$\frac{r^3}{(r^2 + z^2)^{\frac{3}{2}}} = K$$

Assuming K as a reduction factor for the center magnetic flux at defined distance from the coil plane.

This model can be used with an approximating assumption and considering the all solenoid condensed on its edge (Fig. 93): this consists in having a single coil on the edge of the solenoid with a magnetic field on its plane equal to the magnetic field on the edge of the solenoid ( $B_0=B_e$ ).

$$B_z = B_e \frac{r^3}{(r^2 + z^2)^{\frac{3}{2}}}$$

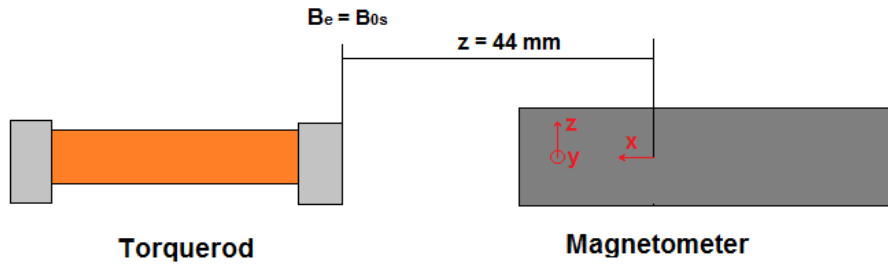


*Fig. 93 Experiment layout scheme*

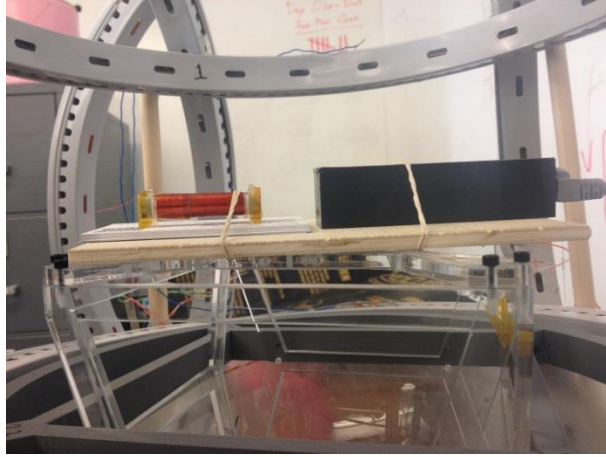


*Fig. 94 Experiment layout*

The maximum current that can be provided to the core is 1 Amp due to limit of the voltage supplier. The profile has been again the same exploited for other torque (Fig. 95).

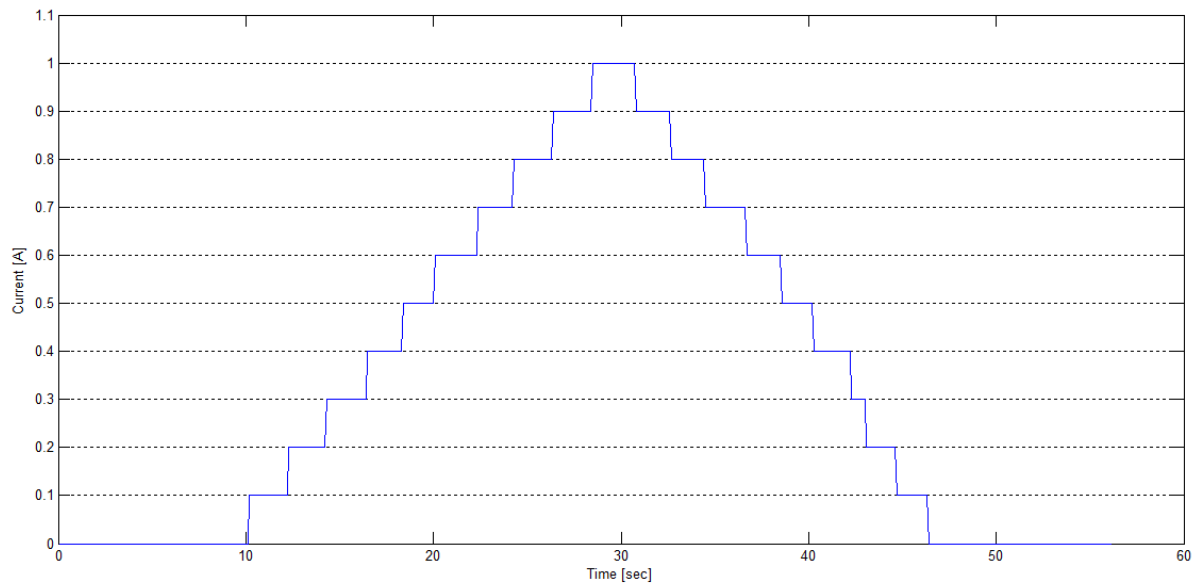


*Fig. 95 Current profile for torquerod experiment*

The results show that the experimental data are definitively higher than the mathematical model (Fig. 96).

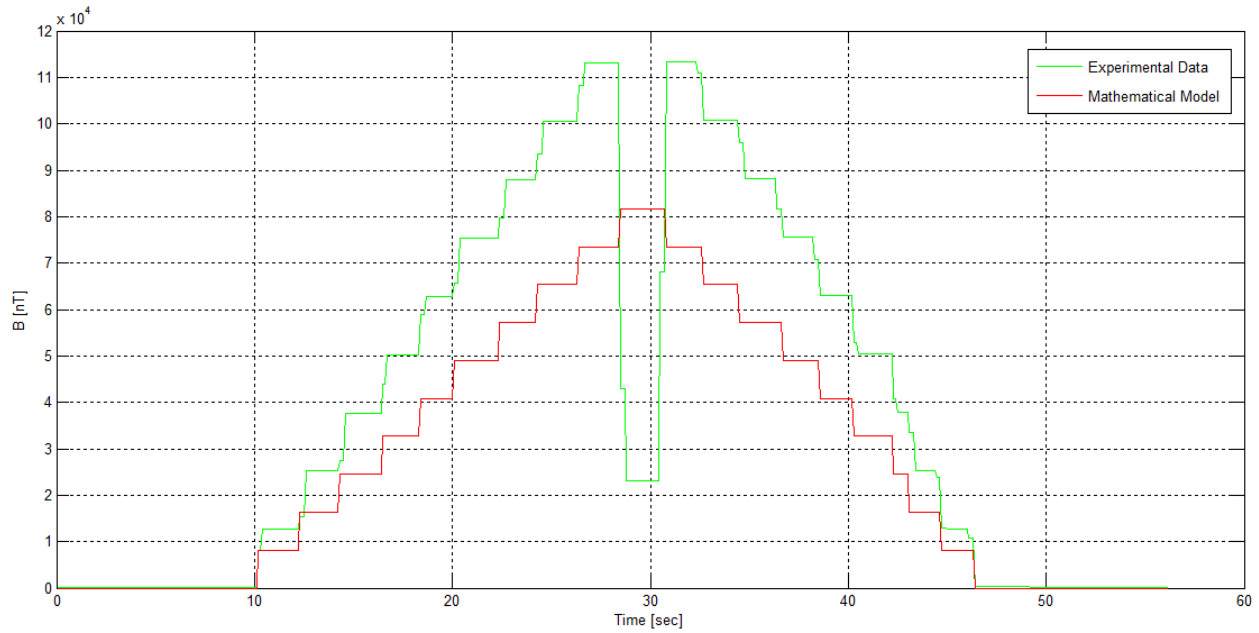


*Fig. 96 Magnetic flux density in x direction; experimental results and mathematical model*

An explication to this has to be found in all the different uncertainties and approximation made to correct the mathematical model according to the measuring point. Furthermore has to be kept in mind that the used permeability is evaluated at high frequency data that, consistently reduce the value leading in that way to lower values.

In addition to this, the model used to reduce the field according to the distance is an approximation being based on analogy with coil model, as well as the edge effect consideration.

The fact that the results differs less than the 50% in spite of all the issues related with the measure is a good indication of the likelihood of the theoretical model for the calculation of the magnetic flux induced by the core. In this model in fact enters the demagnetizing factor that for a torque rod is a key element during the design phase.

It interesting now to invert the process bringing the experimental data to the estimated nominal value in the core simply re-applying the correction factors used for the mathematical model.

In this way it's possible to observe the portion of the H-B operative range of the core interested with the current provided to the solenoid (Fig. 97).

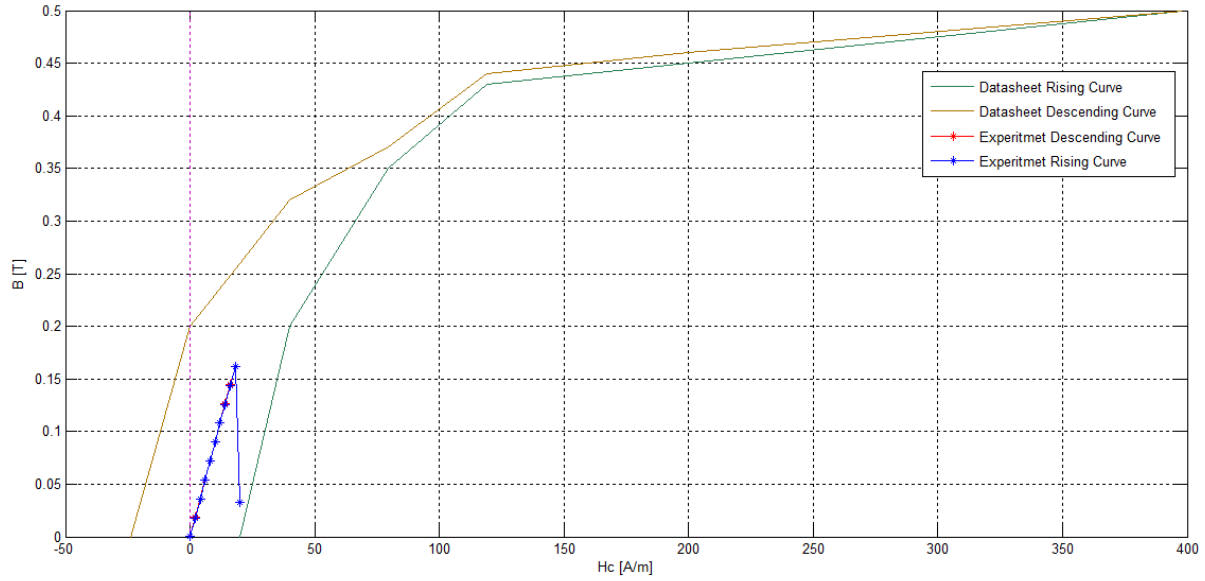


*Fig. 97 Evaluated operative region during experiment*

The core operated in a really small portion contained in the hysteresis loop. This because the current provided that can be assumed realistic for a CubeSat application is too low to lead to higher value.

This has been already observed in which the possibility to exploit the whole loop depends both on the geometry and the available power.

To observe the presence of the residual has been measured defining zero level for the surrounding and then positioning the core unplugged from the supplier at the same measuring point of the experiment.

The measure shows a really small residual present in the core (Fig. 98).

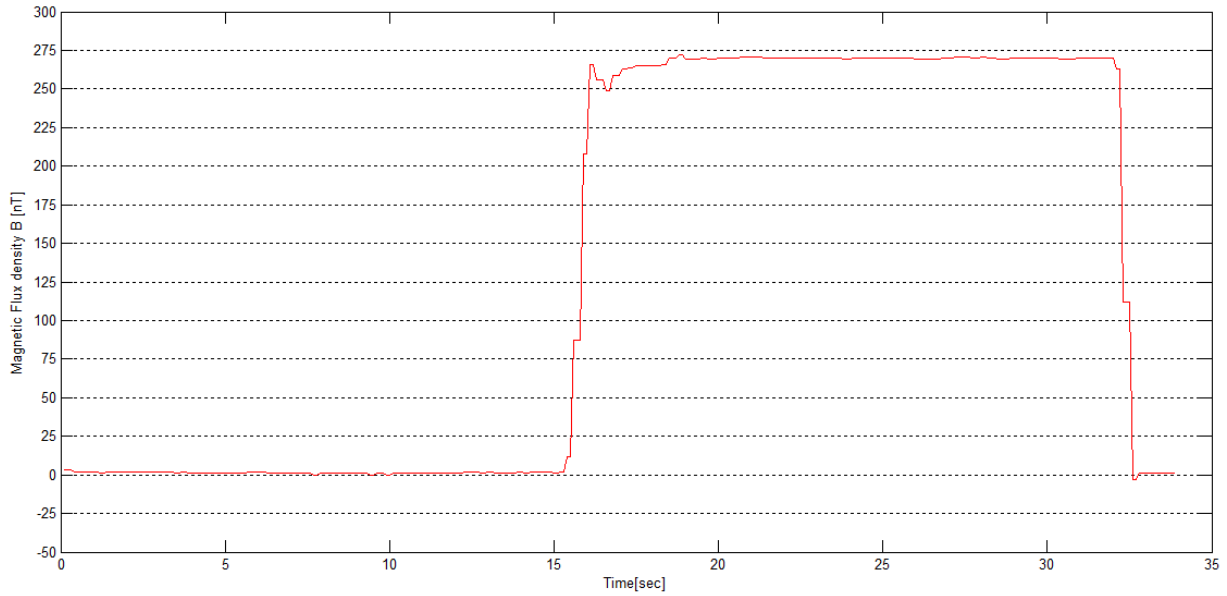


*Fig. 98 Remanence of the core (measured in experiment configuration)*

The value of 275 nT measured at the defined distance has to be related to the maximum magnetic flux experienced by the core during the experiment. The ratio between the two indicates a residual equal to 0.0026 that means absolutely insignificant residual magnetic flux. This analysis is completely independent of the eventual mistakes committed in the evaluation of the space variation of the magnetic flux, being both influenced in the same way. Bringing the value to the center of the core exploiting the same relation used above it's possible to estimate a residual around 500000 nT (Fig. 99). Of course the relation of 0.0026 with respect to the maximum value experienced in the center of the core is maintained.

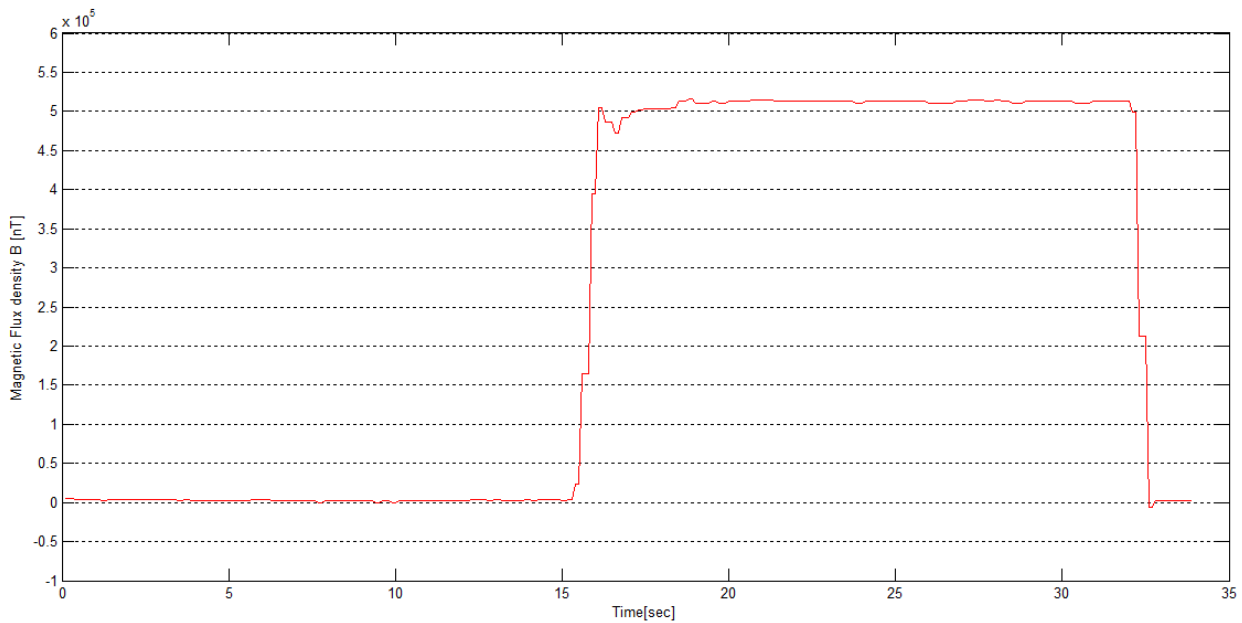


*Fig. 99 Evaluated remanence inside the core*

A possible explication for such a low value of residual can be related first of all to the nature of the core: a ferrite core designed for high frequency cycle presents in general lower value of residual with respect to the other soft ferromagnets. Second important consideration is that the operating region of the core was really reduced with respect to the typical hysteresis loop. In this region the permeability has been constant that lead to the idea that the eventual presence of strong residual could be related to the change of permeability, as a sort of memory effect similar to the residual deformation of material stretched. This can't be anyway assumed as universal behavior being too many the variables involved. Each torquerod designed should therefore tested in real working condition in order to define all the properties related and eventually design proper demagnetizing circuit.



## 6. Design of a 3axis torquerod for CubeSat

The consideration in term of core's shape and volume put several constraints in the design of torquerod for nanosatellite application. The increase in magnetic dipole could not justify the increase in mass and volume of the system if this is not properly designed. For CubeSat applications, volume and mass are also critical aspects and the performance of every system is often limited to this two constraints. That's why should be not a bad issue to reduce as much as possible the impact of the system on this two parameters.

The magnitude of these parameters is not the only issues. In general also the shape interference in the internal volume should be considered: air core and embedded coil could in a certain way considered as services subsystem in a nanosatellite being integrated in the side panel with the structure and consisting in a reduction of the useful volume that does not interrupt the inner useful room (Fig. 101, Fig. 100).

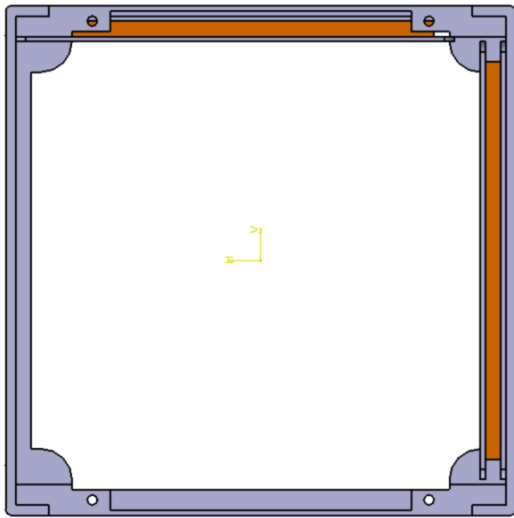


*Fig. 100 Air core magnetorquer integration*

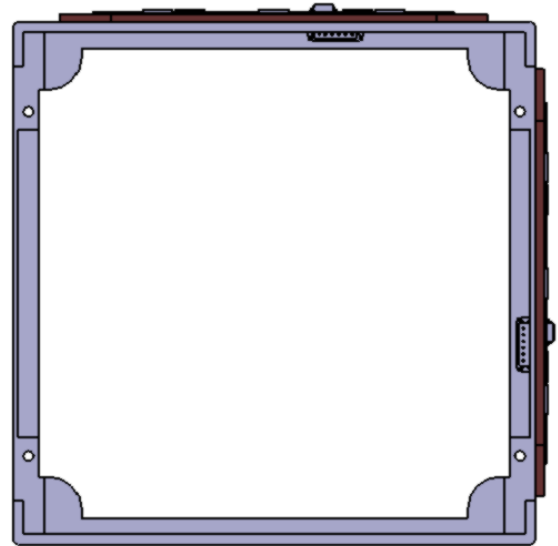


*Fig. 101 Embedded magnetorquer integration [8]*

With a simple model it's possible to consider the volume average internal volume reduction of the two systems. The case refers to a simple structure with the two magnetorquer used to lead measurements: air core coil on the left and embedded coil on the right (Fig. 102). The useful volume is not fragmented but it's only reduced in the 3 direction in which the torquers are mounted.

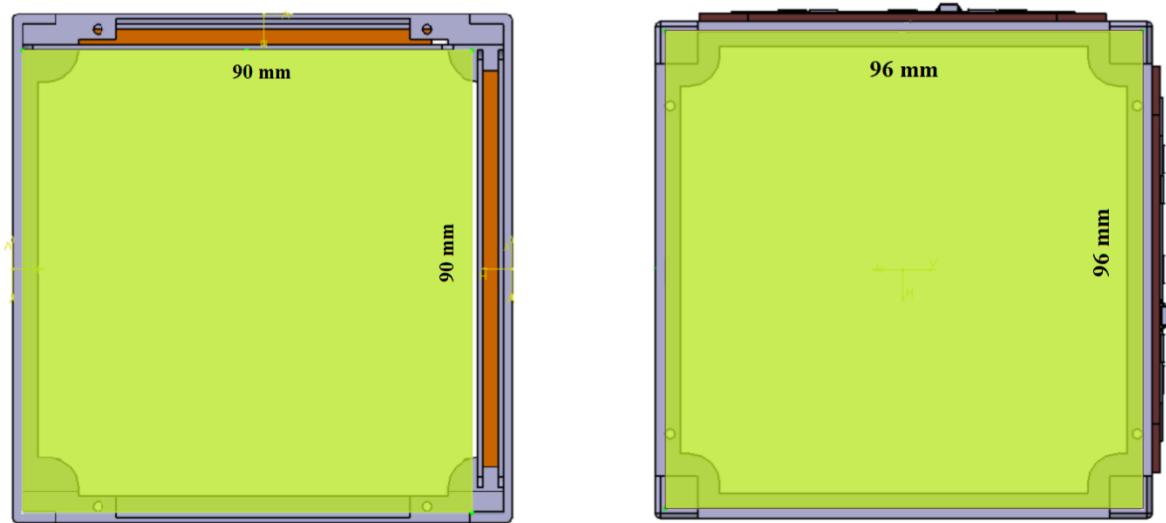


*Fig. 102 Air core and embedded magnetorquer average encumbrance*

The value of the example shows that for the embedded coil the internal useful volume is not affected by the presence of the device, because of its suitable fitting position in the side panels. The volume of  $884736\text{mm}^3$  can be assumed as maximum useful volume for CubeSat internal components in conservative analysis. Considering typical air core torquers, the expected internal useful volume is reduced to  $729000\text{mm}^3$ . This consists in an average reduction of the internal room equal to 0.823 of the first case.

The torquerod for its shape and volume has in general higher interference with the internal layout of the satellite, fragmenting the internal usable volume in smaller ones.

In this scenario is not proper to compare the three kinds of magnetorquers considering only the value of mass, volume and performances. This issue can drastically affect the layout and the design of the entire satellite.

The idea to design a suitable torquerod system for CubeSat is to reproduce the most shape of the encumbrance of the other types of magnetorquer. In this way a more honest comparison between different kinds of solution can be made evaluating the useful volume reduction.

Considering CubeSat structure and CubeSat standard the idea is to exploit the inner volume of the columns trail in order to position the torquerod and exploit the whole available length (Tab. 12). The radius of the core is limited in order to remain the

most in the side volume inside the structure. The system has to be connected directly to the structure as well as the other magnetorquer (Fig. 103, Fig. 104). This concept differs then the one of commercial torquerod available, where the rod is directly mounted on the control board.

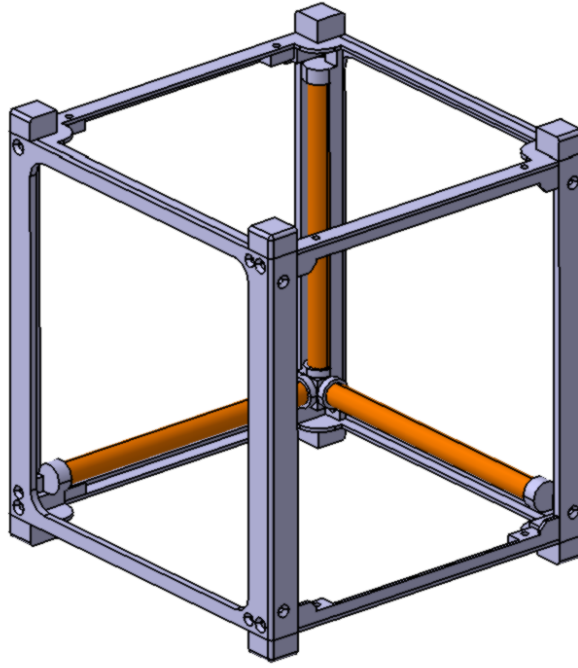
The choice of the material can be made observing the designing issues analyzed before: in the example presented the magnetic flux density reached in the core was far from the magnetic flux density saturation because of the effect of the demagnetizing factor. Knowing the volume and the  $L/r$  ratio of the core it can be possible to define the proper wire that satisfy magnetic dipole requirements and adjust the number of turns to decrease the power consumption according to constraints.

The alloy 79 or alloy 50 seems to be a proper choice for a CubeSat torquerod system, depending on the shape of the core.

	Length [mm]	Diameter [mm]	Material
<b>Core</b>	76	6	Alloy 79

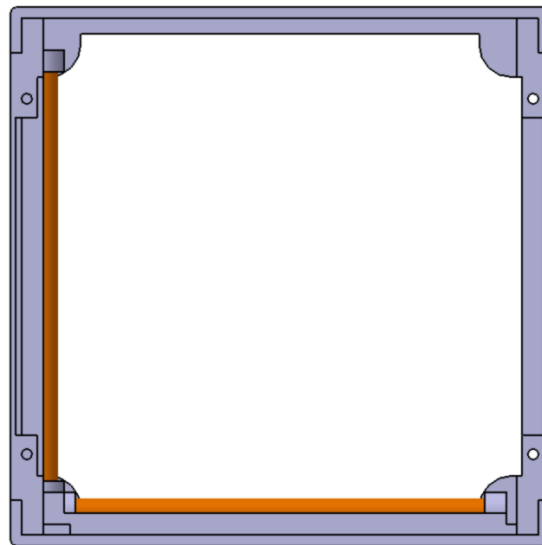
*Tab. 12 Designed core properties*

Once decided the core dimension and material and in that way the average encumbrance of the system it's possible to image to wound the core with the wire to completely cover the available surface.



Istantanea di SNAME - SDATA SORA

*Fig. 103 Designed torquerod integrated in CubeSat structure (1)*



Istantanea di SNAME - SDATA SORA

*Fig. 104 Designed torquerod integrated in CubeSat structure (2)*

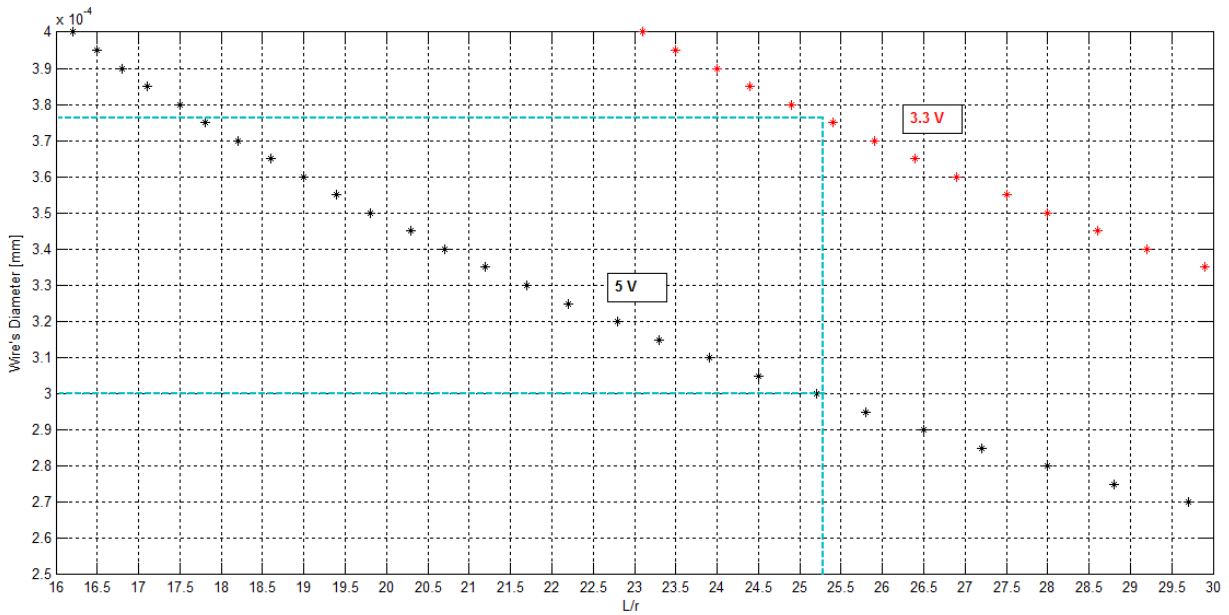


*Fig. 105 Optimal wire's diameter evaluation*

For the defined core, the optimal wire diameter to exploit the core under not over the saturation region would be from 0.3 to 0.38 mm (Fig. 105). Using a thinner wire would not permit to reach saturation level and in that way to exploit the core the most as possible, while using a thicker wire would increase the power consumption without having significant advantages from the core. Of course the choice of the optimal wire diameter doesn't take in consideration the power consumption that can result really high if not compensated with the number of turns. Increasing the number of turns increases also the mass, the encumbrance of the system and introduces difficulties in the manufacturing. Not only, exploiting the saturation level would consist in higher residual dipole that couldn't be compatible with the mission requirements. Due to all these issues can be reasonable to exploit the value as the maximum wire's diameter available for the system.

Designing the system exploiting 0.3 mm wire, the power consumption results really high just for 3.3V supply, depending on the number of turns (Fig. 106).

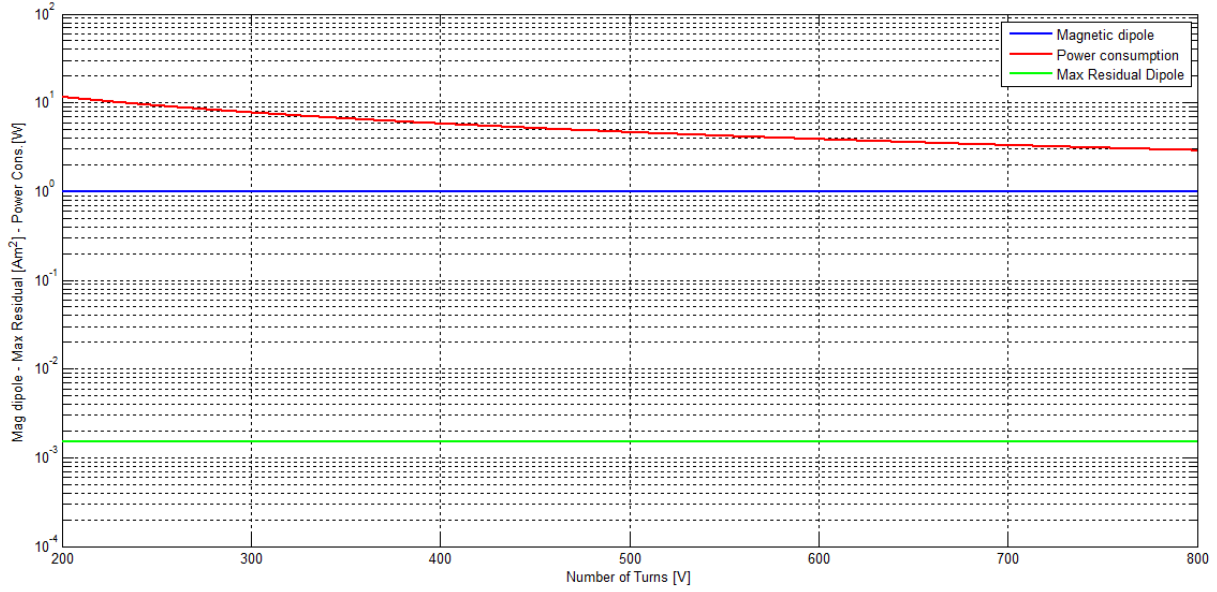


*Fig. 106 Performances for 0.3 mm wire's diameter*

The magnetic dipole is close to 1 Am<sup>2</sup> while the residual is in the order of 0.002 Am<sup>2</sup>. Even if would appear a good performance the power consumption results really high with elevated current (>1A) through the wire despite the huge number of turns. For a 5V supply (PWM) the condition would be even worse. More it has be considered that 800 turns with a 0.3 mm wire is not a negligible value in terms of encumbrance because it would lead to really thick winding in the order of 1.5 mm. This value would basically double the diameter of the entire torquerod.

Reducing the wire diameter is the best choice to reduce the power consumption for two positive aspects: the current is automatically reduced because of the increase of resistivity, while the thin wire permits to increase the number of turns reducing the impact on the system (Fig. 107).

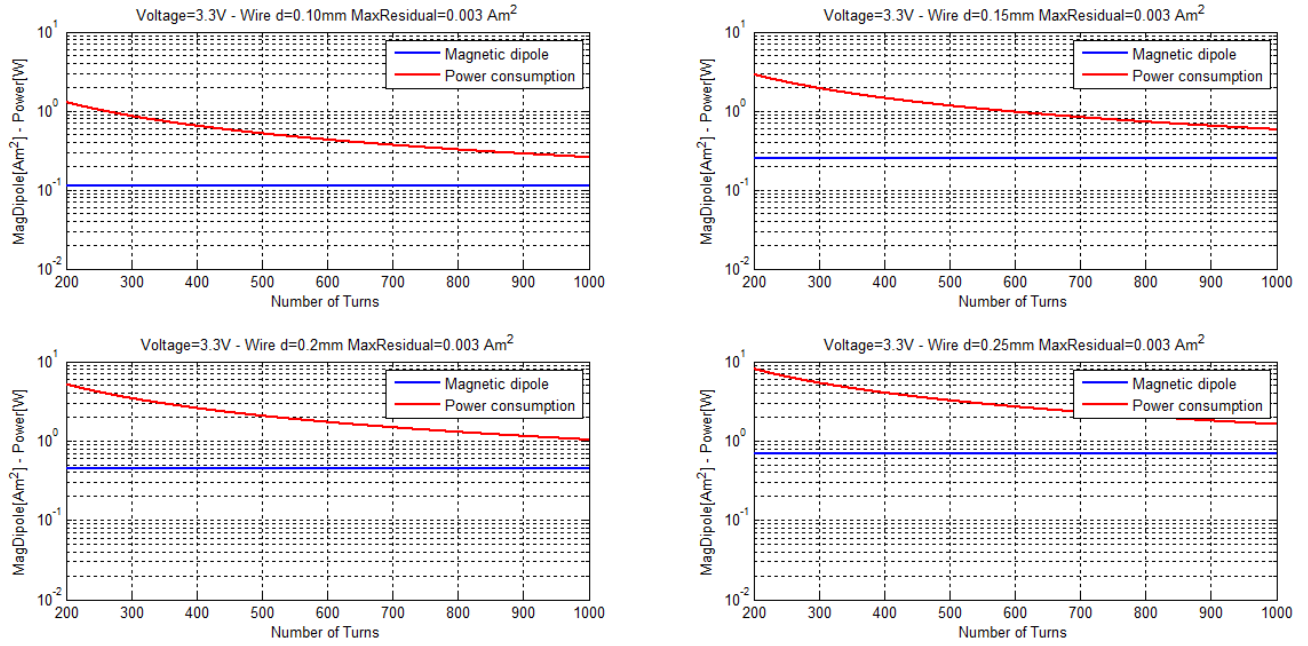


Fig. 107 Different possible performances for different wire's diameter @3.3V

According to the graphs above, a 0.25mm wire could be considered already over the limit of common power consumption and current for a 3.3 V supply.

For a 5.5V supply the presented wire's diameter could be completely out of power constraints while it's necessary to exploit thinner wire (Fig. 108).

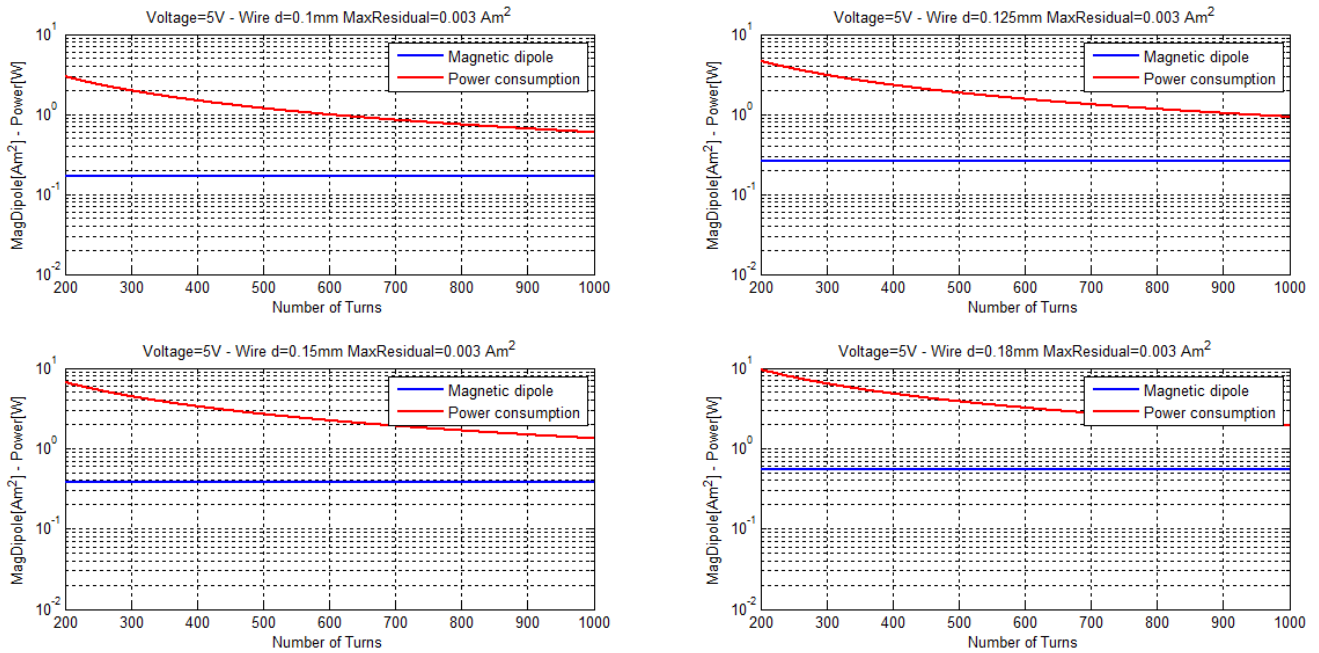


Fig. 108 Different possible performances for different wire's diameter @5V

Increasing the number of turns respecting manufacturing limits would offer even better solution for the presented torque rod. The results obtained permit to converge through the optimal solution: assuming 0.4-0.5 mm winding thickness as limit, the maximum number of turns available with a wire not thicker than 0.18 mm would be 800-900. Exploiting these parameters it's possible to design different magnetorquer with different performances (Fig. 109).

In order to obtain a magnetic dipole around  $0.5 \text{ Am}^2$  for 3.3V supply a 0.18 mm wire diameter can be exploited. The performance of this kind of torquerod are represented below:

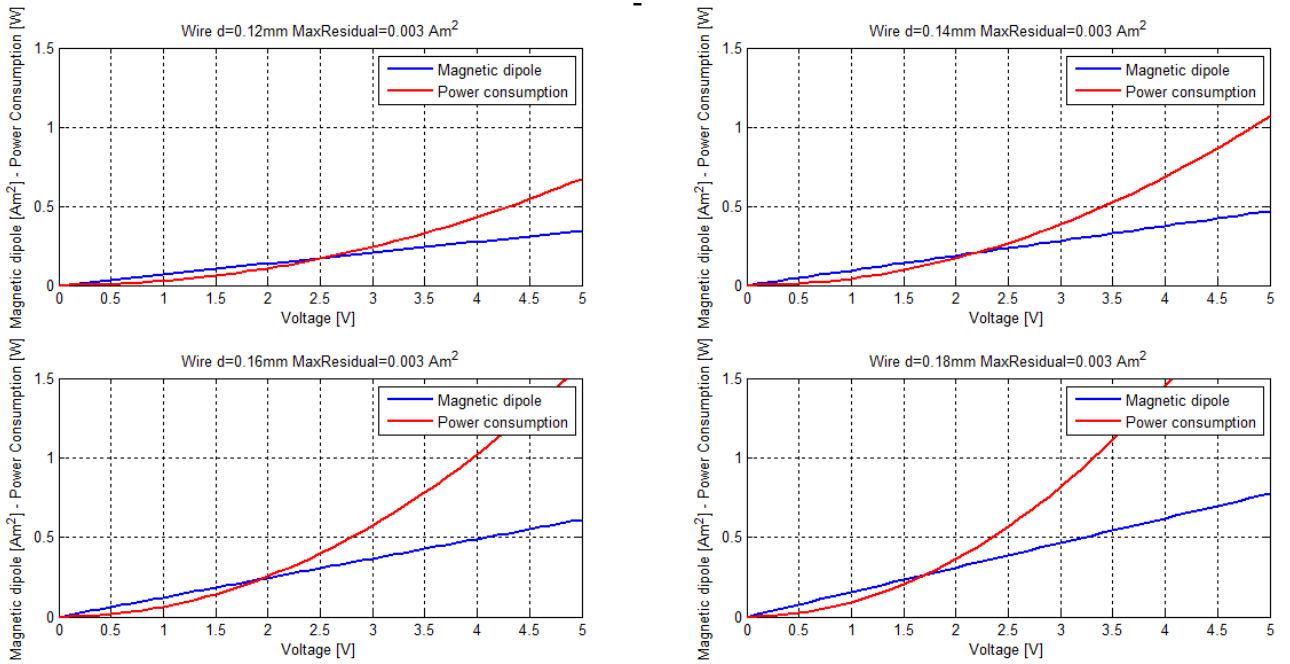


Fig. 109 Operative range for different designs (850 turns and variable wire's diameter)



## 7. Magnetorquer preliminary design

Defining a CubeSat mission it's important to properly define the needed subsystem and their main characteristic. Among them magnetorquer sizing and design is fundamental for a proper attitude control system. As already presented there are several issues in the choice and the design of a magnetorquer. In most of case there could be some issues that lead to the choice of one kind of magnetorquer instead of another. In the really first preliminary design, in which there is more flexibility in power and mass budgets, this choice as well as the design of the main features can be done completely arbitrarily. This could lead to a solution that is not optimal for the final project of the whole satellite, forcing during the development to change some specifics or worst of case to revisit some part of the design and some requirements. The more the preliminary design has been made far from the optimal condition, the more the mistake would cost in term of time and money in the satellite development. For that reason it's important to properly design the system appropriately close to the optimal condition in the initial stages of the design of the satellite.

However, as presented, it's not easy to define a universal strategy to converge towards the optimal condition in terms of requirements and constraints.

It's important to define at least some input parameter to reduce the variables of the dimensioning equations. The idea is to exploit the methodology presented fixing as initial parameter the characteristic dimension (occupied volume) of the system and the voltage supply for the system in nominal operative range.

This can allow to produce different matrix in which the power consumption, the magnetic dipole and the mass depends on the wire and the manufacturing of the system (number of turns or spiral concentration). Comparing simultaneously this matrices it's possible to put on evidence the minors that meet the requirement for each of the 3 parameters. The intersections of these matrices minor, if exists, already represents the range such that, for the initial parameters imposed, represents the optimality conditions. When the intersection matrix doesn't exist means that the optimal condition is not obtainable for the defined dimensions and nominal voltage, suggesting the idea to redefine the initial parameter or understand the margin of variability of requirements/constraints.

Once the 3 possible configuration has been defined it's possible to confronts the performance of the 3 device and determine which one should be used for the

mission. The cost of manufacturing is another important issue not negligible that has to be taken in consideration for the choice.

The designing procedure is characterized represented in the graph and characterized by 3 different phases. The first phase in the blue square is the preliminary inputs and constraints/requirements. The second phase in the red square is the matrices generation for each kind of magnetorquer. The third phase is the comparison between the different possible solutions for each kind of technology.

## 2nd Phase

### 1st Phase

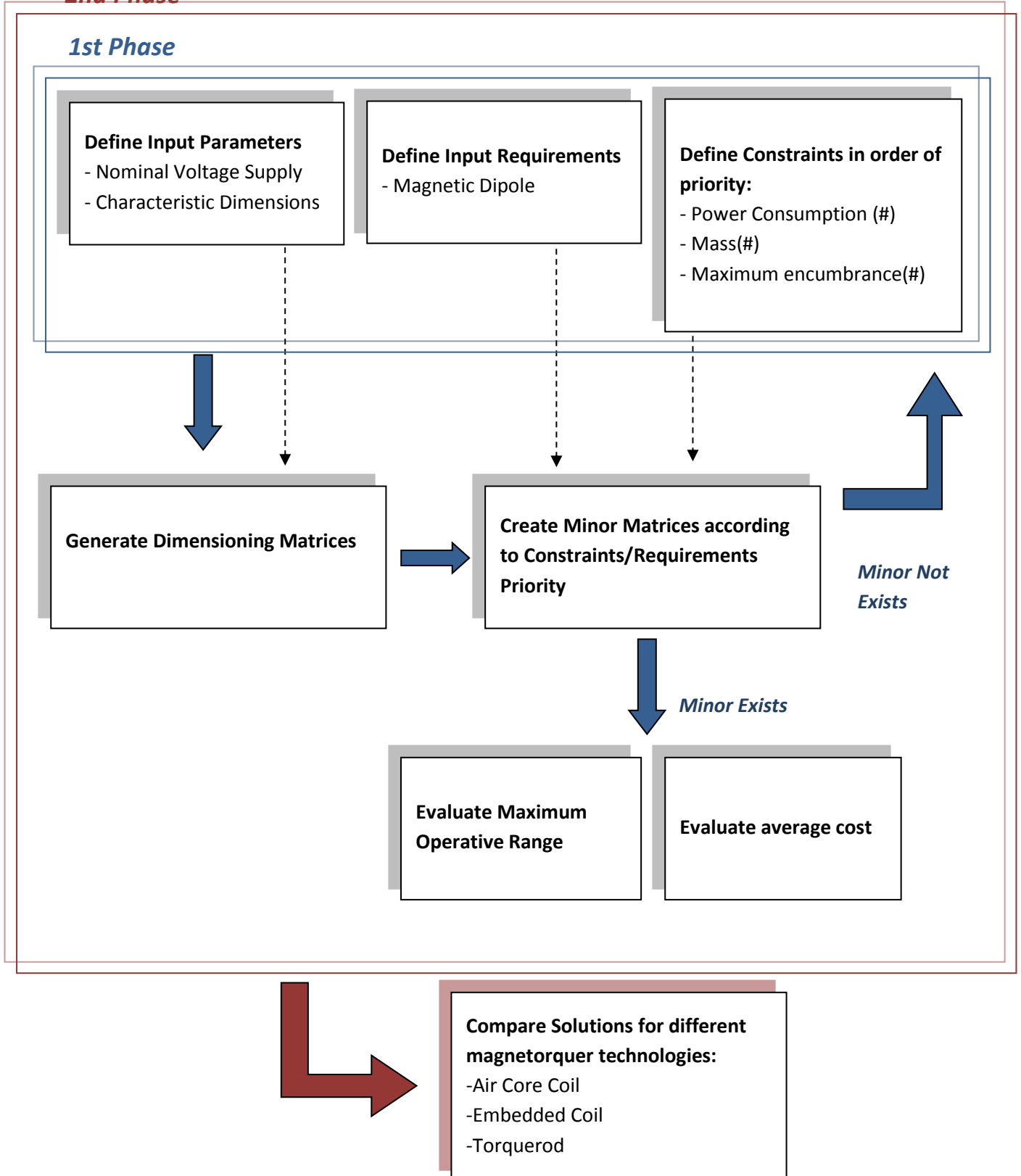


Fig. 110 Magnetorquer optimal design procedure

An example of the dimensioning procedure is presented below.

To understand the main difference between the different magnetorquer, has been taken in consideration different cases that slightly differ from each others. For each one has been exploited the procedure to design each kind of magnetorquer.

Case 1										
Magnetorquer					Air Core					
Input										
Voltage Supply [V]					3.3					
Side Dimension [mm]					76					
Constraints/Requirements										
Requested Magnetic Dipole [Am <sup>2</sup> ]					>0.08					
Maximum Power Consumption [W]					<1					
Maximum Mass [Kg]					<0.03					
Possible Design										
Wire Diameter [mm]	0.18		0.19		0.20		0.021		0.22	
	Min	Max	Min	Max	Min	Max	Min	Max	Min	Max
Number of Turns	52	289	58	260	64	234	71	212	81	194
Winding Thickness [mm]	0.56	3.1	0.69	3.1	0.85	3.1	1.0	3.1	1.2	3.1
Magnetic Dipole [Am <sup>2</sup> ]	0.0831	0.0893	0.0930	0.0991	0.1031	0.1094	0.1136	0.1200	0.1247	0.1310
Power [P]	0.179	0.996	0.221	0.994	0.273	0.999	0.332	0.992	0.398	0.991
Mass [Kg]	0.0135	0.0299	0.0144	0.0299	0.0154	0.0299	0.0166	0.0299	0.0180	0.0299
Support Thickness [mm]	3		3		3		3		3	

Tab. 13 Case 1 scenario - AirCore

In this case the optimal design consists in five different possibilities depending on the kind of wire used. Each possibility defines a maximum and minimum range for

the manufacturing as well as the main performance. It's possible to evaluate a hypothetical operative range for each of the five solutions keeping in consideration the mean value in terms of number of turns.

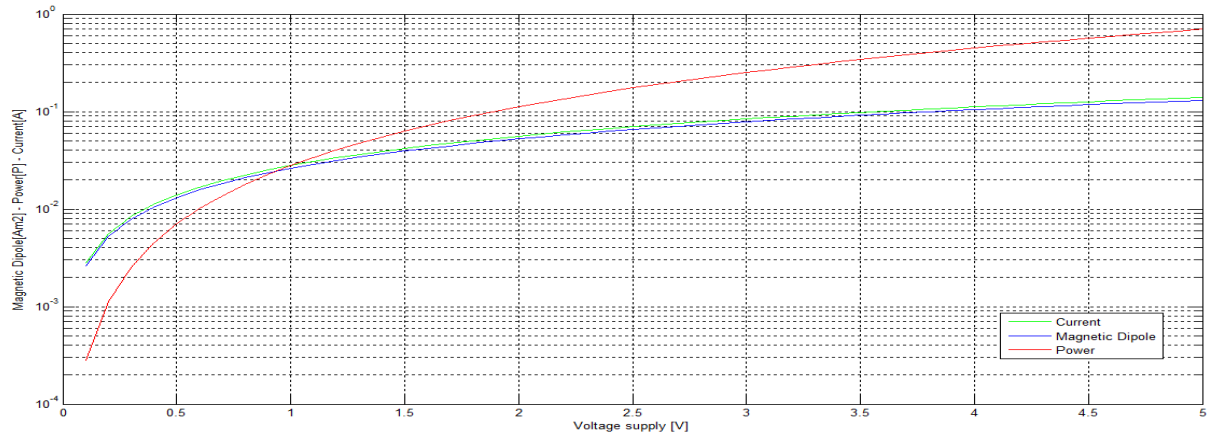


*Fig. 111 Design 1 AirCore*

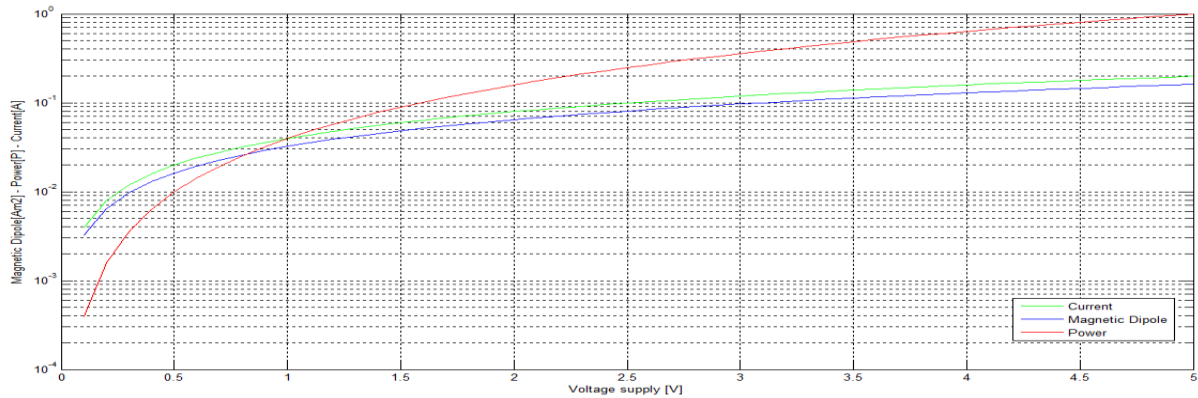


*Fig. 112 Design 2 AirCore*

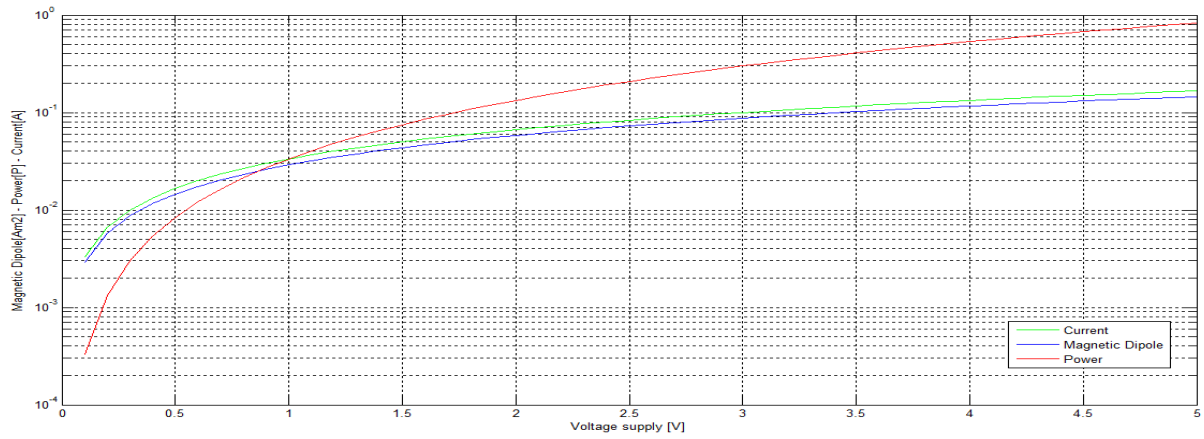


*Fig. 113 Design 3 AirCore*

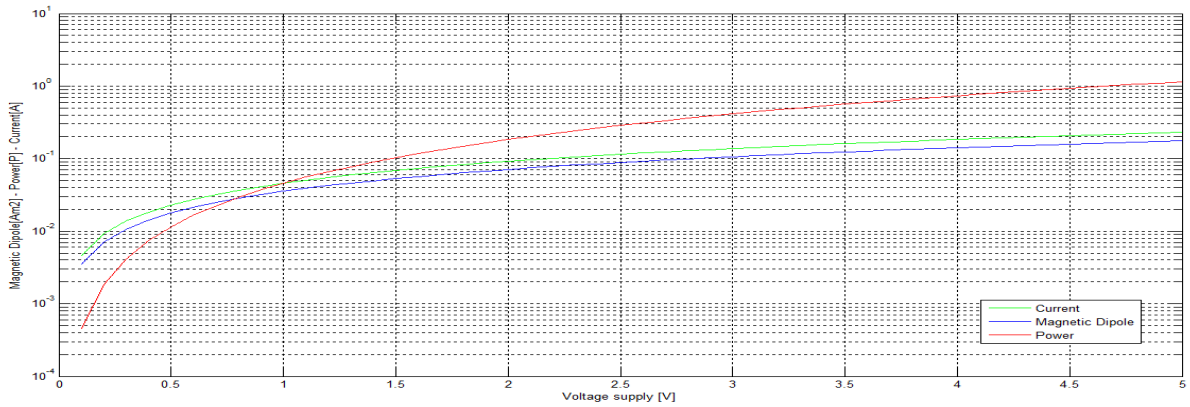


*Fig. 114 Design 4 AirCore*

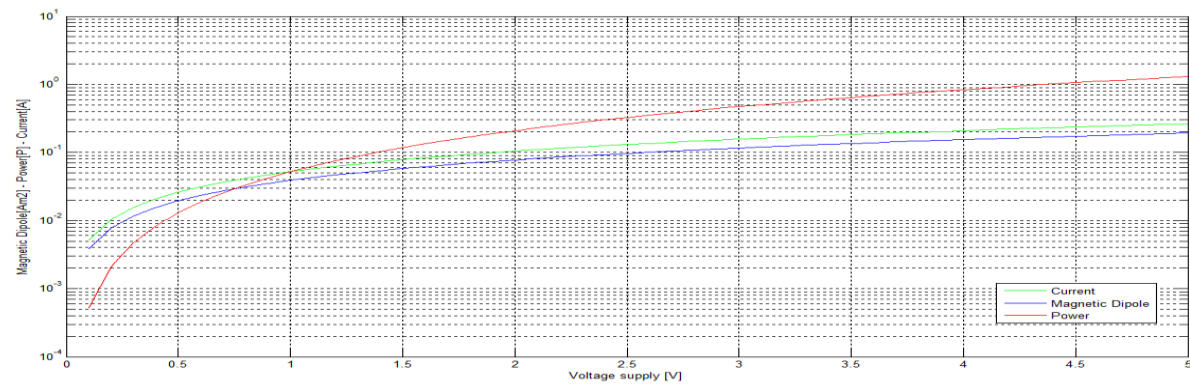


*Fig. 115 Design 5 AirCore*

According to the requested performance it's possible to choose one solution instead of another. Really important is to observe the operative range in order to determine the margin of functionality for each design.

Case 1										
Magnetorquer					Embedded coil					
Input										
Voltage Supply [V]					3.3					
Side Dimension [mm]					76					
Constraints/Requirements										
Requested Magnetic Dipole [Am <sup>2</sup> ]					>0.08					
Maximum Power Consumption [W]					<1					
Maximum Mass [Kg]					<0.03					
Possible Design										
Trace Diameter	0.55		0.60		0.65		0.070		0.75	
	Min	Max	Min	Max	Min	Max	Min	Max	Min	Max
Number of Turns	20	21	22	30	25	30	27	30	30	30
Internal Dimension [mm]	0.044	0.046	0.027	0.041	0.024	0.033	0.022	0.027	0.019	0.019
Magnetic Dipole [Am <sup>2</sup> ]	0.0800	0.0805	0.0834	0.0873	0.0914	0.0938	0.0996	0.101	0.108	0.108
Power [P]	0.938	0.979	0.765	0.0991	0.0840	0.0973	0.916	0.995	0.994	0.994
Mass [Kg]	0.0184	0.0185	0.0188	0.0195	0.0193	0.0197	0.0196	0.0199	0.020	0.0199
Number Layer	3		3		3		3		3	
Board Thickness	1.6		1.6		1.6		1.6		1.6	

Tab. 14 Case 1 scenario - EmbeddedCoil

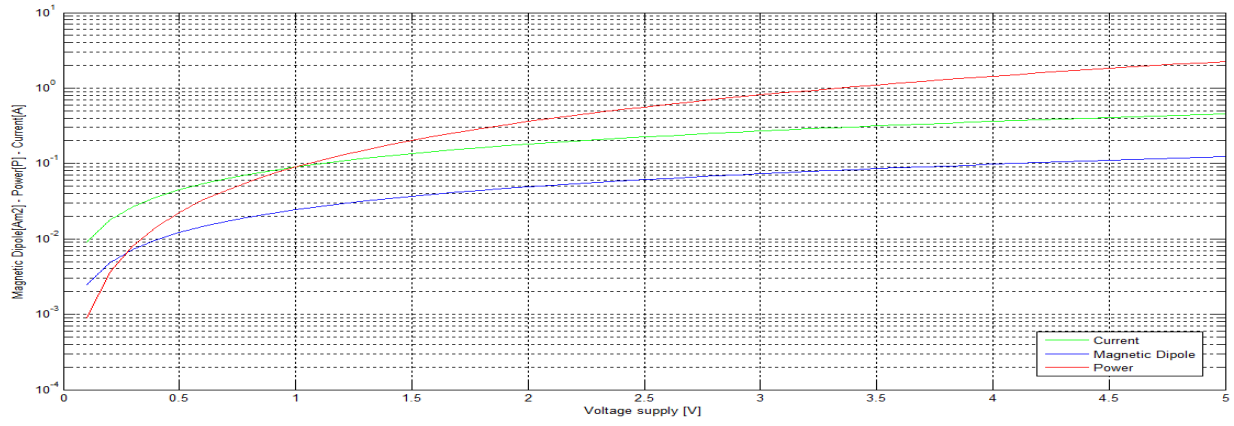


*Fig. 116 Design 1 EmbeddedCoil*

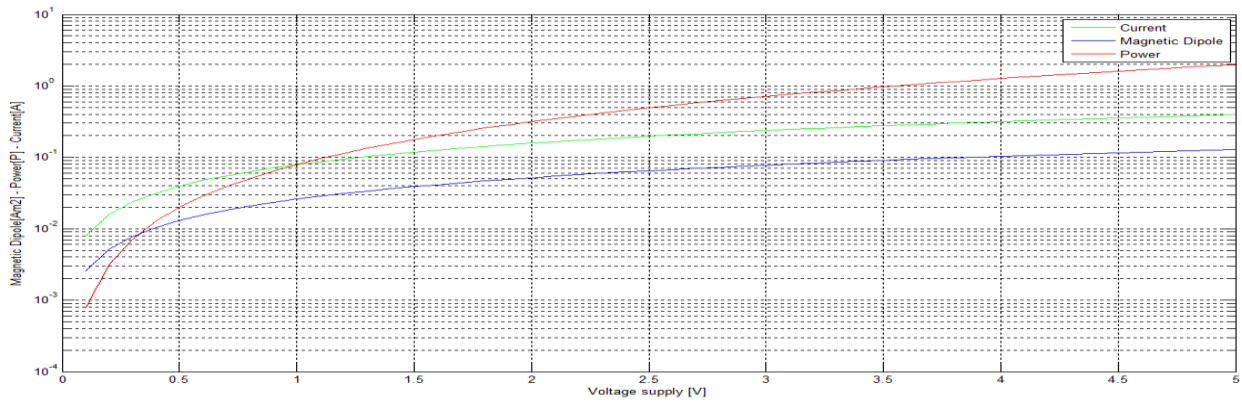


*Fig. 117 Design 2 EmbeddedCoil*

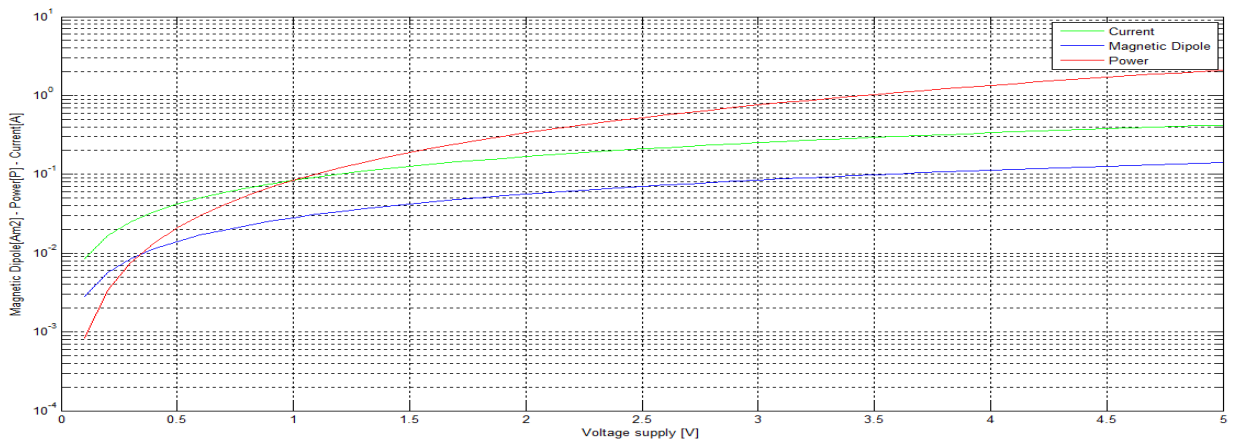


*Fig. 118 Design 3 EmbeddedCoil*



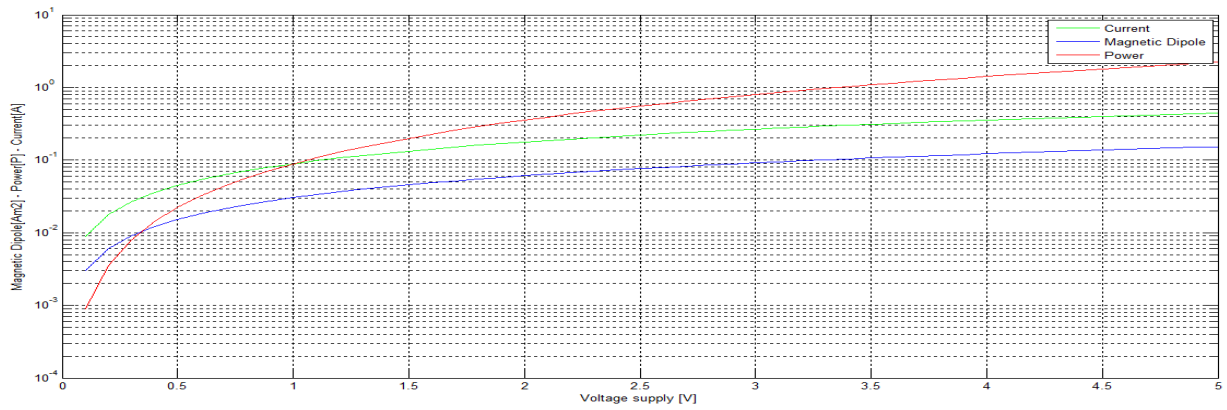


Fig. 119 Design 4 EmbeddedCoil

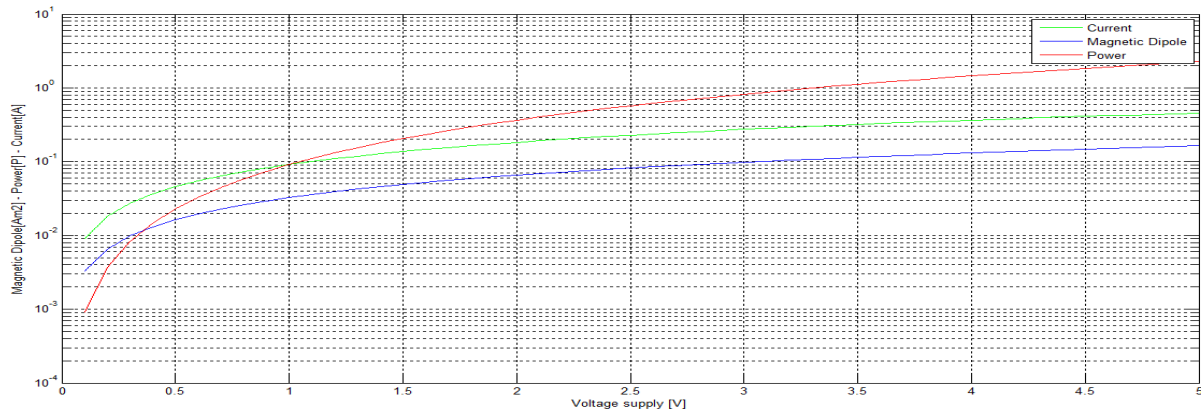


Fig. 120 Design 5 EmbeddedCoil

Case 1									
Magnetorquer				Torque Rod					
Input									
Voltage Supply [V]				3.3					
Core Dimension [mm]				6 x 76					
Constraints/Requirements									
Requested Magnetic Dipole [Am <sup>2</sup> ]				>0.08					
Maximum Power Consumption [W]				<1					
Maximum Mass [Kg]				<0.03					
Possible Design									
Wire D [mm]		0.10		0.11		0.13		0.14	
	Min	Max	Min	Max	Min	Max	Min	Max	

<b>Number of Turns</b>	258	800	312	800	372	686	486	534
<b>Winding Thickness [mm]</b>	0.1	0.2	0.11	0.22	0.12	0.24	0.14	0.14
<b>Magnetic Dipole [Am<sup>2</sup>]</b>	0.157	0.157	0.190	0.190	0.227	0.227	0.266	0.266
<b>Power [P]</b>	0.322	0.999	0.389	0.999	0.541	0.997	0.746	0.997
<b>Mass [Kg]</b>	0.0290	0.0299	0.0291	0.0299	0.0294	0.0299	0.0296	0.0299

*Tab. 15 Case 1 scenario - TorqueRod*

The scenario can be satisfied using air core, embedded coil or torquerod. As it's possible to see the torquerod solution would ensure really high magnetic dipoles even three times the minimum required one.

On the contrary the solution is border line with respect to the mass constraints because of the presence of the core that alone, cover almost the available mass budget. What's more the possibilities offered by the torquerod involve huge number of turns that introduce difficulties in the practical manufacturing of the system. Due to the short length of the single turn, even for high number of turns the power consumption can result pretty high with respect to the air core.

Modifying one of the constraints the situation changes. Reducing the requested power consumption 300 mW it's possible to notice that for the defined input doesn't exist the possibility to satisfy requirements and constraints using embedded coil, while almost could be possible with torquerod. This example put on evidence one of the limit of embedded coil that is related to high current absorbed. The scenario instead is still compatible exploiting air core coils, of course reducing the flexibility in the system design.

On the contrary, reducing the mass constraints could be impossible to exploit the same torquerod system, while embedded coil and air core still could be satisfying.

<b>Case 2</b>	
<b>Magnetorquer</b>	<b>Air Core</b>
<b>Input</b>	
<b>Voltage Supply [V]</b>	3.3
<b>Side Dimension [mm]</b>	76

Constraints/Requirements						
Requested Magnetic Dipole [Am <sup>2</sup> ]	>0.08					
Maximum Power Consumption [W]	<0.30					
Maximum Mass [Kg]	<0.03					
Possible Design						
Wire Diameter [mm]	0.18		0.19		0.20	
	Min	Max	Min	Max	Min	Max
Number of Turns	173	289	196	263	217	237
Winding Thickness [mm]	1.8	3.1	2.3	3.1	2.8	3.1
Magnetic Dipole [Am <sup>2</sup> ]	0.0835	0.0863	0.0930	0.0950	0.1031	0.1038
Power [P]	0.179	0.299	0.221	0.299	0.273	0.298
Mass [Kg]	0.0219	0.0299	0.0248	0.0299	0.0282	0.0299
Support Thickness [mm]	3		3		3	

Tab. 16 Case 2 scenario - AirCore

Changing the requirements instead of the constraints the torquerod would become the only available solution. Increasing the requested magnetic dipole up to 0.2 only this system can permit to reach the goal respecting the constraints in power and size.

This is of course the advantage of the core that permits to increase of order of magnitude the magnetic dipole for a fixed power, but increasing also size and mass of the whole system.

Case 3	
Magnetorquer	Torque Rod
Input	
Voltage Supply [V]	3.3
Core Dimension [mm]	6 x 76
Constraints/Requirements	
Requested Magnetic Dipole [ $\text{Am}^2$ ]	>0.2

Maximum Power Consumption [W]	<1			
Maximum Mass [Kg]	<0.03			
Possible Design				
Wire Diameter [mm]	0.12		0.13	
	Min	Max	Min	Max
Number of Turns	373	686	436	584
Winding Thickness [mm]	0.1	0.2	0.11	0.22
Magnetic Dipole [Am²]	0.227	0.227	0.266	0.266
Power [P]	0.541	0.999	0.745	0.999
Mass [Kg]	0.0294	0.0299	0.0296	0.0299

*Tab. 17 Case 2 scenario - TorqueRod*

The scenario can be satisfied using only a torquerod. The flexibility in the design is reduced and, in order to satisfy the requirement in power consumption, many turns are requested.

## 8. Cost Analysis

Besides the technical issues it's important to evaluate also the economic aspects of each kind of magnetorquer. Air core magnetorquer are basically the easiest solution both in terms of manufacturing and cost. Considering that this consists basically in a wounded wire on a proper support, the average price is connected to the quality and the cost of chosen wire. Magnetic wire can have several different prices according to the standard and the certificates offered by the supplier. General for the wire presented in the previous analysis the cost vary from a minimum of 0.5 \$/m to a maximum of 3.29 \$/m. Typical length for an air core are in the order of 50-100 m. The cost of the support depends of course on the manufacturing procedure.

A torquerod has similar cost concerning the wire that is exactly the same exploited for air core. Typical lengths for this system are reduced, being around 10 to 20 m. As obvious the key element of this system is the core that determines the quality of the device. According to different products also here the cost may significantly vary. Generally for a NiFe alloy 79 and alloy 50 are provided in long bars with different diameter. A 1m bar with 0.8 to 1.2 mm diameter can have a cost that

varies from 100 to 200\$. Different cores of different material can present higher cost according to the standard guaranteed by the supplier. As well as air core magnetorquer the cost of the support depends on the manufacturing procedures.

In general is really difficult to determine the total cost for the realization of a single device because of the uncertainties connected with the manufacturing procedures. In general it's possible to notice that this kind of magnetorquer are relatively cheap if self-made and the average price of materials for single device can be considered to be in worst case around 500 to 700\$.

Different consideration can be made for embedded coil. In this case the cost of the realization is totally defined by the cost of the PCB designed. The problem in this case is due to the need to have a multilayer board in order to have a satisfying device. Also the trace height can influence the price. The cost of a PCB doesn't increase linearly with the number of layer. In general the cost of production can vary from a minimum of 100\$ to a maximum of 1000\$ for a board with many layers and specific arrangements.

Even if the cost of this solution could appear much higher than the previous ones, it has to be considered the nature of this devices: embedded coils are part of a more complex subsystem that is represented by the side panels of a nanosatellite: generally in these are comprised also the conditioning circuit for the solar panels and other devices (sensors). For that reason the cost of an embedded coil can't be considered as a standalone cost as subsystem but it is part of a bigger portion of the whole satellite.

For that reason it's not easy to define compare properly the cost of this solution with respects to the previous ones.

## 9. Conclusion

The analysis led permitted to understand the advantages and disadvantages of each solution presented.

The following table take resume the main features of the three kind of magnetic control trying to give a qualitative assessment that allows to address the choice towards the most appropriate solution according to the type of mission. A rating from 1 to 3 points summarizes the main disadvantages and disadvantages of each configuration.

	Air Core	Embedded Coil	Torquerod
<b>Magnetic Dipole</b> The magnitude of the dipole that can be provided	★	★	★ ★ ★
<b>Power Consumption</b> The average power requested for normal operative condition	★ ★ ★	★	★ ★
<b>Mass</b> The mass of the system with supports and arrangements	★ ★	★ ★ ★	★
<b>Volume</b> The volume of the system with supports and arrangements	★ ★	★ ★ ★	★
<b>Volume Interference</b> The interference of the system with continuous internal volume	★ ★	★ ★ ★	★
<b>Integration</b> Simplicity of integration in the satellite, taking into account the need of additional elements (screws, connectors)	★ ★	★ ★ ★	★
<b>Efficiency</b> Ratio between the average dipole and the requested power	★ ★	★	★ ★ ★
<b>Control</b> Simplicity of controlling method	★ ★ ★	★ ★ ★	★ ★
<b>Cost</b> Cost for manufacturing	★ ★ ★	★ ★	★ ★

Related Issues	<ul style="list-style-type: none"> <li>• Limited number of turns on the plane</li> </ul>	<ul style="list-style-type: none"> <li>• Presence of residual dipole</li> <li>• Eventual need of demagnetizing circuit</li> </ul>
----------------	--	---

*Tab. 18 Magnetorquer resume*

The work presented offered an analysis of the main three magnetorquer solution. For each of these has been found the mathematical model and the design equation that permit to dimension the proper system. Each model has been compared with experimental measure on different prototype in order to check margins of reliability of the mathematical model and investigate related unexpected issues. The dimensioning equations have been exploited to define a universal designing flow chart that could permit to obtain the optimal preliminary design according to the required performances starting from defined inputs. The equation integrated in iterative tools and the methodologies presented are fully parametric in each variable, in order to completely rescale the system to a bigger satellite with completely different budget and requirements.

The mission requirements and constraints defined in the concept design of the whole satellite are fundamental to determine the most appropriate solution. This phase is really important because in most of case, obtaining the maximum magnetorquer strength could not be the real needed solution. These devices in fact don't offer a controlling torque whose magnitude permits a precise pointing maneuver, and more they exploit an external field (magnetic field) that vary during the orbit and in that way also the controlling law depends in a certain way on the position of the satellite. The torquerod are the only solution that permits to reach higher value of the controlling torque, but also here it has to be carefully evaluated their real purpose: this systems, as well as air core and embedded coil, are often used to detumble and desaturate the wheels that instead are the main device to perform faster and more accurate maneuvers. In this scenario may not be necessary to have substantial dipole moments at the expense of the disadvantages in terms of mass and volume.

## Bibliography

- [1] Cal Poly SLO, Cubesat design specification Rev.12, The Cubesat Program, 2009.
- [2] W. J.R.Wertz, Space Mission Analysis and Design.
- [3] M. Glass, «Principles of Design of Magnetic Devices for Attitude Control of Satellites,» *The Bell System Technical Journal*, 1967.
- [4] George Mason University, [Online]. Available: [http://bass.gmu.edu/~pceperle/WebProjts19xx/st1/mag\\_torq.htm](http://bass.gmu.edu/~pceperle/WebProjts19xx/st1/mag_torq.htm). [Consultato il giorno July 2014].
- [5] A. Aydinlioglu, Design development and production of electromagnetic coils for attitude control of a pico satellite, Aachen, University of Applied Sciences, 2006.
- [6] Tunghai University, Department of Applied Physics, [Online]. Available: [http://phys.thu.edu.tw/~hlhsiao/mse-web\\_ch20.pdf](http://phys.thu.edu.tw/~hlhsiao/mse-web_ch20.pdf). [Consultato il giorno April 2014].
- [7] S. A. Puig, Modeling Linear and Nonlinear Soft Ferromagnetic Materials, Department de Fisica, Universitat Autònoma de Barcelona, 2013.
- [8] © 2013 GomSpace ApS., «NanoPower P110 Series Datasheet,» [Online]. [Consultato il giorno April 2014].
- [9] «Wikipedia, Permeability(Electromagnetism),» [Online]. Available: [http://en.wikipedia.org/wiki/Permeability\\_\(electromagnetism\)](http://en.wikipedia.org/wiki/Permeability_(electromagnetism)). [Consultato il giorno May 2014].
- [10] © 2010 Spectrolab, Inc, «28.3% Ultra Triple Junction (UTJ) Solar Cells Datasheet,» [Online]. Available: <http://www.spectrolab.com/DataSheets/cells/PV%20UTJ%20Cell%205-20-10.pdf>. [Consultato il giorno May 2014].
- [11] © EOPortal 2000 - 2014, «DTUSat-2 (image credit: DTU),» [Online]. Available: <https://directory.eoportal.org/web/eoportal/satellite-missions/d/dtusat-2>. [Consultato il giorno June 2014].
- [12] G. Franceschetti, «Magnet Permanenti,» [Online]. Available: [http://web.mclink.it/MC5690/capitolo1\\_3.html](http://web.mclink.it/MC5690/capitolo1_3.html). [Consultato il giorno April 2014].
- [13] L. L. Harner, «A Simplified Method of Selecting Soft Magnetic Alloys,» Carpenter Technology Corporation, May 1999. [Online]. Available: <http://www.carttech.com/techarticles.aspx?id=1624>. [Consultato il giorno May 2014].
- [14] «Ed Fagan Inc. Soft Magnetic,» Ed Fagan Inc., [Online]. Available: <http://www.edfagan.com/magnifer-7904-hymu-80-hipernom-moly-permalloy-80-rod-sheet-coil-square-bar.php>. [Consultato il giorno May 2013].
- [15] «Aperam Alloys,» Aperam, [Online]. Available: [www.aperam.com/alloys-imphy](http://www.aperam.com/alloys-imphy). [Consultato il giorno June 2014].
- [16] K. V. GmbH, «Magnifer® 7904,» August 2000. [Online]. [Consultato il giorno April 2014].
- [17] V. G. & C. KG. [Online]. Available: <http://www.vacuumschmelze.com/en/products.html>. [Consultato il giorno April 2014].
- [18] M. M. Mohamad Fakhari Mehrjardi, «Design and Manufacturing of a Research Magnetic Torquer Rod,» *Contemporary Engineering Sciences*, vol. 3, n. 5, pp. 227-236, 2010.
- [19] Étienne du Trèmolet de Lacheisserie; Damien Gignoux; Michel Schlenker, Magnetism: material and application, Springer, 2005.



- [20] F.-R. P. Catalog, «4077375211 Datasheet,» 3 July 2013. [Online]. Available: [http://www.fair-rite.com/catalog\\_pdfs/4077375211.pdf](http://www.fair-rite.com/catalog_pdfs/4077375211.pdf). [Consultato il giorno June 2013].
- [21] R. Clark, «Magnetism: quantities, units and relationships,» 2013. [Online]. Available: <http://info.ee.surrey.ac.uk/Workshop/advice/coils/terms.html#ind>. [Consultato il giorno April 2014].